



Virginia Commonwealth University
VCU Scholars Compass

Theses and Dissertations

Graduate School

2014

Understanding ligand binding, selectivity and functions on the G protein-coupled receptors: A molecular modeling approach

Saheem Zaidi
Virginia Commonwealth University

Follow this and additional works at: <https://scholarscompass.vcu.edu/etd>

 Part of the [Pharmacy and Pharmaceutical Sciences Commons](#)

© The Author

Downloaded from

<https://scholarscompass.vcu.edu/etd/596>

This Dissertation is brought to you for free and open access by the Graduate School at VCU Scholars Compass. It has been accepted for inclusion in Theses and Dissertations by an authorized administrator of VCU Scholars Compass. For more information, please contact libcompass@vcu.edu.

© Saheem A. Zaidi _____ 2014
All Rights Reserved

UNDERSTANDING LIGAND BINDING, SELECTIVITY AND FUNCTIONS ON THE G
PROTEIN-COUPLED RECEPTORS: A MOLECULAR MODELING APPROACH

A dissertation submitted in partial fulfillment of the requirements for the degree of Doctor of
Philosophy at Virginia Commonwealth University

By

Saheem Asghar Zaidi

Director: Dr. Yan Zhang, Ph.D.
Associate Professor,
Department of Medicinal Chemistry

Director: Dr. Glen E. Kellogg, Ph.D.
Associate Professor,
Department of Medicinal Chemistry

Virginia Commonwealth University
Richmond, Virginia
6th May, 2014

ACKNOWLEDGMENTS

It gives me immense pleasure to convey my gratitude to many people who have helped in this endeavor. First and foremost, heartfelt thanks to my family, especially my father, *Dr. Aijaz A. Zaidi*, who was the most positive influence in my life. I'm grateful to mother, *Mrs. Naheed Zaidi*, and my sisters, *Sabika* and *Falak*, for being a constant source of love and strength.

I have deepest appreciation for my advisors, *Dr. Yan Zhang*, *Dr. Glen E. Kellogg* and *Dr. Philip D. Mosier*, for accepting me in their research labs when I was a novice, and five years later, for still excusing my nescience. I'm thankful to them for providing me with the guidance, support and challenges throughout my program. I'm grateful for their patience while reviewing this dissertation, and also for financially supporting me.

I thankfully acknowledge number of colleagues I worked with and learned from in the past five years, particularly *Dr. Hardik Parikh*, *Dr. Yunyun Yuan*, *Dr. Christopher Arnatt*, *Dr. Orgil Elbegdorj*, *Dr. Dwight Williams*, *Thomas Raborg*, *Jeremy Chojnacki* and *Ahmad Obaidullah*.

My friends have provided me with great support throughout these five years. I owe a special thanks to *Sharmeen*, *Mohit*, *Paumil*, *Kunal*, among others.

I'm grateful to *Dr. Frank Fang* and *Dr. Neel Scarsdale* for reviewing and evaluating my research along with *Dr. Yan Zhang, Dr. Glen E. Kellogg and Dr. Philip D. Mosier*.

Finally, I would like to acknowledge School of Pharmacy, Virginia Commonwealth University for accepting me the program and providing me with all the opportunities that I had in past five years.

TABLE OF CONTENTS

Acknowledgment.....	ii
List of Figures.....	viii
List of Tables.....	xii
List of abbreviations.....	xiii
Abstract.....	xv
Chapter 1: Introduction.....	1
Chapter 2: Predicting receptor-ligand interactions in C-C chemokine receptor type 5	
2.1 Introduction.....	9
2.2 Methods and Results.....	15
2.2.1 Homology modeling of CCR5.....	15
2.2.2 Ligand sketching.....	17
2.2.3 Ligand docking and binding site validation.....	17
2.2.4 Docking modes of anibamine.....	26
2.2.5 Generation of water sites inside the homology model.....	28
2.3 Discussion.....	33
Chapter 3: Modeling selectivity of naltrexone derived antagonists for opioid receptors	

3.1 Introduction.....	40
3.1.1 Early research in opioid receptor identification and characterization.....	40
3.1.2 Opioid receptor signaling.....	43
3.1.3 μ -opioid receptor (MOR).....	45
3.1.4 κ -opioid receptor (KOR).....	47
3.1.5 δ -opioid receptor (DOR).....	48
3.1.6 Importance of MOR selective antagonists.....	49
3.2 Binding mode characterization of 6 α - and 6 β - <i>N</i> -heterocyclic substituted naltrexamine derivatives	
3.2.1 Introduction.....	53
3.2.2 Methods.....	57
3.2.2.a Sequence analysis.....	57
3.2.2.b Receptor models.....	57
3.2.2.c Ligand models.....	58
3.2.2.d Ligand docking.....	58
3.2.2.e Conformational analysis.....	59
3.2.3 Results.....	59
3.2.3.a Sequence alignment analyses.....	59
3.2.3.b Conformational analysis.....	63
3.2.3.c Docking studies of the opioid universal antagonist NTX.....	64
3.2.3.d Analysis of the NAP and NAQ morphinan backbone binding.....	67
3.2.3.e NAP and NAQ in the MOR.....	67

3.2.3.f NAP and NAQ in the KOR.....	69
3.2.3.g NAP and NAQ in the DOR.....	72
3.2.3.h Validation of docking mode by site-directed mutagenesis.....	75
3.2.4 Conclusions.....	76
3.3 Modeling pharmacological profile switch from mu-opioid receptor selectivity to mu/kappa opioid dual selectivity of 14-heteroaromatic substituted naltrexone derivatives	
3.3.1 Introduction.....	80
3.3.2 Methods.....	85
3.3.3 Results.....	87
3.3.4 Conclusions.....	91
3.4 Characterization of the selectivity profile of NAQ derivatives	
3.4.1 Introduction.....	93
3.4.2 Methods.....	95
3.4.3 Results.....	99
3.4.3.a Binding mode of NNQ in MOR.....	100
3.4.3.b Binding mode of NNQ in KOR.....	101
3.4.3.c Binding mode of NNQ in DOR.....	103
3.4.4 Conclusions.....	104
3.5 Discussion.....	107
Chapter 4: Understanding GPCR activation mechanism through molecular dynamic simulations	
4.1 Introduction.....	120
4.1.1 GPCR conformational diversity and crystallized GPCR agonist complex.....	120

4.1.2 GPCR micro-switches.....	125
4.1.3 Bimodal and multimodal models for GPCR activation.....	128
4.1.4 Unified GPCR activation model.....	131
4.1.5 Modeling active state receptor for KOR.....	134
4.1.6 Accelerated molecular dynamics.....	136
4.2 Methods.....	138
4.2.1 Generation of receptor models.....	138
4.2.2 Generation of topology and parameter files.....	142
4.2.3 Generation of lipid embedded receptor complex.....	142
4.2.4 Conventional molecular dynamics run.....	143
4.2.5 Accelerated molecular dynamics run.....	144
4.3 Analysis.....	145
4.3.1 Stability of the accelerated system.....	145
4.3.2 Trajectory analysis.....	146
4.3.2.a Analysis of KOR-JDTic lipid embedded complex.....	146
4.3.2.b Analysis of KOR-RB-64 lipid embedded complex.....	151
4.3.2.c Analysis of apoprotein KOR lipid embedded complex.....	161
4.4 Discussion.....	164
Chapter 5: Conclusions.....	172

LIST OF FIGURES

2.1. A typical time evolution of HIV-1 tropism.....	12
2.2 .CCR5 antagonists.....	14
2.3. Sequence alignment of CCR5 (target) and CXCR4 (template).....	16
2.4A. Representation of best-selected model.....	17
2.4B. Ramachandran plot of the model.....	17
2.5. Hydrophobic ligand binding pocket of CCR5.....	18
2.6. Docking poses of maraviroc inside CCR5 homology model.....	21
2.7. Docking poses of vicriviroc inside CCR5 homology model.....	22
2.8. Docking poses of aplaviroc inside CCR5 homology model.....	23
2.9. Docking poses of SCH-c inside CCR5 homology model.....	24
2.10. Docking poses of TAK-779 inside CCR5 homology model.....	25
2.11. Docking poses of anibamine inside CCR5 homology model.....	27
2.12. Generated water map with 29 waters in the ligand binding pocket.....	29
2.13. First docking mode of maraviroc with superimposed interacting waters.....	32
2.14. Second docking mode of maraviroc with superimposed interacting waters.....	32

2.15. First docking mode of TAK-779 with superimposed interacting waters.....	32
3.1. Summary of the GPCR signaling pathways.....	45
3.2. Opioid receptor selective antagonists.....	52
3.3. Naltrexone a universal opioid antagonist.....	54
3.4. Naltrexone docked in the homology models of the MOR, DOR, and KOR.....	55
3.5. Identified potent and selective MOR antagonists.....	56
3.6. Sequence alignment of opioid receptors and bovine rhodopsin.....	62
3.7. Conformational analysis of NAP inside a water box.....	63
3.8. Docked poses of naltrexone inside the three opioid receptors.....	66
3.9 Docked poses of NAP and NAQ in the mu opioid receptor.....	68
3.10. Docked poses of NAP and NAQ in the kappa opioid receptor.....	71
3.11. Docked poses of NAP and NAQ in the delta opioid receptor.....	74
3.12 Morphinan skeleton of NTX indicating 14 th position of substitution.....	80
3.13. Second binding mode of naltrexone inside MOR homology model.....	81
3.14. First generation NOP and second generation NNP 14 th substituted NTX derivatives.....	85
3.15A. Superimposed binding mode of NOP in three opioid receptors.....	88
3.15B. Binding mode of NNP in the MOR.....	89
3.15C. Superimposed binding modes of paraNOP and paraNNP.....	90
3.16. NNQ, 6nitro derivative of NAQ.....	94
3.17. MOR-NNQ-lipid bilayer-aqueous box representation.....	97
3.18. NNQ binding mode inside the MOR.....	101
3.19. NNQ binding mode inside the KOR.....	102

3.20 NNQ binding mode inside the DOR.....	104
4.1. DRY and NPxxY motif.....	127
4.2. Movement in P-I-F motif in response to co-crystallization with ergotamine.....	128
4.3. Bimodal and multimodal GPCR activation models.....	130
4.4. Proposed GPCR activation mechanism.....	132
4.5. Salvinorin A and RB-64.....	133
4.6. Schematic representation of the accelerated MD.....	136
4.7. Cartoon representation of KOR demonstrating point of linkage of RB-64.....	137
4.8. Placement of JDtic inside KOR as observed in the crystal structure.....	138
4.9. Position of sodium inside KOR.....	139
4.10. Co-variance matrix for aMD trajectory of KOR-JDtic system.....	145
4.11 Eigenvalues associated with principal components for KOR-JDtic system.....	146
4.12. Projection of the receptor conformational space unto two principal components.....	147
4.13. Overlaid and aligned conformations for crystal structure and representative structure of the most sampled conformation.....	148
4.14. Co-variance matrix for aMD trajectory of KOR-JDtic system.....	149
4.15. Eigenvalues associated with principal components for KOR-RB-64 system.....	150
4.16. Projection of the receptor conformational space unto two principal components.....	151
4.17. Overlaid and aligned conformations for crystal structure and representative structure of the fourth most sampled conformation.....	152
4.18. Overlaid and aligned conformations for crystal structure and representative structure of the most sampled conformation.....	153
4.19. Evolution of distance between center of mass of phenyl ring of Phe ^{6.44} and nitrogen atom of Pro ^{5.50}	155

4.20. Conformational state of P-I-F motif in the highest sampled population.....	155
4.21. Evolution of distance between hydroxyl oxygen atoms of Tyr ^{5.58} and Pro ^{7.53}	156
4.22. Conformational state of Tyr ^{7.53} and Tyr ^{5.58} in the highest sampled population.....	157
4.23. Evolution of distance between center of mass of the receptor and center of mass of cytoplasmic domain of TM6	158
4.24. Sharp kink in TM6 at His ^{6.52}	159
4.25. Eigenvalues associated with principal components for Apo-KOR system.....	160
4.26. Eigenvalues associated with principal components for Apo-KOR-allosteric sodium system.....	160
4.27. Projection of the receptor conformational space unto two principal components.....	161
4.28. Sampling probabilities of projections.....	161

LIST OF TABLES

2.1. Fold differences of amino acid mutations on inhibition of fusion with viral gp120.....	19
2.2. Water Relevance scores for the generated waters.....	30
3.1. NTX, NAP and NAQ receptor radioligand binding and selectivity profile.....	56
3.2. Functional characterization of ligands <i>In vitro</i> and <i>In vivo</i> studies.....	56
3.3. Non conserved amino acid residue composition of two binding sites in opioid receptors....	61
3.4. Sequence identity among three opioid receptor.....	61
3.5. Fitness scores for each docking modes of NTX, NAP and NAQ.....	66
3.6. Binding of ligands to the site-directed mutated MORs.....	75
3.7. Second generation naltrexamine derivatives.....	78
3.8. Opioid receptor binding affinity and selectivity of O-linked 14-position NTX derivatuves..	83
3.9. Opioid receptor binding affinity and selectivity of N-linked 14-position NTX derivatuves..	84
3.10. Opioid receptor binding affinity and selectivity data for NNQ and NAP.....	94
3.11. NNQ-receptor interaction energies.....	100
4.1. Pharmacological profile of salvinorin A and its C-22 derivative RB-64.....	135
4.2 Summary of conventional MD and accelerated MD simulations.....	145

LIST OF ABBREVIATIONS

GPCR – G protein-coupled receptor

CCR5 – C-C chemokine receptor type 5

HIV-1 – Human Immunodeficiency Virus-1

cDNA – complimentary deoxyribonucleic acid

CXCR4 – C-X-C chemokine receptor type 4

PDB – Protein Data Bank

TM – Transmembrane

ECL – Extracellular loop

ICL – Intracellular loop

TFF –TRIPOS Force Field

HINT – Hydrophobic INTERaction

CNS – Central Nervous System

GTP – Guanine Triphosphate

MOR- Mu opioid receptor

KOR – Kappa opioid receptor

DOR – Delta opioid receptor

NTX – Naltrexone

PBC – Periodic Boundary Conditions

PME – Particle Mesh-Ewald

MD – Molecular Dynamics

ABSTRACT

UNDERSTANDING LIGAND BINDING, SELECTIVITY AND FUNCTIONS ON THE G PROTEIN-COUPLED RECEPTORS: A MOLECULAR MODELING APPROACH

By Saheem Asghar Zaidi, Ph.D.

A dissertation submitted in partial fulfillment of the requirements for the degree of Doctor of Philosophy at Virginia Commonwealth University

Virginia Commonwealth University, 2014

Major Director: Dr. Yan Zhang, Ph.D.
Associate Professor, Department of Medicinal Chemistry

Major Director: Dr. Glen E. Kellogg, Ph.D.
Associate Professor, Department of Medicinal Chemistry

The assessment of target protein molecular structure provides a distinct advantage in the rational drug design process. The increasing number of available G protein-coupled receptor crystal structures has enabled utilization of a varied number of computational approaches for understanding the ligand-receptor interactions, ligand selectivity and even receptor response upon ligand binding.

The following dissertation examines the results from three different projects with varied objectives – i) structural modeling of human C-C chemokine receptor type 5 (CCR5) and assessment of the ligand binding pocket of the receptor, ii) assessment of the selectivity profile of naltrexone derivatives on the three opioid receptors (μ -opioid, κ -opioid, δ -opioid) with an aim towards designing selective μ -opioid receptor antagonists, and iii) structural modeling of the ‘active’ state conformation of the κ -opioid receptor in response to agonist binding and determination of a plausible molecular mechanism involved in activation ‘switch’ of the κ -opioid receptor.

In absence of a crystal-based molecular structure of CCR5, a homology model of the receptor was built and the ligand binding pocket was validated. On the basis of evaluation of the ligand-receptor interactions on the validated binding pocket, structural and chemical modifications to anibamine, a natural plant product, were proposed to enhance its receptor binding.

The selectivity of naltrexone (a universal antagonist) was assessed with respect to the three opioid receptors by employing ligand docking studies and the ‘message-address’ concept. Multiple address sites were identified on the opioid receptors and structural modifications were proposed for the naltrexone derivatives for their enhanced selectivity.

In the third project, structural modeling of the active state conformation of the κ -opioid receptor covalently bound to a salvinorin A derivative (agonist) was attempted via molecular dynamics simulations. Although the obtained molecular model lacked the signature ‘agonist-like’ conformations, the result provides a template for such studies in the future.

CHAPTER 1

INTRODUCTION

G protein-coupled receptors (GPCRs) are the large family of proteins expressed on plasma membrane that function as the receivers of extracellular chemical and physical stimuli. In seminal studies reported in the late 1960s, Lefkowitz and coworkers demonstrated the first evidence of biologically active receptors by the exhibition of intracellular reactions in response to the extracellular binding of hormones tagged with radioactive iodine molecules.¹ The group later isolated the gene encoding for the receptor of the adrenaline hormone and successfully cloned the β_2 adrenergic receptor.² Around the same time, two groups working independently published the first complete amino acid sequence of rhodopsin. Results from the previous study demonstrating the presence of C-terminus of rhodopsin in the cytoplasm and the hydrophobic profiling of the amino acid sequence, taken together, led to the first two-dimensional model of rhodopsin.^{3,4} The rhodopsin was imagined as a serpentine originating extracellularly, spanning the membrane seven times with seven α helical domains, connected by three intracellular and three extracellular loops, and terminating in the cytoplasm.⁵ The similarities between the β_2 adrenergic receptor and rhodopsin were soon realized, and it was suggested that they might

belong to a family of a larger group of proteins with similar structures but completely different functions. The family was later termed as the GPCRs, and since then more than 800 genes coding for GPCRs have been identified. The members of the GPCR family are known to mediate in a number of physiological functions, including neurotransmission, cardiac function, hormone responses, inflammation, transmission of infectious diseases, and functions regarding vision, taste and odor.⁶

GPCRs are the frequent targets for therapeutic interventions and approximately one-fourth of the currently prescribed drugs target GPCRs. Historically, structures for the biologic ligands are generally identified before the structures of their cognate receptors. Hence, the computational modeling efforts for the development of GPCR ligands were based on the ‘similarity principle’, according to which structurally similar compounds are likely to possess similar biological properties.⁷ The lead compounds for these studies are often identified through large-scale screenings or are based on the endogenous ligands.

The ligand-based methods have proved to be a great tool in ligand design; however, molecular structure elucidation of the first GPCR, bovine rhodopsin, was a giant leap forward. The relatively high quality and detailed structure of inactive ‘dark’ state rhodopsin covalently bound to 11-*cis* retinal has paved the way for structure-based drug design.⁸ This structure elucidation was followed by solution of several other rhodopsin structures, and for a number of years rhodopsins were the only available templates for GPCR homology modeling approaches. The primary reason for this was the abundance of rhodopsin availability from the bovine source and also because of its higher tolerance to the detergents used for extracting the receptor from its native lipid bilayer. Furthermore, the distinct mechanism of the rhodopsin activation allowed for

the ability to precisely time its activation by light and to monitor its functional state by monitoring the spectroscopic properties of retinal.⁹ Several rhodopsin based homology models have been used for virtual screening to identify ligands and to study binding of known ligands. However, these studies had varying success rates because, in spite of sharing many common structural features with other family A GPCRs, the overall homology is generally less than 25% and also because of a distinct receptor activation mechanism that lacks activation through a diffusible ligand.¹⁰

The first crystal structures with diffusible ligands to be solved were turkey β_1 and human β_2 -adrenergic receptors.^{11,12} Those elucidations required significant innovations in crystallization techniques including co-crystallization with structured peptides such as antibody fragments or T4-lysozyme, and thermostabilizing mutations. The continued efforts have realized several more GPCR crystal structures including adenosine A_{2A} , dopamine D_3 , histamine H_1 , muscarinic M_2 and M_3 , μ -opioid receptor, κ -opioid receptor, δ -opioid receptor, C-X-C chemokine receptor 4, C-C chemokine receptor 5, etc.¹³⁻¹⁷

Although the structural coverage by these crystallized GPCRs is still not complete, it does provide a much more diverse pool for template selection in homology modeling. Moreover, these crystallized GPCRs are targets for several ligands. The structure elucidation of target receptors has provided for detailed ligand-receptor interaction studies with increased confidence. The insights gained from these analyses, along with the accumulated experience on ligand-based methods and structure-function relationship studies, promise newer, more potent and selective ligands.

Recently the crystal structures for the ‘active’ state apoprotein form of rhodopsin, called opsin, have also been solved, including one in complex with the C-terminal part of transducin G protein.¹⁸ Similarly, crystal structures for β -adrenergic receptors were elucidated in a ternary complex composed of the receptor, a G protein or a G protein surrogate, and an agonist.^{19,20} These molecular structures are considered to be the ‘fully active’ conformations of the receptor. Several other ‘active-like’ structures have also been solved, including adenosine A_{2A}, muscarinic M₂, 5-HT_{1B} and 5-HT_{2B} receptors.²¹⁻²³ The examination of the inactive and the active forms of GPCRs has enhanced understanding about the changes in conformational states required for receptor signaling and has also led to proposed GPCR activation mechanisms. This opens the door for several computational approaches for studying the receptor response to the ligand binding, the mechanism of activation of receptor, functional selectivity of the ligands, understanding basal activity and inverse agonism, etc.

The following sections report structure based approaches aided by the availability GPCR crystal structures, including homology modeling of a receptor based on a template, ligand-receptor interaction studies on the receptor homology model and on the crystal structures, and long term receptor-ligand molecular dynamics simulations to understand the receptor activation mechanism.

Chapter 2 details the structure based drug design strategy in the absence of target protein crystal structures. Anibamine, a natural plant product, is a C-C chemokine receptor type 5 antagonist and our lab has recently reported its total synthesis.²⁴ The rational design of more potent anibamine analogs required the understanding of ligand-receptor interactions. Hence, homology model of the receptor was built, and we propose the ligand binding mode and identify

the interactions involved in the receptor binding. Furthermore, the role of waters in the ligand binding pocket of CCR5 was explored.

Chapter 3 discusses the modeling approaches for designing selective μ -opioid receptor (MOR) antagonists based on the ‘message-address’ concept. The lead compounds were synthesized previously based on the homology models of the opioid receptors. The work presented here, validates the ‘address’ site conceived in the earlier study and also proposes alternate ‘address’ sites on the receptor.

Chapter 4 details the method and the approach for building ‘active-like’ model of κ -opioid receptor (KOR) in complex with covalently bound agonist in plasma membrane like environment. This study was undertaken to discern the mechanism of κ -opioid receptor activation in response to an agonist.

Reference:

- (1) Lefkowitz, R. J.; Roth, J.; Pricer, W.; Pastan, I. Radioreceptor assay of adrenocorticotrophic hormone: New approach to assay of polypeptide hormones in plasma. *Science* **1970**, *170*, 633–635.
- (2) Dohlman, H. G.; Caron, M. G.; Lefkowitz, R. J. Structure and function of the beta 2-adrenergic receptor--homology with rhodopsin. *Kidney Int Suppl.* **1987**, *23*, S2-13.
- (3) Hargrave, P.; McDowell, J.; Curtis, D.; Wang, J.; Juszczak, E.; Fong, S.; Rao, J.; Argos, P. The structure of bovine rhodopsin. *Biophys. Struct. Mech.* **1983**, *9*, 235–244.
- (4) Ovchinnikov, Y.; Abdulaev, N.; Feigina, M.; Artamonov, I.; Zolotarev, A.; Kostina, M.; Bogachuk, A.; Miroshnikov, A.; Martinov, V.; Kudelin, A. The complete amino- acid-sequence of visual rhodopsin. *Bioorganicheskaya Khimiya* **1982**, *8*, 1011–1014.
- (5) Flight, M. H. Structure-Led Design. *Nature* **2013**, *502*, S50-S52.
- (6) Costanzi, S.; Siegel, J.; Tikhonova, I. G.; Jacobson, K. A. Rhodopsin and the others: a historical perspective on structural studies on G protein-coupled receptors. *Curr. Pharm. Des.* **2019**, *15*, 3994–4002.
- (7) Martin, Y. C.; Kofron, J. L.; Traphagen, L. M. Do Structurally Similar Molecules Have Similar Biological Activity? *J. Med. Chem.* **2002**, *45*, 4350–4358.
- (8) Palczewski, K. Crystal Structure of Rhodopsin: A G Protein-Coupled Receptor. *Science* **2000**, *289*, 739–745.
- (9) Deupi, X. Relevance of Rhodopsin Studies for GPCR Activation. *Biochim. Biophys. Acta* **2013**, *1837*, 674–682.
- (10) Congreve, M.; Langmead, C.; Marshall, F. H. *The Use of GPCR Structures in Drug Design.*; 1st ed.; Elsevier Inc., 2011; Vol. 62, pp. 1–36.
- (11) Warne, T.; Serrano-Vega, M. J.; Baker, J. G.; Moukhametzianov, R.; Edwards, P. C.; Henderson, R.; Leslie, A. G. W.; Tate, C. G.; Schertler, G. F. X. Structure of a beta1-Adrenergic G-Protein-Coupled Receptor. *Nature* **2008**, *454*, 486–491.
- (12) Cherezov, V.; Rosenbaum, D. M.; Hanson, M. a; Rasmussen, S. G. F.; Thian, F. S.; Kobilka, T. S.; Choi, H. J.; Kuhn, P.; Weis, W. I.; Kobilka, B. K.; Stevens, R. C. High-Resolution Crystal Structure of an Engineered Human beta2-Adrenergic G Protein-Coupled Receptor. *Science* **2007**, *318*, 1258–1265.

- (13) Tan, Q.; Zhu, Y.; Li, J.; Chen, Z.; Han, G. W.; Kufareva, I.; Li, T.; Ma, L.; Fenalti, G.; Li, J.; Zhang, W.; Xie, X.; Yang, H.; Jiang, H.; Cherezov, V.; Liu, H.; Stevens, R. C.; Zhao, Q.; Wu, B. Structure of the CCR5 Chemokine Receptor-HIV Entry Inhibitor Maraviroc Complex. *Science* **2013**, *341*, 1387–1390.
- (14) Wu, B.; Chien, E. Y. T.; Mol, C. D.; Fenalti, G.; Liu, W.; Katritch, V.; Abagyan, R.; Brooun, A.; Wells, P.; Bi, F. C.; Hamel, D. J.; Kuhn, P.; Handel, T. M.; Cherezov, V.; Stevens, R. C. Structures of the CXCR4 Chemokine GPCR with Small-Molecule and Cyclic Peptide Antagonists. *Science* **2010**, *330*, 1066–1071.
- (15) Granier, S.; Manglik, A.; Kruse, A. C.; Kobilka, T. S.; Thian, F. S.; Weis, W. I.; Kobilka, B. K. Structure of the Δ -Opioid Receptor Bound to Naltrindole. *Nature* **2012**, *485*, 400–404.
- (16) Manglik, A.; Kruse, A. C.; Kobilka, T. S.; Thian, F. S.; Mathiesen, J. M.; Sunahara, R. K.; Pardo, L.; Weis, W. I.; Kobilka, B. K.; Granier, S. Crystal Structure of the M-Opioid Receptor Bound to a Morphinan Antagonist. *Nature* **2012**, *485*, 321–326.
- (17) Wu, H.; Wacker, D.; Mileni, M.; Katritch, V.; Han, G. W.; Vardy, E.; Liu, W.; Thompson, A. A.; Huang, X. P.; Carroll, F. I.; Mascarella, S. W.; Westkaemper, R. B.; Mosier, P. D.; Roth, B. L.; Cherezov, V.; Stevens, R. C. Structure of the Human K-Opioid Receptor in Complex with JD1c. *Nature* **2012**, *485*, 327–332.
- (18) Scheerer, P.; Park, J. H.; Hildebrand, P. W.; Kim, Y. J.; Krauss, N.; Choe, H. W.; Hofmann, K. P.; Ernst, O. P. Crystal Structure of Opsin in Its G-Protein-Interacting Conformation. *Nature* **2008**, *455*, 497–502.
- (19) Rasmussen, S. G. F.; DeVree, B. T.; Zou, Y.; Kruse, A. C.; Chung, K. Y.; Kobilka, T. S.; Thian, F. S.; Chae, P. S.; Pardon, E.; Calinski, D.; Mathiesen, J. M.; Shah, S. T. A.; Lyons, J. A.; Caffrey, M.; Gellman, S. H.; Steyaert, J.; Skiniotis, G.; Weis, W. I.; Sunahara, R. K.; Kobilka, B. K. Crystal Structure of the β 2 Adrenergic Receptor-Gs Protein Complex. *Nature* **2011**, *477*, 549–555.
- (20) Rasmussen, S. G. F.; Choi, H.-J.; Fung, J. J.; Pardon, E.; Casarosa, P.; Chae, P. S.; DeVree, B. T.; Rosenbaum, D. M.; Thian, F. S.; Kobilka, T. S.; Schnapp, A.; Konetzki, I.; Sunahara, R. K.; Gellman, S. H.; Pautsch, A.; Steyaert, J.; Weis, W. I.; Kobilka, B. K. Structure of a Nanobody-Stabilized Active State of the β (2) Adrenoceptor. *Nature* **2011**, *469*, 175–180.
- (21) Wacker, D.; Wang, C.; Katritch, V.; Han, G. W.; Huang, X.-P.; Vardy, E.; McCorvy, J. D.; Jiang, Y.; Chu, M.; Siu, F. Y.; Liu, W.; Xu, H. E.; Cherezov, V.; Roth, B. L.; Stevens, R. C. Structural Features for Functional Selectivity at Serotonin Receptors. *Science* **2013**, *340*, 615–619.

- (22) Kruse, A. C.; Ring, A. M.; Manglik, A.; Hu, J.; Hu, K.; Eitel, K.; Hübner, H.; Pardon, E.; Valant, C.; Sexton, P. M.; Christopoulos, A.; Felder, C. C.; Gmeiner, P.; Steyaert, J.; Weis, W. I.; Garcia, K. C.; Wess, J.; Kobilka, B. K. Activation and Allosteric Modulation of a Muscarinic Acetylcholine Receptor. *Nature* **2013**, *504*, 101–106.
- (23) Lebon, G.; Warne, T.; Edwards, P. C.; Bennett, K.; Langmead, C. J.; Leslie, A. G. W.; Tate, C. G. Agonist-Bound Adenosine A2A Receptor Structures Reveal Common Features of GPCR Activation. *Nature* **2011**, *474*, 521–525.
- (24) Li, G.; Watson, K.; Buckheit, R. W.; Zhang, Y. Total Synthesis of Anibamine, a Novel Natural Product as a Chemokine Receptor CCR5 Antagonist. *Org. Lett.* **2007**, *9*, 2043–2046.

CHAPTER 2

PREDICTING RECEPTOR-LIGAND INTERACTIONS IN C-C CHEMOKINE RECEPTOR

TYPE 5

2.1 Introduction

The C-C chemokine receptor type 5 (CCR5) belongs to the superfamily of membrane bound G protein-coupled receptors (GPCRs) and is highly expressed on macrophages and CD4 T cells. Phylogenetic analysis places CCR5 in the chemokine receptor cluster within the γ -subgroup of Rhodopsin-type receptors, along with angiotensin/bradykinin related receptors and many orphan receptors.^{1,2} Like the majority of the receptors in the cluster, CCR5 is also known interact with endogenous peptide ligands such as CCL3 (MIP-1 α), CCL4 (MIP-1 β), CCL5 (RANTES), CCL8, CCL11, CCL14 and CCL16. These ligands are C-C type or β -chemokines, which are characterized by the presence of two adjacent cysteines near the N-terminus.³ These chemokine ligands, along with several others, are vital chemoattractants for several mononuclear cell types to the site of inflammation and to the secondary lymphatic tissues acting via interaction with the

chemokine receptor. Hence, they play an important role in immune response to foreign antigens, tissue damage and other physiological insults. The type of mononuclear cell stimulated depends on the ligand and receptor involved, e.g., C-C chemokines stimulate leucocytes such as monocytes, lymphocytes and basophils.⁴ They are also reported to have functions in angiogenesis, haematopoiesis, embryonic development and metastasis.⁵ However, CCR5 along with CXCR4, a closely related chemokine receptor, attracted major attention in late 1990s when they were reported to be important co-receptors along with CD4 for *in vivo* HIV-1 portal into human cells.⁶

By the early 1990s it was clear that the CD4 expression was a necessary but not sufficient condition for HIV-1 entry into human cells. This was concluded based primarily on two observations. Firstly, recombinant CD4 receptor permitted viral entry only when expressed on human cells. Secondly, viral strains showed distinct tropism. Some viral strains showed efficient fusion/infectivity on T-lymphocytes, while having poor fusion/infectivity for primary macrophages. These strains were called T-tropic and were also syncytium-inducing strains. Other strains were more infective towards macrophages and were termed M-tropic or non-syncytium inducing strains.⁷ Viral isolates obtained from recently infected individuals showed presence of predominantly M-tropic strains; however, an increasing amount of T-tropic strains were seen in later stages of AIDS in many patients.⁸ Since studies from hybrid cell models negated the presence of inhibitors, existence of a co-receptor for the HIV-1 virus was postulated. Unbiased cDNA cloning experiments studying the ability of cDNA library to allow fusion/infection T-tropic strains on CD4 expressing cells revealed that C-X-C chemokine type 4 (CXCR4) as a co-receptor for T-tropic strains.⁹ Nonetheless, CXCR4 was still regarded as an

“orphan” receptor that was termed fusin. In a major breakthrough, study C-C chemokines like RANTES, MIP-1 α and MIP-1 β were reported to be important suppressors of M-tropic strains with little/no effect on T-tropic strains of HIV-1.¹⁰ These chemokines were later identified to bind at CCR5. Within a period of a week in 1996, five independent groups identified CCR5 as a co-receptor for M-tropic HIV-1 strains by employing both CCR5 ligand-induced loss of function and recombinant CCR5 induced gain of function studies.¹¹⁻¹⁵ Further definitive evidence came from the discovery of the mutant CCR5 allele with 32 base pair deletions, termed CCR5 Δ 32, which resulted in a truncated protein at trans-membrane domain 5 that is not expressed at the cell surface.¹⁶⁻¹⁹ Homozygotes of this mutant allele are found with a frequency of \sim 1% among the North American Caucasian population and this frequency was significantly higher in an exposed but uninfected population. Further studies revealed that the individuals with such mutant homozygotes were completely resistant to M-tropic HIV-1 strains, but they remained susceptible to T-tropic strains.^{16,17,20-22} Later studies have reported CCR5 to be a crucial co-receptor for viral transmission and replication during the early and clinically dormant phase of the disease. Furthermore, CCR5-tropic viruses are reported to be exclusively responsible for more than half of the HIV-1 infected population, even during late-phase disease, while in the remaining population HIV-1 also uses CXCR4 as a co-receptor.⁸

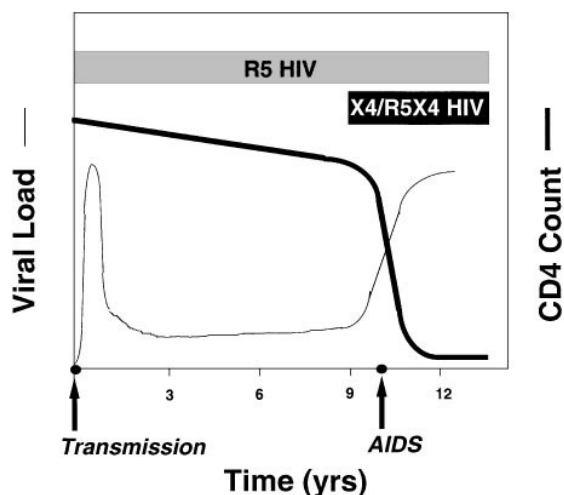


Figure 2.1. A typical time evolution of HIV-1 tropism indicating viral load (thin line), CD4 count (thick line), CCR5 tropism (grey bar) and CXCR4 tropism (black bar). Reprint from reference 6.

Another frontier for CCR5 receptor and related chemokines for drug discovery is developing an effective immunotherapeutic approach for curbing progression of certain malignancies and cancers.²³ Several reports have associated expression levels of chemokines such as CCL5 and CCL2 with pro-malignant activity of certain cancers.²⁴ CCL5 levels are correlated independently with clinical outcomes in stage II breast cancer, and thus is a diagnostic marker. Estrogen receptor α (ER- α) expression levels along with CCL5 levels are significant prognostic indicators in such cases.²⁵ Unregulated expression levels of CCL5 and surface expression of CCR5 has also been reported in many human prostate adenocarcinoma cells, *In vitro* studies on such cell lines have also revealed decreased tumor cell proliferation and invasion via receptor inhibition by CCR5 antagonists (TAK 779).²⁶ Various mechanisms have been advanced to explain the pro-cancer activity of CCR5 and related chemokines including stimulation of cell proliferation activity, pro-angiogenesis functions, increased metastasis and creation of immunologically privileged sites around cancer cells.²³

Several molecules have been reported to inhibit CCR5 function and they can be classified into four major classes – small molecules, modified peptides, N-terminal modified ligands (small molecule attached N-terminally to the peptide) and humanized monoclonal anti-CCR5 antibodies. The majority of small molecule CCR5 antagonists have been identified following high-throughput screening and subsequent optimization.²⁷ TAK-779 was the first reported small molecule antagonist. However, it suffered from toxicity and low bioavailability issues. SCH-C was first CCR5 antagonist to advance to clinical efficacy studies. In this case, the potential cardiac side effects due prolonging of QTc interval in cardiac cells caused early termination of the studies. Further optimization of the compound led to vicriviroc that showed greater selectivity towards the CCR5 receptor over muscarinic and hERG, thus reducing the potential of cardiac side effects. Aplaviroc was another potential candidate, but its clinical trials were discontinued because of increased occurrence of idiosyncratic hepatotoxicity. Maraviroc has been the only successful FDA approved CCR5 targeting drug for HIV-1 infected patients. It showed better pharmacokinetic and pharmacodynamic profile with sustained reduction in viral load owing to its prolonged receptor occupancy ($t_{1/2} > 5$ days).

Anibamine, an alkaloid isolated from *Aniba panurensis*, was identified as a CCR5 antagonist with micromolar level inhibition of HIV-1 gp120 binding. Anibamine has also been shown to inhibit prostate cancer cell proliferation, adhesion and invasion. Anibamine provides a novel structural skeleton that can be further embellished to improve its CCR5 binding and antagonist activity. Our lab has recently published the total synthesis of anibamine and several ligands of this class with varying degree of antagonistic activity against CCR5. However, development of the anibamine analogs required guidance on the probable interactions involved

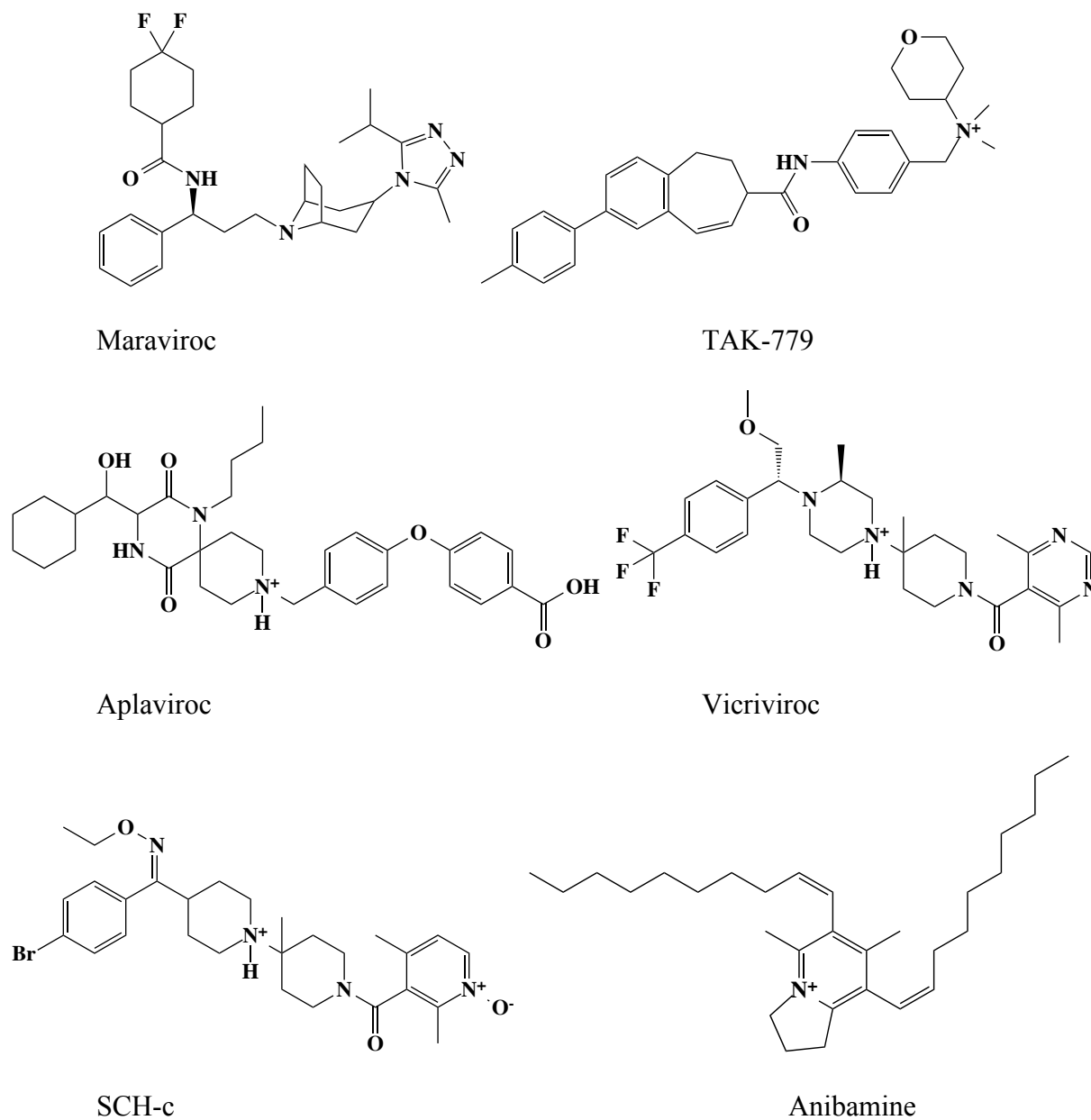


Figure 2.2. CCR5 antagonists

between the receptor and the ligand. The non-availability of a crystal structure for CCR5 hindered the process. The purpose of this project was to develop a usable CCR5 protein homology model, including the identification and validation of the small molecule binding

pocket through computational methods with a goal of helping the development of effective anibamine cognate ligands.

2.2 Methods and Results

2.2.1 Homology Modeling of CCR5

Homology modeling relies on the similarity between the amino acid sequence of the “target” protein and an experimentally determined three-dimensional structure of a homologous “template” protein. At the time of this project, only five types of GPCR crystal structure had been resolved – bovine rhodopsin²⁸, turkey β_2 adrenergic receptor²⁹, human β_1 adrenergic receptor³⁰, human adenosine A_{2A} receptor³¹ and human CXCR4 chemokine receptor³². The amino acid sequences of the above receptors along with the target CCR5 protein were retrieved from the UniProtKB server.³³ A PSI-BLAST search (protein-protein BLAST) was performed with default settings on the amino acid sequences for template identification. Expectedly, the closely related C-X-C Chemokine receptor type 4 showed highest level of identity (34%) and similarity (56%). Additionally, cysteine residues responsible for disulfide bonding between extracellular loop (ECL) 2 and the top of transmembrane helix 3, and between the top of helix 1 and ECL3 were conserved and aligned. The alignment was further refined using CLUSTALX2 with default settings. And the additional modifications were done manually.³⁴ (Figure 2.3)

The small molecule ligand bound crystal structure of C-X-C Chemokine receptor type 4, retrieved from RCSB database (PDB ID – 3ODU)³², was chosen as the template among other available CXCR4 structures. The comparative modeling program MODELLER 9v7³⁵ was employed to generate a total of 100 models using the *automodel* class, where models are built

while violating minimum restraints obtained from the template protein structure. The best model was selected on the basis of the inbuilt scoring functions of MODELLER (MOLPDF, DOPE, GA341), as well as its ability to accommodate the known ligand of CCR5 (maraviroc) inside its orthosteric ligand-binding site. Ramachandran analysis of the selected model, using the online server MOLPROBIDITY³⁶, showed 96.9% residues in favored regions and 99.3% residues in allowed regions, with only two residues outside the allowed region and those were present at a fairly large distance from the putative ligand binding pocket. (Figure 2.4)

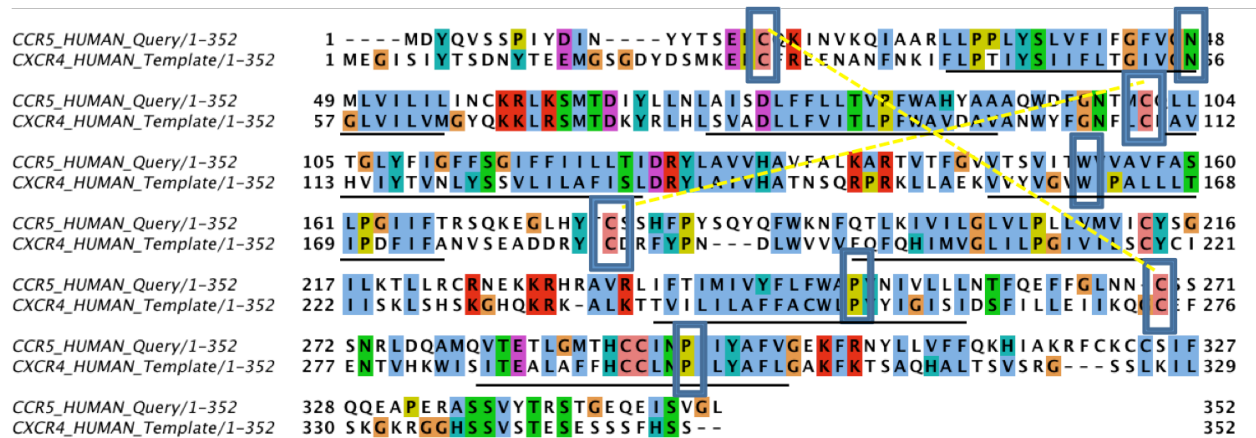


Figure 2.3. Sequence alignment of CCR5 (target) and CXCR4 (template). Disulfide bond between cysteines shown in yellow dashed lines

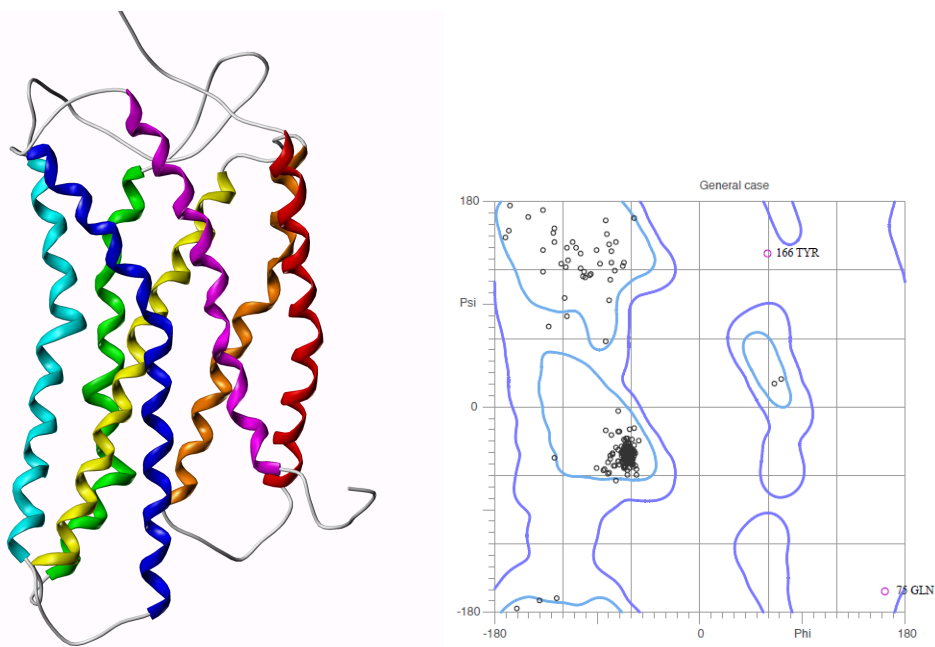


Figure 2.4. A. Representation of best-selected model **B.** Ramachandran plot of the model

2.2.2 Ligand Sketching

The molecular structures of the ligands (maraviroc, SCHc, TAK779, aplaviroc, vicriviroc and anibamine) were sketched in Sybyl 8.1, and Gasteiger-Hückel charges were assigned before energy minimization (10,000 iterations) under the TRIPOS force field (TFF).

2.2.3 Ligand Docking and binding site validation

GOLD 5.1, an automated genetic algorithm based docking program, was used to perform the docking studies with standard default settings unless specified otherwise.³⁷ The binding site on the optimized CCR5 receptor model was defined to include all atoms within 10 Å of the carboxylate carbon atom of Glu283, and a distance constraint of 5 Å was defined between the quaternary nitrogen atom of the ligands and the carboxylate oxygen of the Glu283 side chain.

Based on the fitness scores (GOLD score) the best 50 GOLD-docked solutions were selected and merged onto the receptor model. The interactions between ligand and receptor within the binding pocket were optimized; clashes and strain energies were removed by energy minimizing the combined receptor-ligand structures (1000 iterations under Tripos force field). These optimized models were then subjected to hydrophobic analysis with the HINT program.³⁸ The obtained ligand binding pocket was validated using site directed mutagenesis studies retrieved from the literature.³⁹ (Table 2.1) The orthosteric site of CXCR4 is more spacious and wider than most of the other GPCRs crystallized up to that time. This structural characteristic of the template was also transferred to the CCR5 model. The ligand binding site was effectively made up of three large hydrophobic sites – the inter-helical region between transmembrane (TM) 3, TM5 and TM6 at the bottom of the pocket, between TM3 and TM5, and close to TM2. (Figure 2.5)

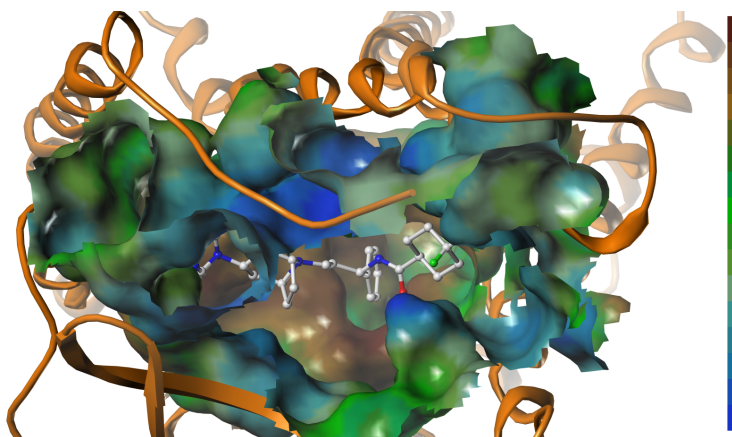


Figure 2.5. Predominantly hydrophobic ligand binding pocket of CCR5 homology model with hydrophobic gradient scale, brown (hydrophobic) and blue (hydrophilic).

Table 2.1. Fold differences of amino acid mutation on inhibition of fusion with viral gp120 (from reference 39)

Location	Mutant	Maraviroc	Aplaviroc	SCH-C	Vicriviroc	TAK779
N-ter	K26A	0.5	6.6	1.5	2.0	1.3
TM1	L33A	0.2	1.7	28	22	32
TM1	Y37A	1.7	0.6	208	395	273
	Y37F	2.5	0.4	0.3	0.5	16
TM2	F79A	7.1	21	27	192	8.3
TM2	W86A	83	477	1367	1205	378
TM3	T105A	1.1	8.9	17	2.9	0.4
TM3	Y108A	207	16	60	51	146
	Y108F	51	22	9.2	46	111
TM3	F109A	0.6	2620	1.9	27	7.0
TM3	F113A	0.2	8.8	1.3	9.8	0.7
ECL2	K191A	3.4	6.3	8.9	2.0	3.7
TM5	I198A	256	110	75	83	0.6
TM5	Y251A	69	0.2	0.3	3.3	4.4
	Y251F	28	1.9	0.2	0.4	0.1
TM7	E283A	11118	1273	2077	12109	5.5
TM7	T284A	5.7	4.2	0.9	0.9	39

i) Maraviroc binding pose

The majority of the docking solutions for maraviroc showed interactions with similar residues. However, based on the internal ligand conformation, two clusters of docking poses were obtained. In both of the poses, the isopropyl triazole ring had hydrophobic interactions with Trp86 and Tyr89 (pocket 1); however, the position of the difloro cyclohexyl and the phenyl ring switched. In first pose, the cyclohexyl ring resided in the hydrophobic pocket formed by Ile198, Phe109, Phe112, Trp248 and Phe251 (pocket 2), and the phenyl ring had hydrophobic

interactions with the alkyl part of Lys191 (pocket 3). In this pose the quaternary nitrogen was involved in interactions with Glu283 and Tyr251. (Figure 2.6A)

As indicated earlier, in the second docking pose of maraviroc the phenyl ring of the ligand showed interactions with the hydrophobic residues of pocket 2 and the cyclohexyl ring showed interactions with the hydrophobic residues of pocket 3. This pose also had interactions between Glu283 and the quaternary nitrogen, a shift in the position of Tyr251 was observed that allowed hydrogen-bonding interactions between the hydroxyl of Tyr251 and the amide nitrogen of the ligand. (Figure 2.6B) Overall, both docking poses had general agreement with the site-directed mutagenesis results.

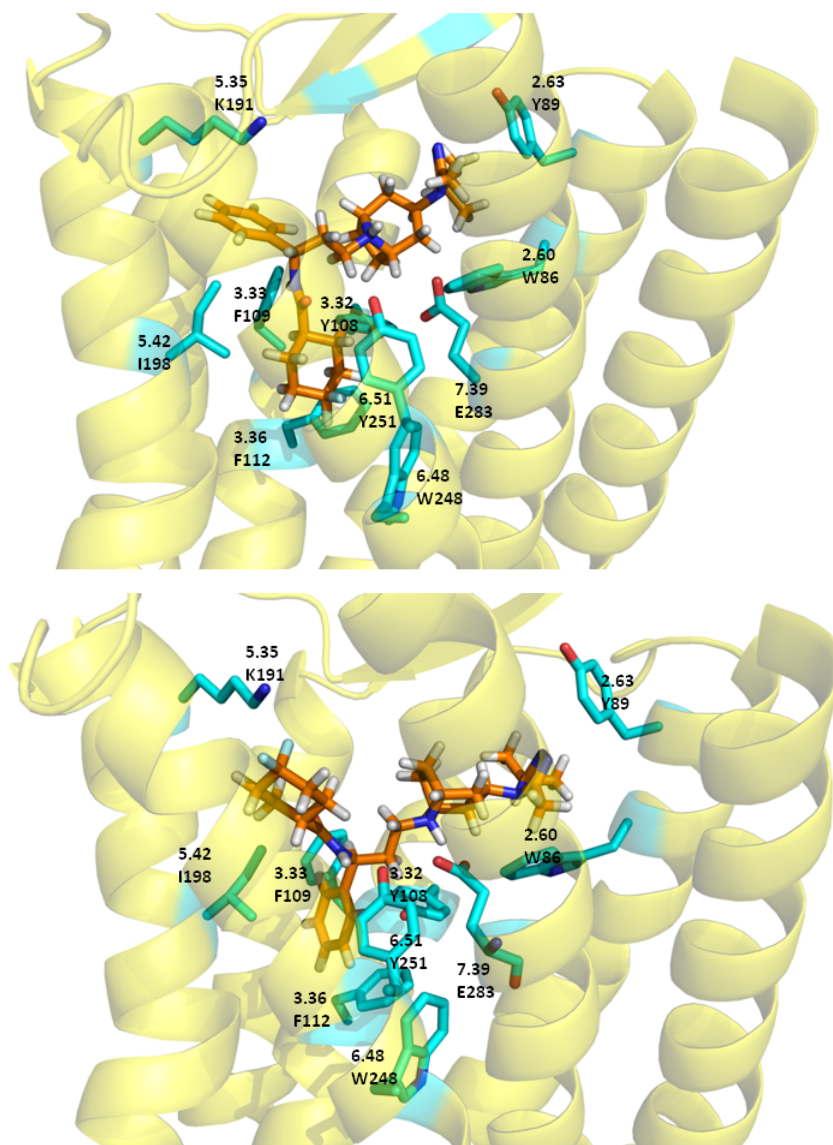


Figure 2.6. Docking poses of maraviroc inside CCR5 homology model. A. Pose 1 (Goldscore = 61.04, HINT score = 444) B. Pose 2 (Goldscore = 60.26, HINT score = 431).

ii) Vicriviroc binding pose

Similar to maraviroc two docking poses were also observed for vicriviroc with interactions in similar regions but with different conformations of the ligand. Residues present in pocket 1 and

pocket 2 were seen to be involved in both the observed docking poses, along with the ionic interactions between the quaternary nitrogen of the ligand and carboxylate group of Glu283.

(Figure 2.7)

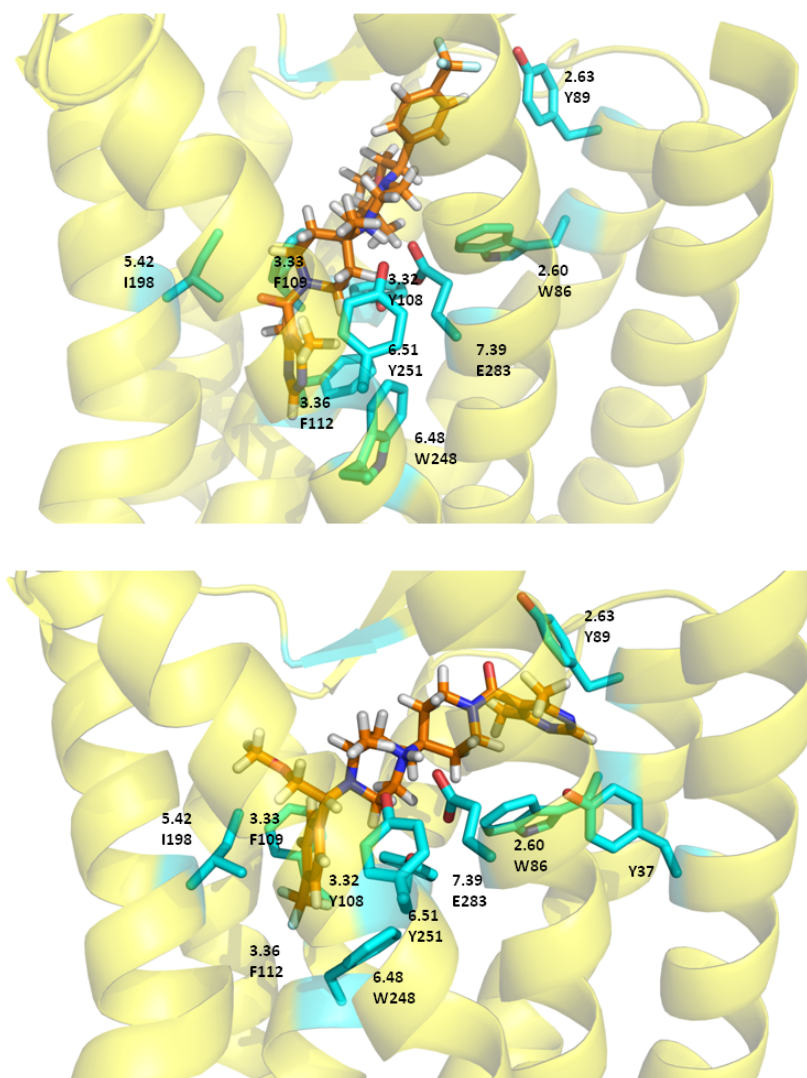


Figure 2.7. Docking poses of vicriviroc inside CCR5 homology model. A. Pose 1 (Goldscore = 58.92, HINT score = 701) B. Pose 2 (Goldscore = 51.70, HINT score = 736).

iii) *Aplaviroc binding pose*

Two poses were also observed for aplaviroc inside CCR5 homology model. Interactions, however, were primarily limited to pocket 2 and pocket 3. Apart from the ionic interactions between Glu283 and the quaternary nitrogen (observed in both poses), plausible hydrogen bonding interactions were also observed between the ligand and extracellular loop 2 (for pose 1) and Asn194 of TM5. (Figure 2.8)

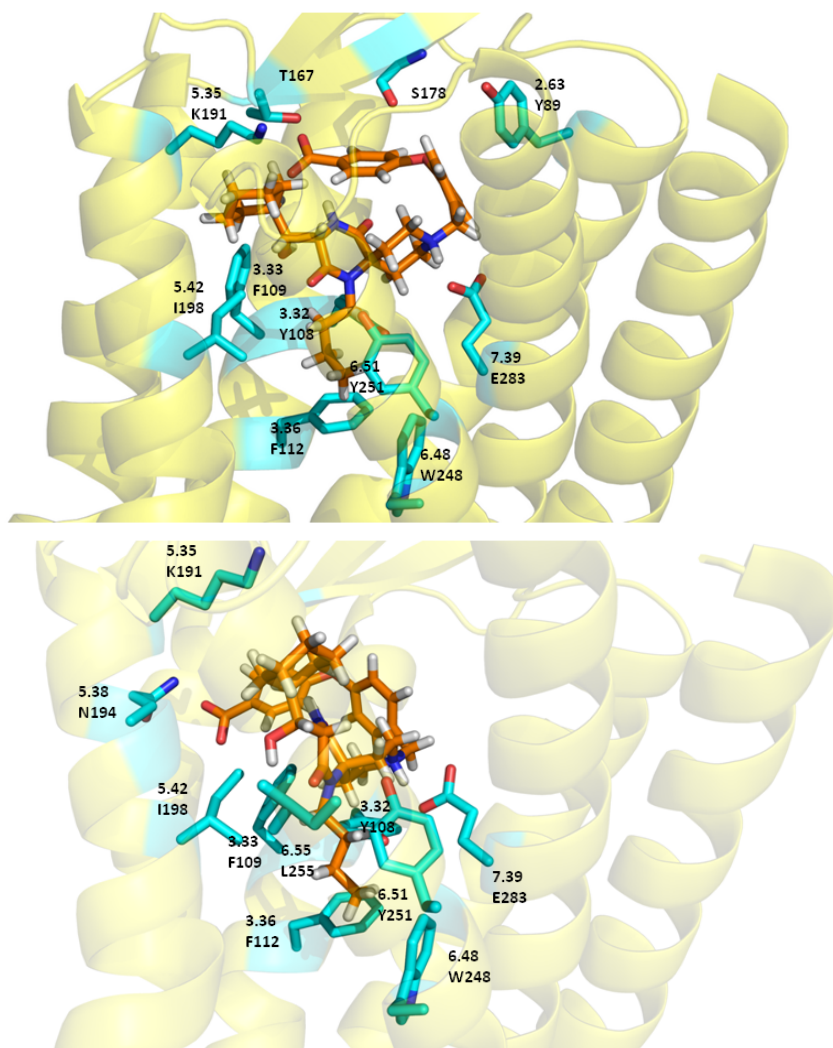


Figure 2.8. Docking poses of aplaviroc inside CCR5 homology model. A. Pose 1 (Goldscore = 49.07, HINT score = 1395) B. Pose 2 (Goldscore = 46.20, HINT score = 698).

iv) SCH-C binding pose

Pose 1 for SCH-C interactions were observed in pocket 1, 2 and 3, while for pose 2, interactions were observed in pocket 1 and 2. Interactions with the acidic glutamate residue and quaternary nitrogen atom of the ligand were observed in both the binding modes. (Figure 2.9)

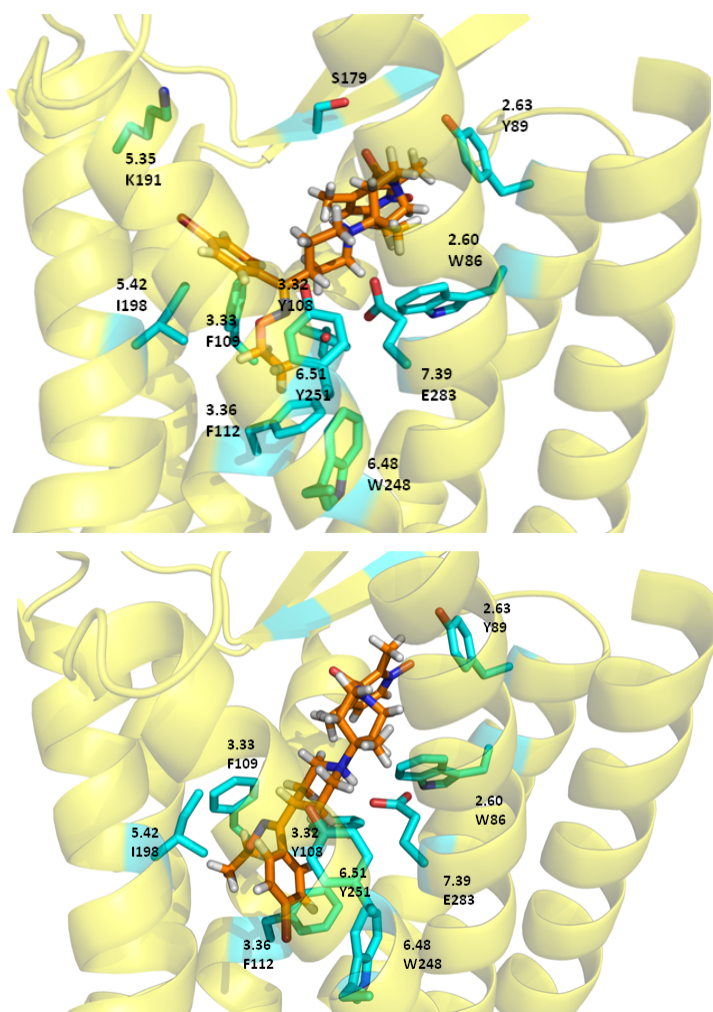


Figure 2.9. Docking poses of SCH-C inside CCR5 homology model. A. Pose 1 (Goldscore = 59.75, HINT score = 834) B. Pose 2 (Goldscore = 54.10, HINT score = 398).

v) *TAK-779 binding pose*

Only one dominant docking pose was observed for TAK779, and the major point of departure from the binding poses of the other docked ligands was greater than 5 Å distance between carboxylate group of Glu283 and the quaternary nitrogen, and between the amide nitrogen. (Figure 2.10) This suggests a limited effect of the Glu283 on TAK-779 binding, which is in agreement with the site-directed mutagenesis studies. While the effect of glutamate mutation to alanine at position 283 was remarkably high for other ligands (>2000 to > 12000), its effect on TAK-779 was limited to 5.5 fold. (Table 2.1)

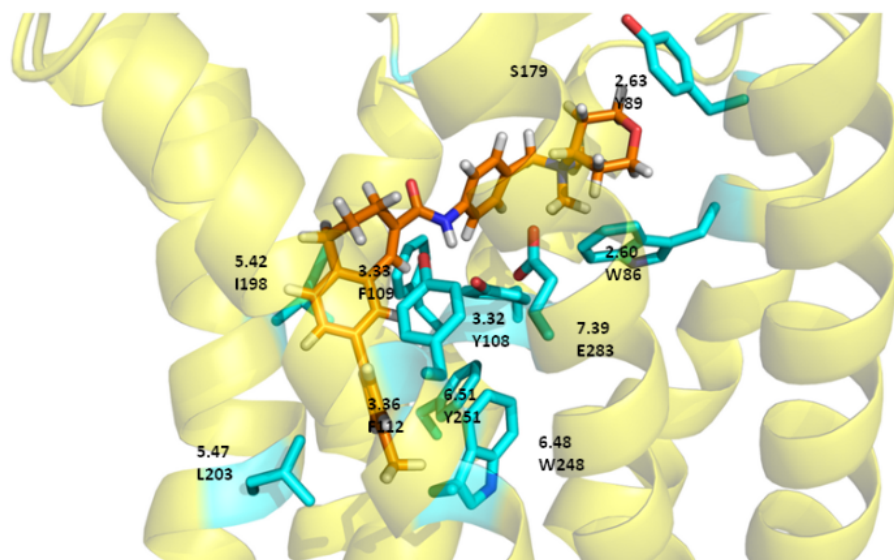


Figure 2.10. Docking poses of TAK-779 inside CCR5 homology model. Goldscore = 37.13, HINT score = 919.

The site-directed mutagenesis studies described above validated the binding modes of multiple ligands following automated docking and minimization of the ligand-receptor complexes. This, in turn, validates the orthosteric binding site of CCR5 modeled based on the CXCR4 template.

2.2.4 Docking modes of anibamine

The minimized structure of anibamine was then docked onto the validated homology model ligand binding pocket of CCR5, employing the same parameters as used for the earlier docked antagonists. In all the major docking poses the heterocyclic moiety of the anibamine was placed close to Glu283 due to the distance constraint, which allowed interaction between the quaternary nitrogen of the heterocyclic ring and the carboxylate oxygen of the Glu283 residue. However, the alkyl moiety adopted a varied number of conformations primarily because the open and spacious nature of the orthosteric binding pocket does not deter the highly flexible alkyl chain from exploring different conformations. (Figure 2.11) Analysis of the HINT scores revealed decreased hydrophobic interactions between the anibamine and the receptor residues. Moreover, high flexibility of the ligand is likely to result in less frequent and less tight interactions with the protein surface.

The results indicate that in designing a more active analogue, the anibamine side chains should be made less flexible, and the possible inclusion of aromatic moieties would also improve π - π interactions with the aromatic residues lining the CCR5 ligand binding pocket.

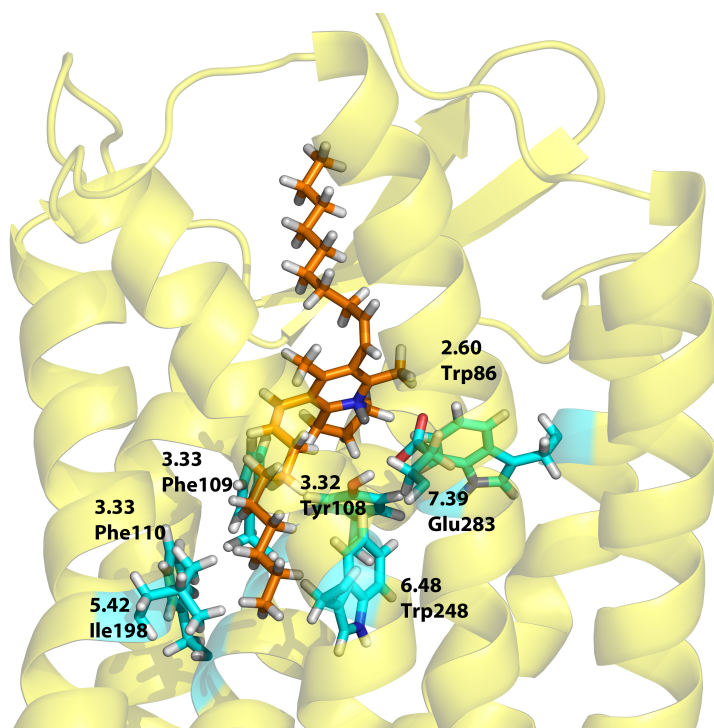
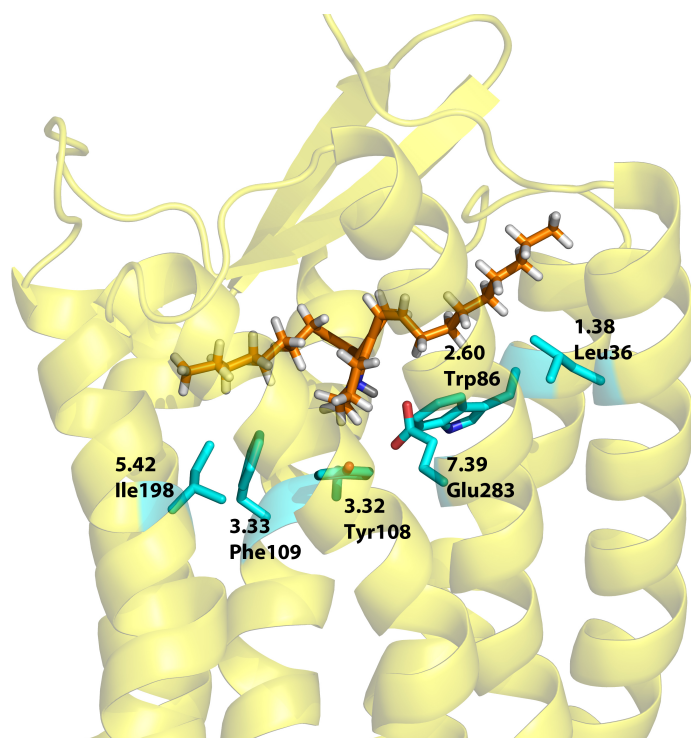


Figure 2.11. Docking poses of anibamine inside CCR5 homology model. A. Pose 1 (Goldscore = 39.55, HINT score = -448) B. Pose 2 (Goldscore = 35.02, HINT score = -334).

2.2.5 Generation of water sites inside the homology model

Water molecules can play a very significant role in directing the binding of a small molecule ligand. The water molecules often form hydrogen bonding bridges between the ligand and the protein, and thus contribute to the binding enthalpy. Waters, however, can also effect entropic change in the system. A protein-bound “ordered” water molecule along with the water network surrounding it may be displaced by an incoming ligand, thereby increasing disorder/entropy of the system and increasing the binding free energy. The recently elucidated 1.8 Å resolution crystal structures of the A_{2A} adenosine receptor and the delta opioid receptor indicate the presence of clusters of water molecules that may play a significant role in defining ligand binding and selectivity. However as of yet, the high degree of resolution required to resolve crystal waters has not been possible in the majority of GPCR crystal structures.

To explore the possible contribution of water molecules, a ‘water map’ inside the homology model of CCR5 was generated using the water Relevance program.⁴⁰ The water Relevance relies on two factors - Hydrophobic INTERactions (HINT), a non-Newtonian force field based on experimentally determined $\log P_{\text{Octanol/Water}}$, for calculation of interactions; and a Rank algorithm to assess potential hydrogen bonding ability. The Relevance of waters is then quantified as a probability score; waters with higher probability are assessed as ‘conserved’ or tightly bound to the protein and those with lower scores as defined as ‘non-conserved’ or less tightly bound.⁴⁰

In theory, a ‘conserved’ water molecule can only be displaced by an atom or group of atoms that can substitute for all the interactions the outgoing water molecule was involved in. If the conserved water molecule is present at the solvent accessible surface, it is often surrounded

by a ‘structured’ shell of water molecules. The displacement of the ‘conserved’ water would also disrupt the ‘structured’ shell of water molecules surrounding it, and hence provide the binding event with an entropic impetus. So, designing molecules with such water displacement effects can have significant improvement in the binding profiles of such ligands.

The water map for the docking site of the homology model was generated using Solvate feature of HINT/Sybyl 8.1 within 5 Å margin of the docking site and a grid resolution of 1 Å in 2 cycles (2*VDW atom size model, contact distance of 4.0 and VDW bump = 1.10). 29 water molecules were generated by the search and 29 waters-receptor model complex were then minimized for 1000 iterations. The 29 generated waters were then checked for degree of conservation using the water Relevance feature of HINT/Sybyl 8.1. The water molecules with relevance greater than 0.50 were defined as ‘conserved’. (Figure 2.12) (Table 2.2)

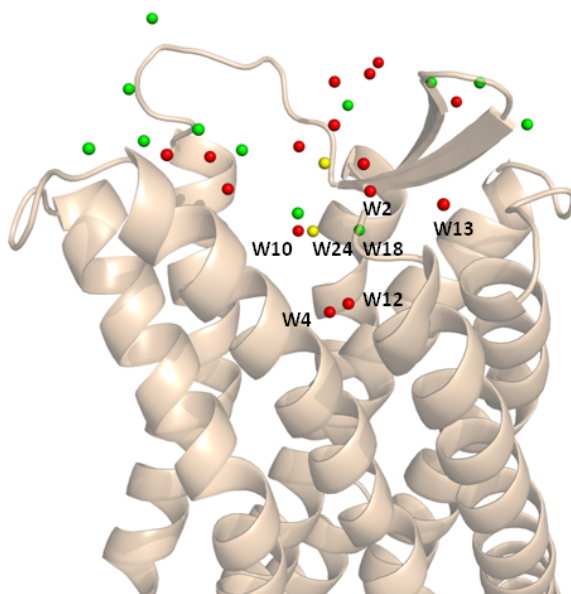


Figure 2.12. Generated water map with 29 waters in the ligand-binding pocket, Red (Conserved), Yellow (Conserved primarily due to inter-water contacts), Green (non-conserved). Waters found within 5 Å of docked ligand poses are labeled.

Table 2.2. Water Relevance scores for the generated waters.

Water name	Total			With CCR5			Inter-water		
	HINT Score	Rank	Relevance	HINT Score	Rank	Relevance	HINT Score	Rank	Relevance
Wat1	474	3.56	0.86	416	1.39	0.61	59	2.17	0.41
Wat2	259	5.27	0.92	188	2.78	0.64	72	2.48	0.46
Wat3	249	2.47	0.63	175	1.29	0.42	74	1.18	0.34
Wat4	600	2.18	0.80	600	2.18	0.80	0.1	0.00	-0.04
Wat5	692	3.63	0.93	592	1.33	0.67	100	2.30	0.47
Wat6	242	2.42	0.62	230	2.42	0.62	12	0.00	-0.04
Wat7	362	3.85	0.84	356	2.70	0.72	6	1.15	0.28
Wat8	320	4.12	0.85	349	2.872	0.74	-29	1.25	0.25
Wat9	235	2.37	0.61	235	2.37	0.61	1	0.00	-0.04
Wat10	196	2.39	0.59	57	1.20	0.32	139	1.19	0.38
Wat11	258	3.70	0.79	144	2.39	0.54	114	1.31	0.39
Wat12	352	2.14	0.67	357	2.15	0.67	-5	0.00	-0.04
Wat13	229	3.31	0.73	32	0.00	-0.04	197	3.31	0.73
Wat14	119	2.14	0.47	101	2.14	0.45	18	0.00	-0.04
Wat15	141	5.13	0.80	118	3.83	0.68	23	1.31	0.30
Wat16	5	1.02	0.25	4	1.02	0.26	1	0.00	-0.04
Wat17	192	2.17	0.56	190	1.27	0.41	2	0.91	0.24
Wat18	-91	1.01	0.17	-90	1.01	0.18	-1	0.00	-0.04
Wat19	-83	1.86	0.18	-76	1.86	0.20	-7	0.00	-0.04
Wat20	66	2.00	0.39	75	1.17	0.34	-10	0.84	0.21
Wat21	132	2.07	0.48	-44	0.00	-0.04	176	2.07	0.53
Wat22	183	2.16	0.55	144	2.16	0.51	38	0.00	-0.04
Wat23	123	2.10	0.47	95	2.10	0.44	28	0.00	-0.04
Wat24	221	2.33	0.60	-32	0.00	-0.04	254	2.33	0.62
Wat25	136	2.12	0.49	13	0.00	-0.04	124	2.12	0.48
Wat26	6	0.00	0.04	-21	0.00	-0.04	27	0.00	-0.04
Wat27	19	1.98	0.32	17	1.98	0.33	2	0.00	-0.04
Wat28	125	2.22	0.49	121	1.20	0.38	5	1.02	0.26
Wat29	110	0.99	0.32	-19	0.00	-0.04	128	0.99	0.33

To explore the possible roles of waters in ligand binding, the docking modes of the previously docked ligands were superimposed on the generated water map. Five possible water mediated interactions scenarios were observed – a) the conserved waters may act as bridge between the ligand and the protein, b) the conserved waters may get displaced once the ligand binds, c) the conserved waters may not form a bridge, also need not be displaced, d) the non-conserved waters may get displaced, e) the non-conserved waters may form a bridge once the ligand binds. (Figure 2.13, 2.14 and 2.15)

Waters 4 and 12 were conserved waters mapped close to Glu283 residue. The site-directed mutagenesis studies have indicated that Glu283 is critical for binding, and it is considered to bind to the quaternary amine moiety present in most of the high affinity allosteric inhibitors of CCR5. Point mutation at this residue results in 1,000 to 10,000- fold decrease in the fusion inhibition of viral gp120 for most of the ligands, except for TAK779 where the inhibition drop is less than 10-fold. According to our model, both Waters 4 and 12, or at least one of these, are displaced during the receptor binding of the ligands. However in the case of TAK779, these waters may not be displaced, and may act as a bridge. This suggests that binding of the allosteric inhibitors of CCR5 may be entropy driven due to displacement of the conserved highly ordered waters molecules along with their associated water network.

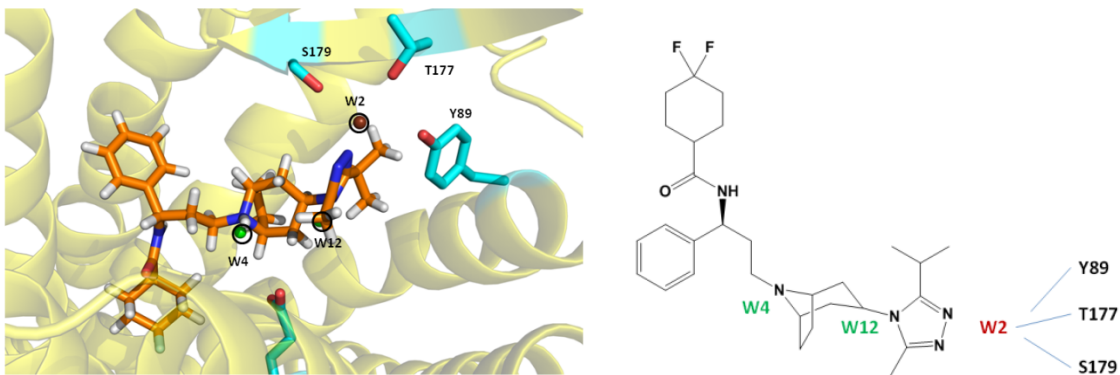


Figure 2.13. First docking mode of maraviroc with superimposed interacting waters. W4 and W12 (green) conserved but displaced, W2 (brown) conserved and bridges ligand and residues S179, T177 and Y89, Solvent accounting scores for W2, for protein 246 and for ligand -36.

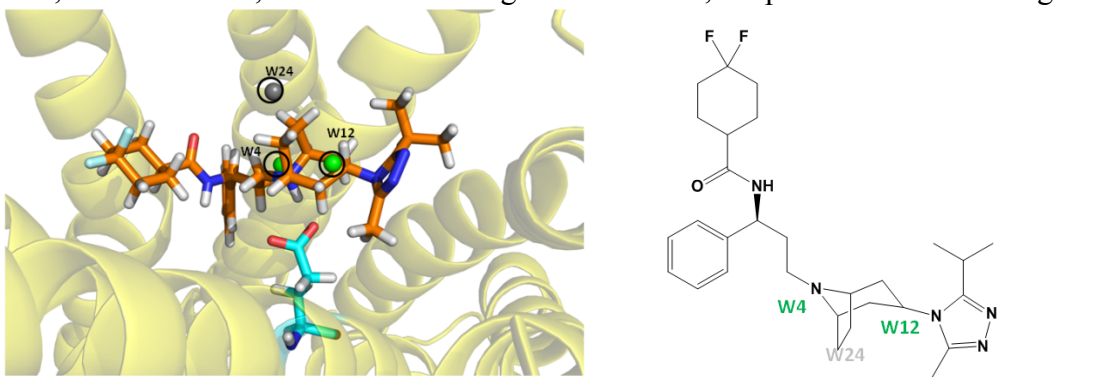


Figure 2.13. Second docking mode of maraviroc with superimposed interacting waters. W4 and W12 (green) conserved but displaced, W24 (grey) non-conserved and displaced.

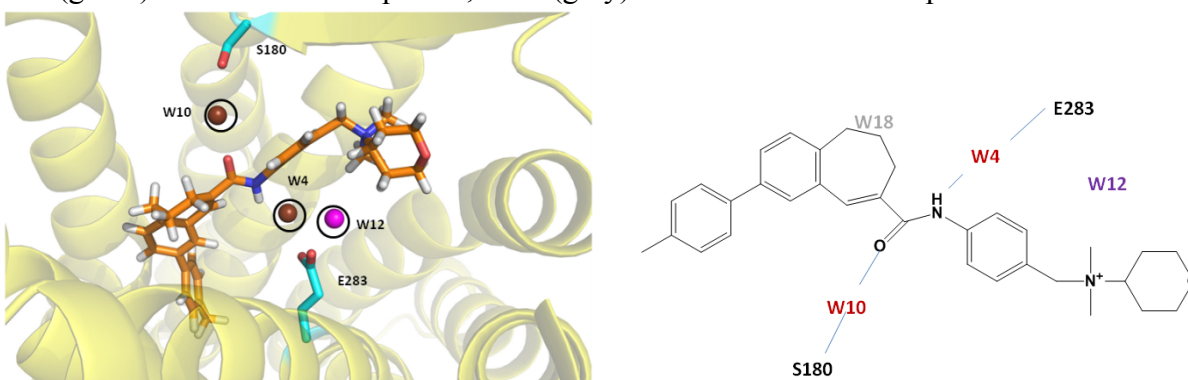


Figure 2.14 Docking mode of TAK779 with superimposed interacting waters. W4 and W10 (brown) conserved and bridges ligand and the protein, W12 (magenta) conserved and close but not displaced, W18(grey) non-conserved and displaced. Solvent accounting scores for W4, for protein 489, for ligand -63; W10 for protein 92, for ligand 32; W12 for protein 339, for ligand -92

2.3 Discussion

The homology model of CCR5 was built using the closely related CXCR4 template. The ligand binding pocket of the homology model was then validated by analyzing the obtained docking poses for known the CCR5 antagonists against the site-directed mutagenesis studies available in the literature. This validation, in turn, also validates the scoring function used in the docking studies. Anibamine (the lead compound) was docked in the validated docking site of the homology model. Comparison of binding modes of anibamine with binding modes of other antagonists suggested that incorporation of constrained hydrophobic moieties to the heterocyclic skeleton would be beneficial for the receptor binding. Based on this model, second generation of anibamine analogs with the amine linked aromatic substituents of the heterocyclic skeleton were synthesized. Third generation of anibamine analogs with further substitutions on the aromatic substituents are now being tested (the homology model of this chapter has been superseded by the elucidation of the crystal structure of CCR5⁴¹). However, the process described here provides a good template for receptor based design in the absence of protein structure.

Furthermore, the possible roles of the structural water molecules in the binding site were also explored. Our modeling studies suggest that the remarkable effect of Glu283 on the ligand binding of CCR5 antagonists could be entropically driven due to the displacement of highly ordered waters molecules along with disruption of their associated water network. Possible hydrogen bonding bridges formed by waters were identified for both conserved and non-conserved waters. Although HINT scores for interactions between ligand and the waters were not high, the presence of potential hydrogen bonding groups cannot be neglected. The potential roles that waters may play in protein-ligand interactions are often overlooked, particularly for GPCRs.

We suggest that protein binding pockets can be mapped for water molecules using HINT and the water Relevance programs, that the generated positions and degree of conservation of water molecules can help in identifying the possible roles that water, both enthalpic and entropic, may play in protein-ligand binding.

Reference:

- (1) Fredriksson, R.; Lagerström, M. C.; Lundin, L.-G.; Schiöth, H. B. The G-Protein-Coupled Receptors in the Human Genome Form Five Main Families. Phylogenetic Analysis, Paralogon Groups, and Fingerprints. *Mol. Pharmacol.* **2003**, *63*, 1256–1272.
- (2) Katritch, V.; Cherezov, V.; Stevens, R. C. Structure-Function of the G Protein-Coupled Receptor Superfamily. *Annu. Rev. Pharmacol. Toxicol.* **2013**, *53*, 531–556.
- (3) Allen, S. J.; Crown, S. E.; Handel, T. M. Chemokine: Receptor Structure, Interactions, and Antagonism. *Annu. Rev. Immunol.* **2007**, *25*, 787–820.
- (4) Choi, W. T.; An, J. Biology and Clinical Relevance of Chemokines and Chemokine Receptors CXCR4 and CCR5 in Human Diseases. *Exp. Biol. Med.* **2011**, *236*, 637–647.
- (5) Gerard, C.; Rollins, B. J. Chemokines and Disease. *Nat. Immunol.* **2001**, *2*, 108–115.
- (6) Berger, E. A.; Murphy, P. M.; Farber, J. M. Chemokine Receptors as HIV-1 Coreceptors: Roles in Viral Entry, Tropism, and Disease. *Annu. Rev. Immunol.* **1999**, *17*, 657–700.
- (7) Berger E. A. HIV entry and tropism: the chemokine receptor connection. *AIDS* 1997, S3–S16.
- (8) Miedema, F.; Meyaard, L.; Koot, M.; Klein, M. R.; Roos, M. T. L.; Groenink, M.; Fouchier, R. A. M.; Van't Wout, A. B.; Tersmette, M.; Schellenkens, P. T. A.; Schuitemaker, H. Changing virus-host interactions in the course of HIV-1 infection. *Immunol. Rev.* **1994**, *140*, 35–72.
- (9) Feng, Y.; Broder, C. C.; Kennedy, P. E.; Berger, E. A. HIV-1 Entry Cofactor: Functional cDNA Cloning of a Seven-Transmembrane, G Protein-Coupled Receptor. *Science* **1996**, *272*, 872–877.
- (10) Cocchi, F.; Devico, A. L.; Garzino-demo, A.; Arya, S. K.; Gallo, R. C.; Lusso, P.; Cocchi, F.; Devico, A. L.; Garzino-demo, A.; Arya, S. K.; Gallo, R. C.; Lussot, P. Identification of RANTES, MIP-1 α , and MIP-1 the Major HIV-Suppressive Factors Produced by CD81 T Cells. *Science* **1995**, *270*, 1811–1815.
- (11) Deng, H.; Liu, R.; Ellmeier, W.; Choe, S.; Unutmaz, D.; Burkhart, M.; Di Marzio, P.; Marmon, S.; Sutton, R. E.; Hill, C. M.; Davis, C. B.; Peiper, S. C.; Schall, T. J.; Littman, D. R.; Landau, N. R. Identification of a major co-receptor for primary isolates of HIV-1. *Nature* **1996**, *381*, 661-666.
- (12) Dragic, T.; Litwin, V.; Allaway, G. P.; Martin, S. R.; Huang, Y.; Nagashima, K. A.; Cayan, C.; Maddon, P. J.; Koup, R. A.; Moore, J. P.; Paxton, W. A. HIV-1 entry into

- CD4⁺ cells is mediated by the chemokine receptor CC-CKR-5. *Nature* **1996**, *381*, 667-673.
- (13) Alkhatib, G.; Combadiere, C.; Broder, C. C.; Feng, Y.; Paul, E.; Murphy, P. M.; Berger, E. A. CC CKR5 : A RANTES, MIP-1 α , MIP-1 β Receptor HIV-1 as a Fusion Cofactor for Macrophage-Tropic HIV-1. *Science* **1996**, *272*, 1955–1958.
- (14) Choe, H.; Farzan, M.; Sun, Y.; Sullivan, N.; Rollins, B.; Ponath, P. D.; Wu, L.; Mackay, C. R.; LaRosa, G.; Newman, W.; Gerard, N.; Gerard, C.; Sodroski, J. The Beta-Chemokine Receptors CCR3 and CCR5 Facilitate Infection by Primary HIV-1 Isolates. *Cell* **1996**, *85*, 1135–1148.
- (15) Doranz, B. J.; Rucker, J.; Yi, Y.; Smyth, R. J.; Samson, M.; Peiper, S. C.; Parmentier, M.; Collman, R. G.; Doms, R. W. A Dual-Tropic Primary HIV-1 Isolate That Uses Fusin and the Beta-Chemokine Receptors CKR-5, CKR-3, and CKR-2b as Fusion Cofactors. *Cell* **1996**, *85*, 1149–1158.
- (16) Liu, R.; Paxton, W. A.; Choe, S.; Ceradini, D.; Martin, S. R.; Horuk, R.; MacDonald, M. E.; Stuhlmann, H.; Koup, R. A.; Landau, N. R. Homozygous Defect in HIV-1 Coreceptor Accounts for Resistance of Some Multiply-Exposed Individuals to HIV-1 Infection. *Cell* **1996**, *86*, 367–377.
- (17) Samson, M.; Libert, F.; Doranz, B. J.; Rucker, J.; Liesnard, C.; Farber, C.; Saragosti, S.; Lapoum roulie, C.; Cognaux, J.; Forceille, C.; Muyldermans, G.; Verhofstede, C.; Burtonboy, G.; Georges, M.; Imai, T.; Rana, S.; Yi, Y.; Smyth, R. J.; Collman, R. G.; Doms, R. W.; Vassart, G.; Parmentier, M. Resistance to HIV-1 infection in Caucasian individuals bearing mutant alleles of the CCR-5 chemokine receptor gene. *Nature* **1996**, *382*, 722-725.
- (18) Dean, M.; Carrington, M.; Winkler, C.; Huttley, G. A.; Michael, W.; Allikmets, R.; Goedert, J. J.; Buchbinder, S. P.; Vittinghoff, E.; Donfield, S.; Vlahov, D.; Kaslow, R.; Saah, A.; Rinaldo, C.; Detels, R.; O'Brien, S. J. Genetic Restriction of HIV-1 Infection and Progression to AIDS by a Deletion Allele of the CKR5 Structural Gene. *Science* **1996**, *273*, 1856-1862.
- (19) Zimmerman, P. A.; Buckler-White, A.; Alkhatib, G.; Spalding, T.; Kubofcik, J.; Combadiere, C.; Weissman, D.; Cohen, O.; Rubbert, A.; Lam, G.; Vaccarezza, M.; Kennedy, P. E.; Kumaraswami, V.; Giorgi, J. V.; Detels, R.; Hunter, J.; Chopek, M.; Berger, E. A.; Fauci, A. S.; Nutman, T. B.; Murphy, P. M. Inherited Resistance to HIV-1 Conferred by an Inactivating Mutation in CC Chemokine Receptor 5: Studies in Populations with Contrasting Clinical Phenotypes, Defined Racial Background, and Quantified Risk. *Mol. Med.* **1997**, *3*, 23–36.

- (20) Connor, R. I.; Paxton, W. A.; Sheridan, K. E.; Koup, R. A. Macrophages and CD4 + T Lymphocytes from Two Multiply exposed, uninfected individuals resist infection with primary non-syncytium-inducing isolates of Human Immunodeficiency Virus Type 1. *J. Virol.* **1996**, *70*, 8758-8764.
- (21) Rana, S.; Besson, G.; Cook, D. G.; Rucker, J.; Smyth, R. J.; Yi, Y.; Guo, H. H.; Du, J. G.; Peiper, S. C.; Lavi, E.; Samson, M.; Libert, F.; Liesnard, C.; Vassart, G.; Doms, R. W.; Parmentier, M. Role of CCR5 in Infection of Primary Macrophages and Lymphocytes by Macrophage-Tropic Strains of Human Immunodeficiency Virus: Resistance to Patient-Derived and Prototype Isolates Resulting from the Delta ccr5 Mutation. *J. Virol.* **1997**, *71*, 3219-3227.
- (22) Paxton, W. A.; Martin, S. R.; Tse, D.; O'Brien, T. R.; Skurnick, J.; VanDevanter, N. L.; Padian, N.; Braun, J. F.; Kotler, D. P.; Wolinsky, S. M.; Koup, R. A. Relative resistance to HIV-1 infection of CD4 lymphocytes from persons who remain uninfected despite multiple high-risk sexual exposures. *Nature* **1996**, *2*, 412-417.
- (23) González-Martin, A.; Mira, E.; Mañes, S. CCR5 as a Potential Target in Cancer Therapy: Inhibition or Stimulation? *Anticancer. Agents Med. Chem.* **2012**, *12*, 1045–1057.
- (24) Soria, G.; Ben-Baruch, A. The Inflammatory Chemokines CCL2 and CCL5 in Breast Cancer. *Cancer Lett.* **2008**, *267*, 271–285.
- (25) Yaal-Hahoshen, N.; Shina, S.; Leider-Trejo, L.; Barnea, I.; Shabtai, E. L.; Azenshtein, E.; Greenberg, I.; Keydar, I.; Ben-Baruch, A. The Chemokine CCL5 as a Potential Prognostic Factor Predicting Disease Progression in Stage II Breast Cancer Patients. *Clin. Cancer Res.* **2006**, *12*, 4474–4480.
- (26) Vaday, G. G.; Peehl, D. M.; Kadam, P. a; Lawrence, D. M. Expression of CCL5 (RANTES) and CCR5 in Prostate Cancer. *Prostate* **2006**, *66*, 124–134.
- (27) Scholten, D. J.; Canals, M.; Maussang, D.; Roumen, L.; Smit, M. J.; Wijtmans, M.; de Graaf, C.; Vischer, H. F.; Leurs, R. Pharmacological Modulation of Chemokine Receptor Function. *Br. J. Pharmacol.* **2012**, *165*, 1617–1643.
- (28) Palczewski, K. Crystal Structure of Rhodopsin: A G Protein-Coupled Receptor. *Science* **2000**, *289*, 739–745.
- (29) Cherezov, V.; Rosenbaum, D. M.; Hanson, M. A.; Rasmussen, S. G. F.; Thian, F. S.; Kobilka, T. S.; Choi, H. J.; Kuhn, P.; Weis, W. I.; Kobilka, B. K.; Stevens, R. C. High-Resolution Crystal Structure of an Engineered Human beta2-Adrenergic G Protein-Coupled Receptor. *Science* **2007**, *318*, 1258–1265.

- (30) Warne, T.; Serrano-Vega, M. J.; Baker, J. G.; Moukhametzianov, R.; Edwards, P. C.; Henderson, R.; Leslie, A. G. W.; Tate, C. G.; Schertler, G. F. X. Structure of a beta1-Adrenergic G-Protein-Coupled Receptor. *Nature* **2008**, *454*, 486–491.
- (31) Jaakola, V.; Griffith, M. T.; Hanson, M. A.; Cherezov, V.; Chien, E. Y. T.; Lane, J. R.; Ijzerman, A. P.; Stevens, R. C. The 2.6 angstrom crystal structure of a human A_{2A} adenosine receptor bound to an antagonist. *Science* **2008**, *322*, 1211–1217.
- (32) Wu, B.; Chien, E. Y. T.; Mol, C. D.; Fenalti, G.; Liu, W.; Katritch, V.; Abagyan, R.; Brooun, A.; Wells, P.; Bi, F. C.; Hamel, D. J.; Kuhn, P.; Handel, T. M.; Cherezov, V.; Stevens, R. C. Structures of the CXCR4 Chemokine GPCR with Small-Molecule and Cyclic Peptide Antagonists. *Science* **2010**, *330*, 1066–1071.
- (33) Magrane, M.; Consortium, U. UniProt Knowledgebase: A Hub of Integrated Protein Data. *Database* **2011**, *2011*, bar009.
- (34) Larkin, M. A.; Blackshields, G.; Brown, N. P.; Chenna, R.; McGettigan, P. A.; McWilliam, H.; Valentin, F.; Wallace, I. M.; Wilm, A.; Lopez, R.; Thompson, J. D.; Gibson, T. J.; Higgins, D. G. Clustal W and Clustal X Version 2.0. *Bioinformatics* **2007**, *23*, 2947–2948.
- (35) Fiser, A.; Do, R. K.; Sali, A. Modeling of Loops in Protein Structures. *Protein Sci.* **2000**, *9*, 1753–1773.
- (36) Chen, V. B.; Arendall, W. B.; Headd, J. J.; Keedy, D. A.; Immormino, R. M.; Kapral, G. J.; Murray, L. W.; Richardson, J. S.; Richardson, D. C. MolProbity: All-Atom Structure Validation for Macromolecular Crystallography. *Acta Crystallogr. D. Biol. Crystallogr.* **2010**, *66*, 12–21.
- (37) Jones, G.; Willett, P.; Glen, R. C.; Leach, A. R.; Taylor, R. Development and Validation of a Genetic Algorithm for Flexible Docking. *J. Mol. Biol.* **1997**, *267*, 727–748.
- (38) Kellogg, G. E.; Abraham, D. J. Hydrophobicity: Is LogP(o/w) More than the Sum of Its Parts? *Eur. J. Med. Chem.* **2000**, *35*, 651–661.
- (39) Labrecque, J.; Metz, M.; Lau, G.; Darkes, M. C.; Wong, R. S. Y.; Bogucki, D.; Carpenter, B.; Chen, G.; Li, T.; Nan, S.; Schols, D.; Bridger, G. J.; Fricker, S. P.; Skerlj, R. T. HIV-1 Entry Inhibition by Small-Molecule CCR5 Antagonists: A Combined Molecular Modeling and Mutant Study Using a High-Throughput Assay. *Virology* **2011**, *413*, 231–243.
- (40) Fornabaio, M.; Spyraakis, F.; Mozzarelli, A.; Cozzini, P.; Abraham, D. J.; Kellogg, G. E. Simple, Intuitive Calculations of Free Energy of Binding for Protein-Ligand Complexes. 3. The Free Energy Contribution of Structural Water Molecules in HIV-1 Protease Complexes. *J. Med. Chem.* **2004**, *47*, 4507–4516.

- (41) Tan, Q.; Zhu, Y.; Li, J.; Chen, Z.; Han, G. W.; Kufareva, I.; Li, T.; Ma, L.; Fenalti, G.; Li, J.; Zhang, W.; Xie, X.; Yang, H.; Jiang, H.; Cherezov, V.; Liu, H.; Stevens, R. C.; Zhao, Q.; Wu, B. Structure of the CCR5 Chemokine Receptor-HIV Entry Inhibitor Maraviroc Complex. *Science* **2013**, *341*, 1387–1390.

CHAPTER 3

MODELING SELECTIVITY OF NALTREXONE DERIVED ANTAGONISTS FOR OPIOID RECEPTORS

3.1 Introduction

3.1.1 Early research in opioid receptor identification and characterization

Opium is one of the most ancient drugs and its use has been documented in several historical texts. The word opium comes a Greek word ‘opos’ meaning the juice, in reference to the latex that leaks out from immature poppy pods when incised. Its use in history has been medicinal for analgesia and relief in diarrhea, as well as cultural, for example as a euphoriant in rituals.¹ Initiation of modern research in the field can be traced back to 1806 when Sertürner first isolated the active constituent of opium and named it ‘morphine’ after the Greek god of dreams, Morpheus.^{2,3} Soon codeine was also isolated and with the advancement in surgical sciences in the late 1800s morphine and analogs were being used as analgesics and adjuncts to general anesthetics.¹ However, the increased abuse potential of these compounds was soon realized and efforts were made to develop safer opiates. One such attempt, in 1888, of a drug developed and marketed as more potent than morphine and with no abuse prospect was heroin.⁴ Significant developments have been made since then; however, efforts undertaken to develop compounds

with reduced abuse potential have met only limited success.

In 1942, nalorphine was synthesized and characterized as the first known opioid antagonist. It could reverse respiratory depression caused by morphine and precipitate opiate withdrawal syndrome in opiate addicts, although it did have some analgesic effect too.^{5,6} This was followed by development of several other compounds with a wide range of agonist, antagonist and mixed agonist-antagonist activities.¹ A number of animal studies revealed central nervous system (CNS) as the primary site of action of opiates, and with the advent of radioligand it was soon realized different ligands had different localization profile inside the CNS.⁷⁻⁹ This led to a speculation that more than one type of opioid receptors were present in the body and that these receptors were targets for the endogenous opiates.¹⁰

First evidence for such endogenous opiates came from a study where it was found that that brain extract contains factors that inhibit acetylcholine release in guinea pig ileum and that this inhibition is reversed by naloxone, an opioid antagonist. These factors were termed enkephalins and structural characterization revealed these factors to be pentapeptides: Tyr-Gly-Gly-Phe-Met (Met-enkephalin) and Tyr-Gly-Gly-Phe-Leu (Leu-enkephalin).^{11,12} Soon, other factors were also identified and grouped in under three major classes - enkephalin, dynorphin and β -endorphin.^{13,14} It is now known that a large majority of these endogenous ligands share the enkephalin sequence at N-terminus (either Met- or Leu-enkephalin), and are processed from their respective precursor peptides. Preproenkephalin and preprodynorphin yield a large number of peptides, many of which still remain pharmacologically uncharacterized. For a long time, β -endorphins were the only known endogenous opioid ligands that had a different precursor, β -lipotropin. However, recently newer peptides have been reported, endomorphin 1 and

endomorphin 2, whose precursors have not yet been identified, and also do not have characteristic enkephalin N-terminus.¹⁰

Simultaneous research was also directed towards identification of opioid receptors. Studies identified a peculiar property of cross-tolerance, where patients tolerant to an opioid were also tolerant towards a certain group of other opioids and that these could ameliorate drug withdrawal symptoms of each other. These studies were employed to determine two types of opioid receptors and were named after the drug used to identify them: μ (morphine) and κ (ketocyclazocine).¹⁵ The third type of receptor was identified in a study where enkephelins were found to be more effective than morphine in inhibiting contraction in vas deferens and this effect was not affected by naloxone treatment. These receptors were termed δ opioid (vas deferens).¹⁶

The localization of putative opioid receptors was studied by the shock titration technique where midbrain central gray and periventricular areas on rhesus monkeys were mapped for antinociceptive effect of morphine, and whether this nociception was reversed by naloxone.¹⁷ In further studies, analgesia produced by focal electrical stimulation of these regions were partially reversed by naloxone and other antagonists.¹⁸ Biochemical studies indicating sensitivity towards trypsin and chymotrypsin and insensitivity towards DNase, RNase, neuraminidase and phospholipase C, suggested the protein nature of the receptor. Further experiments indicating sensitivity towards detergents and phospholipase A, that releases fatty acids, suggested plasma membrane bound localization of the receptor.¹⁹

A breakthrough came in early 1990s when all three major types of opioid receptors, μ -, κ , and δ -were cloned. Sequence analysis of these cloned opioid receptors established that they belong to the super- family of G protein-coupled receptors (GPCR) and the sub-family of

rhodopsin receptors.²⁰⁻²² As with any other GPCR, they were found to have seven transmembrane α -helices connected via three extracellular and three intracellular domains. Analysis also revealed that these receptors shared about 60% identity, with the highest homology in the transmembrane region (73–76%) and at the intracellular region (86–100%), while greatest diversity in amino acid sequence was found at the N-terminus (9–10%), extracellular loop (14–72%), and the C-termini (14–20%).²³

3.1.2 Opioid Receptor Signaling

Early studies on opioid receptor pharmacology had shown that guanine nucleotides such as guanine triphosphate (GTP) modulate agonist binding. Opioid agonists were shown to stimulate GTPase activity²⁴ and to inhibit cyclic adenosine monophosphate (cAMP) production.²⁵ Cloning of the opioid receptors allowed detailed studies in understanding of the molecular mechanism of receptor dependent signaling pathways. Pertussis toxin sensitive G-protein, $G\alpha_i$, was demonstrated to be involved inhibition of cyclic adenosine mono phosphate (cAMP) production via opioid receptors.^{26,27}

Classical signal transduction of opioid receptor modulates potassium and calcium ion channels. After an agonist induces dissociation of $G\alpha_i$ from $G\beta\gamma$ subunit, $G\alpha_i$ interacts with the G-protein gated inward rectifying potassium channel, K_{ir3} and deactivates the channel. This leads to hyperpolarization and inhibition of tonic neural activity.²⁸⁻³⁰ This positive modulation of potassium concentration is accompanied by negative modulation of calcium concentration. The

dissociated G β subunit interacts with P/Q, N or L-type Ca²⁺ channel, reducing voltage activation of channel pore opening.^{31,32} (Figure 3.1)

These receptors are also capable of regulating the secondary messenger pathways. Agonist induced receptor activation is often concurrent to phosphorylation of the opioid receptor at C-termini or at intracellular loops where there are at least 15 serine, threonine or tyrosine residues available for phosphorylation.³³ G protein-coupled receptor kinases (GRK) 2/3 are primary kinases involved in opioid receptor phosphorylation.^{34,35} Phosphorylation of the opioid receptor is succeeded by β -arrestin 1/2 recruitment. Surface plasmon resonance (SPR), glutathione S-transferase pull down and immunoprecipitation methods have indicated C-termini of the receptor to be involved in β -arrestin recruitment.³⁶ β -arrestin recruitment is followed by desensitization, sequestration and internalization of the receptor. This phosphorylated arrestin bound opioid receptor complex is not entirely inactive, and recruits alternative signal transduction cascades including mitogen activating protein kinases (MAPKs) e.g. ERK1/2³⁷, c-Jun N-terminal kinase (JNK)³⁸, and p38MAPK³⁹. (Figure 3.1) MAPKs are known to be involved in cell differentiation, proliferation, apoptosis and transcription factor regulation. JNK pathway and p38MAPK are involved in inflammatory stress, cytokine activation and neuropathic pain.³⁶

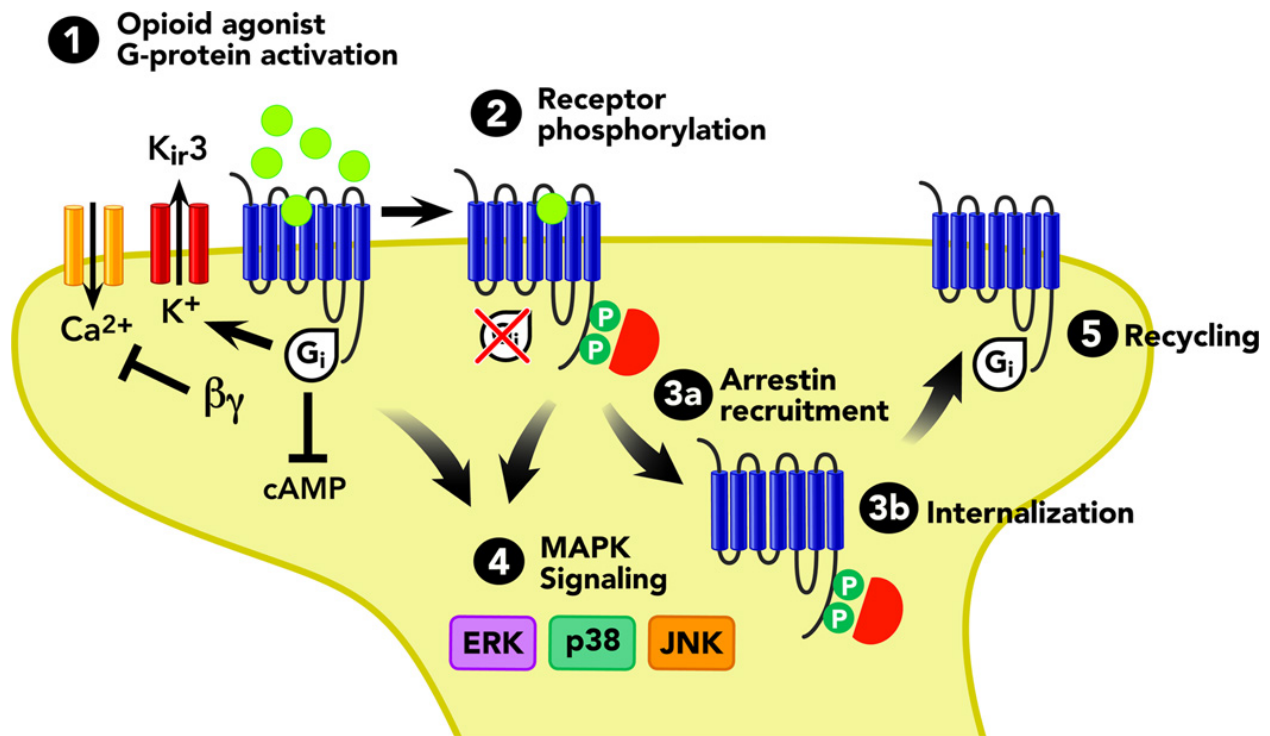


Figure 3.1. Summary of the GPCR signaling pathways. Reprint from reference 33.

3.1.3 μ -opioid receptor (MOR)

MOR is primarily found in the central nervous system either pre- or post-synaptically. Although MOR is distributed throughout the CNS, high densities are observed in the thalamus, striatum, interpeduncular complex, medial habenular nucleus, cortex, superior and inferior colliculi, and in the superficial layers of the spinal cord. MOR is also found in intestinal tracts. MOR is known to be responsible for supraspinal analgesia, respiratory depression, euphoria, sedation, decreased gastrointestinal motility, and physical dependence.³⁶ MOR knockout studies have shown that the primary effects of opioids, either beneficial or detrimental, are borne due to stimulation of MOR. Opioids interacting with MOR are often used for treatment for acute pain, cough, diarrhea and

acute pulmonary edema.⁴⁰ However, these opioids are also activate reward pathway and hence have a huge drug abuse liability. Some MOR agonists are also associated with rapid development of tolerance. Down regulation of opioid receptor due to sustained exposure to opioid agonist was suspected to cause drug tolerance.^{41,42} However, recent evidence suggests receptor desensitization and internalization due to β -arrestin recruitment may play a major role. Opioids associated with high tolerance and drug abuse potential, such as morphine, signal primarily through $G\alpha$ proteins, while compounds that induce receptor internalization after arrestin recruitment, e.g. DAMGO, show reduced tolerance.⁴³

Recently, a 2.8Å resolution X-ray crystal structure of *Mus musculus* MOR in complex with irreversible morphinan antagonist β -funaltrexamine (β FNA) employing T4-lysozyme fusion protein strategy was elucidated (PDBID-4DKL).⁴⁴ The overall architecture of MOR is similar to other previously crystallized GPCRs with proline related kinks in transmembrane (TM) α -helices. A disulphide bond connects two cysteines and thus links extracellular loop 2 (ECL2) and the top of transmembrane 3. ECL2 itself forms a hairpin loop. The ligand binding pocket of MOR, like those of chemokine receptors⁴⁵, is more solvent exposed than other crystallized GPCRs, such as β -adrenergic⁴⁶ and rhodopsin⁴⁷. The exposed nature of MOR ligand binding pocket is consistent with relatively shorter dissociation half lives of opioids compared to ligands interacting with more closed form of binding pockets seen in muscarinic receptor.⁴⁸ However, the ligand binding pocket of MOR is deeper much like that of the β -adrenergic receptors, compared to the shallow pockets in chemokine receptor. Ionic salt bridge 'lock' interactions, as seen in the rhodopsin crystal structure between the conserved DRY (aspartate-arginine-tyrosine) motif at the intracellular site of TM3 and the acidic residue of TM6 is not observed, because of

absence of acidic residue at this position. Instead, arginine of the DRY sequence interacts with the near-by aspartate on the same helix. The DRY aspartate also interacts with a basic arginine at intracellular loop 2 (ICL2), an interaction that is similar to what is observed in β_2 -adrenergic structure; however, in the adrenergic receptor this arginine of ICL2 is replaced by a serine. The crystal structures observed the formation of dimers tightly associated through TM5 and TM6 (buried surface area 1492 Å²) and to a lesser extent through TM1, TM2 and helix 8 (buried surface area 615 Å²).⁴⁴

3.1.4 κ -opioid receptor (KOR)

Kappa receptors are found primarily presynaptically in the limbic and other diencephalic areas, brain stem, spinal cord, and peripheral tissues. They are responsible for spinal analgesia, sedation, dyspnea, dependence, dysphoria, and respiratory depression. They are present in brain regions implicated in reward, cognitive function and stress responses such as ventral tegmental area, nucleus accumbens, prefrontal cortex, hippocampus, etc. KOR disruption is known to cause anti-stress effects. This is in agreement with reports correlating elevated levels of dynorphins under painful and stressful conditions. Thus, the KOR is a good target for conditions such as anxiety, depression, addiction and other stress induced conditions. The anti-stress effect of KOR is associated with C-Jun N-terminus (JNK) pathway, however some reports link the effect with p38MAPK activation.⁴⁹

The X-ray crystal structure of human KOR was also resolved using T4-lysozyme fusion protein with a resolution of 2.9Å and in complex with the KOR selective antagonist JD1c. (PDBID- 4DJH)⁵⁰ Not surprisingly, structure of KOR is similar to MOR with slight departures.

As in the MOR, KOR also lacks an acidic residue at the intracellular region of TM6 to form a ionic salt bridge interaction with TM3 DRY motif. However, KOR forms a hydrogen-bonding interaction with a threonine residue present on TM6, possibly stabilizing the antagonist form of the receptor. Two conformers were seen for ICL2, one with a two turn α -helix and another with a single turn α -helix. Compared to MOR and DOR, KOR has more acidic residues in the ECL2 region. This acidic entrance to the KOR binding pocket may reflect the basic nature of KOR selective dynorphins. A parallel and an anti-parallel (probably artifactual) form of receptor dimers were seen in the KOR crystal structure. The parallel dimer showed association between TM1, 2 and helix 8 with a buried surface area of 1100Å².⁵⁰

3.1.5 δ -Opioid receptor (DOR)

The distribution of DOR is limited to certain regions in CNS including olfactory bulbs, cortex, striatum and amygdala. DOR is also involved in transmission and integration of painful stimuli, peripheral nerve endings and regulation of mood.⁵¹ Compared to the other opioid receptors, DOR is a less explored receptor; however, DOR ligands are known to be involved in analgesia, anxiety, stress and addiction. DOR agonists are reported to increase expression of brain derived neurotropic factor, a factor also linked with some anti depressants.⁵² Recent reports have also indicated suppression of epileptical activity through inhibition of sodium channel.⁵³

The DOR structure is also similar to that of KOR and MOR, as demonstrated by 3.4Å resolution crystal structure of *Mus musculus* DOR in complex with naltrindole (4EJ4).⁵⁴ However, only an antiparallel form of dimers were observed. Recently a 1.8Å resolution structure of human DOR

was elucidated employing BRIL fusion protein (4N6H).⁵⁵ This high-resolution structure revealed an extensive water network surrounding the co-crystallized ligand (naltrindole) and TM7. More significantly a sodium site was observed close to the middle of TM2 and TM3. Use of the BRIL-complex attached to the N-terminus instead of the ICL3 incorporated T4-lysozyme allowed resolution of ICL3, which adopts a ‘closed structure’ that stabilizes the inactive form of receptor in absence of an ionic salt bridge.

3.1.6 Importance of MOR selective antagonists

Opioid antagonists have always been vital tools for characterization of opioid agonists. A ligand is considered as an opioid agonist only if its effects are completely inhibited by an antagonist. Furthermore, selective opioid antagonists have been employed to understand selectivity profiles of many agonists.^{56,57} This is especially important for MOR selective ligands since analgesic, addictive and other notorious properties of opioid agonists are primarily governed through the MOR. This is supported by many MOR knockout studies in mice where these effects were abolished in absence of MORs.⁵⁸⁻⁶⁰ There is an unmet need for a highly selective, nonpeptidyl, reversible and potent MOR antagonist that may help in understanding structure-functional relationships, agonist interactions and activation mechanisms of classical and secondary messenger pathways. However, the utility of a MOR selective antagonist is not limited to the pharmacological toolkit.

UN’s World Drug Report 2012 estimates global annual prevalence of illegal opiate use to be between 0.6 to 0.8%. These numbers are even higher in North America where non-medical use of prescription opioids have aggravated the problem to 3.8 to 4.2% of the adult population.⁶¹

Based on the MOR mechanism, the FDA has approved three drugs – methadone (agonist), buprenorphine (partial agonist) and naltrexone (antagonist) for treatment of long-term opioid dependence and addiction.^{62–64} Methadone and buprenorphine are given as part of morphine replacement therapy. Methadone, being an agonist, can cause fatal respiratory depression and its sudden cessation may precipitate withdrawal syndrome. The latter issue has caused abuse of methadone itself.^{62,65} A partial agonist, buprenorphine, shows similar side effects, albeit to a lesser extent.⁶⁶ The antagonistic action of naltrexone ensures curtailment of issues regarding respiratory depression and drug abuse liability. However, naltrexone is known to precipitate opioid withdrawal symptoms and hence decreases treatment adherence rate and beneficial therapeutic outcomes. Extended release naltrexone formulations have shown some improvement in this regard.^{67,68} The use of naltrexone, however, is still limited to patients with end-stage liver disease and patients requiring chronic pain management.⁶² Nonetheless, this does provide a proof of concept for using opioid antagonists for treatment of opiate addiction.

Alcoholism is another major prevalent substance abuse issue. It has been reported that 7 to 8% of Americans are affected by alcohol abuse, which amounts to a loss of about \$185 billion in U.S. health care costs, lost wages, bodily injury, and property damage annually.⁶⁹ In MOR knockout mice, where abolishment of opiate effects has been reported earlier, strongly diminished reinforcement effects of alcohol, cannabinoids and nicotine are seen.⁷⁰ MOR silencing is also known to effect maintenance of substance abuse, craving and relapse. Opioid antagonists, such as naltrexone and naloxone, are reported to curb abuse and treatment of alcoholism.^{71–76} However, patients on these antagonists have exhibited increased rates of suicides, depression and dysphoria.^{77–79} It is likely that these side effects are caused by the non-

selective nature of the ligands. Recently, nalfemene, an opioid antagonist was approved for “as needed” adjunctive treatment of alcoholism by the European Medicines Agency.⁸⁰ Also, β -funaltrexamine (β -FNA), an irreversible MOR antagonist, is reported to reduce fat intake in fat preferring mice.⁸¹

Several ligands have been developed as potential MOR selective antagonists, including irreversible antagonists such as β -FNA, clocinnamox and methocinnamox.⁸² However, clocinnamox and methocinnamox bind equally well with the three opioid receptors. β -FNA binds equally well with MOR and KOR, and also shows partial agonism towards KOR.⁸³ Covalent binding to the receptor of irreversible antagonists also limits their utility in pharmacological studies. Cyprodime is another extensively studied compound with moderate selectivity and potency towards MOR.^{84,85} Conformationally constrained peptides, such as D-Phe-Cys-Tyr-D-Trp-Orn-Thr-Pen-Thr-NH₂ (CTOP) and D-Phe-Cys-Tyr-D-Trp-Arg-Thr-Pen-Thr-NH₂ (CTAP), are some of the most selective and reversible compounds available.⁸⁶ However, they suffer from poor bioavailability and poor distribution across the blood-brain-barrier.⁸⁷

The ‘Message-Address’^{88,89} concept has been employed previously to design selective KOR (e.g. norBNI⁹⁰ and GNTI⁸⁴) and DOR antagonists (e.g. NTI⁹¹). According to this concept a part of the molecule is essential for activity (message), while additions or modifications can be made at another site (address) resulting in a changed protein recognition profile of the ligand. This is possible only if a receptor has a compatible access to the address part of the ligand. Based on the ‘message-address’ concept and ‘address sites’ identified on the opioid receptor homology models previously reported by our lab, two potential substitution sites on naltrexone were identified and a series of ‘addressed’ ligands were synthesized.^{92,93} The objective of the

following studies was to model the selectivity profile of those naltrexone derived ligands with such substitutions.

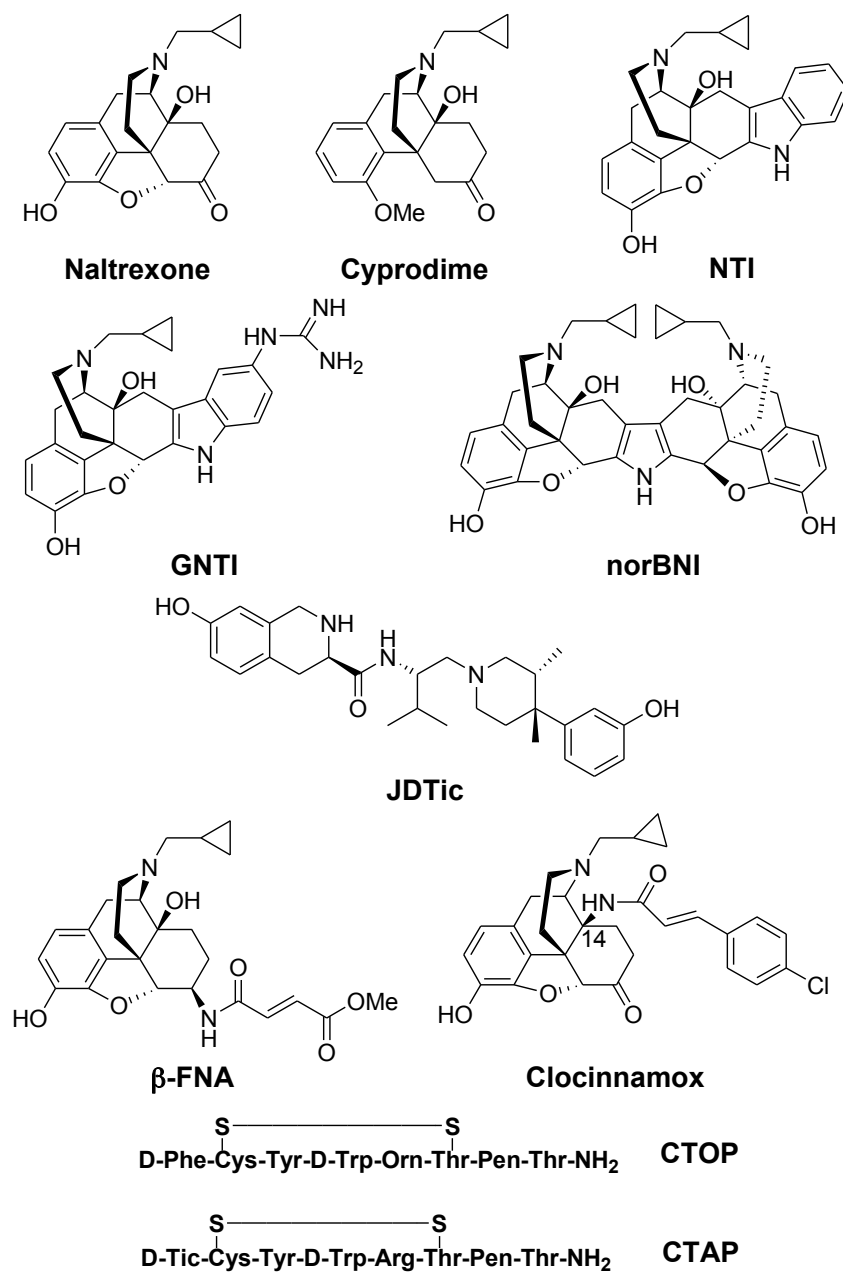


Figure 3.2. Opioid receptor selective antagonists.

3.2 Binding Mode Characterization of 6 α - and 6 β -*N*-Heterocyclic Substituted Naltrexamine Derivatives

3.2.1 Introduction

Naltrexone (NTX) is a universal opioid antagonist with a minimal ‘morphinan’ core and moderate selectivity towards the MOR. (Figure 2. A number of strategies for embellishing this core skeleton has provided KOR and DOR selective antagonists.^{84,90-91} The ‘morphinan’ skeleton can be regarded as the working part of the molecule that interacts with the receptor and conveys a ‘message’ for appropriate receptor response. The embellishments help to distinguish between the receptors and ensure that the ‘message’ is ‘addressed’ accurately. In light of this ‘message-address’ concept, a computational research strategy was devised previously in our lab. Homology models of opioid receptors were built using rhodopsin template and the resulting homology models were subjected to molecular dynamic (MD) simulations to optimize the conformation of the model. Naltrexone, a universal opioid antagonist, was then docked unto the homology models of MOR, KOR and DOR. A comparison of the naltrexone binding pockets inside the MOR, the KOR and the DOR homology models was made following MD simulations for optimization of the binding interactions. The protonated amine moiety of naltrexone was directed towards the conserved acidic aspartate residue inside all the three opioid homology models; however, contrasts were observed in the region towards which the carbonyl group at the position C(6) was directed. (Figure 3.4) In the MOR-naltrexone model, the carbonyl group was directed towards the aromatic residues in extracellular loop 2 (Tyr210 and Phe221) and TM7 (Trp318). In the DOR-naltrexone model, no such aromatic residues were observed in the vicinity of C(6) carbonyl group. In the KOR-naltrexone model, the aromatic binding locus was seen in

extracellular loop 2; however in this binding locus only one residue capable of donating hydrogen for hydrogen bond interactions was observed (Tyr), which is one less than that observed in the case of MOR-naltrexone model (Tyr and Trp). Therefore, it was postulated that the region close to the top of TM7 and ECL2 in MOR, inhabited by Trp318 and Tyr210, could be regarded as a plausible ‘address’ site on the MOR. To this effect, a series of amine-linked 6(C)-substituted naltrexone derivatives were synthesized, with substitutions that can possibly differentiate between the MOR and the DOR models (incorporation of aromatic group) and between the MOR and the KOR models (incorporation of a hydrogen bond acceptor in the aromatic group). To study the effect chirality at the 6(C) position may have, both α and β configurations were synthesized and studied *in vitro* radioligand binding assays and $[S^{15}]GTP\gamma S$ binding functional assays. Of all the compounds tested NAP and NAQ showed optimal selectivity and least partial agonism with respect to DAMGO (a MOR selective agonist). (Table 3.1 and 3.2) These compounds also exhibited antinociception activity by blocking the effect of morphine in mouse tail immersion tests. (Figure 2.5)

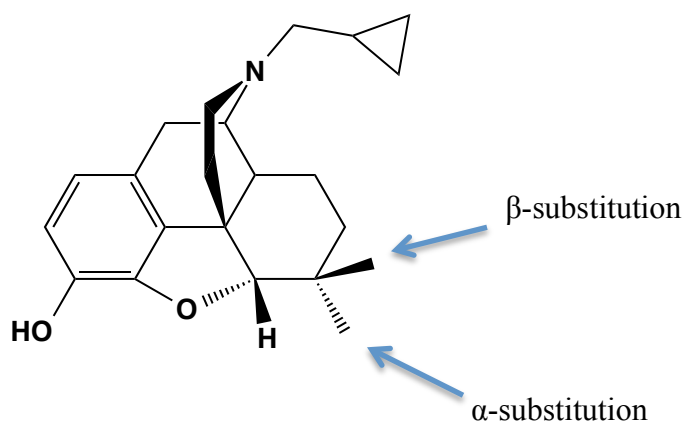


Figure 3.3. Naltrexone a universal opioid antagonist. ‘Morphinan’ skeleton of naltrexone with arrows indicating two possible steric substitutions at 6(C) position.

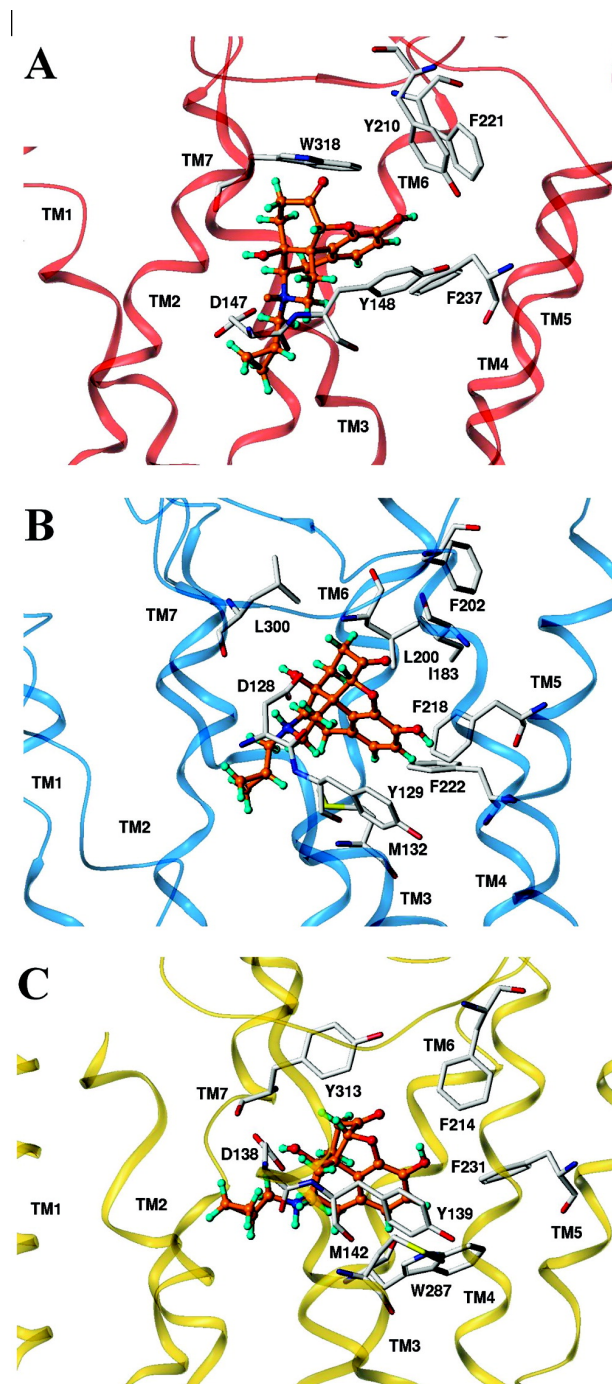


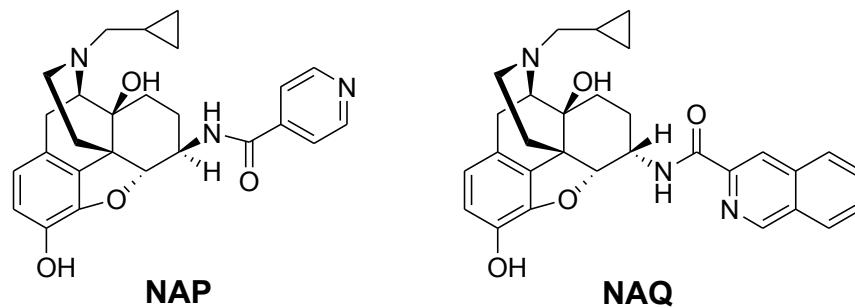
Figure 3.4. Naltrexone (NTX) docked in the homology models of the MOR, DOR, and KOR. NTX is in ball and stick, and colored as carbon, red-orange; hydrogen, cyan; oxygen, red and nitrogen, blue; the amino acid residues are in stick and colored as carbon, grey; oxygen, red and nitrogen, blue. The receptor homology models are in ribbon. NTX is in A) MOR, red; B) DOR, cyan; and C) KOR, yellow. Reprint from reference 92.

Table 3.1. NTX, NAP and NAQ receptor radioligand binding and selectivity profile

Compound	MOR binding (K_i)	KOR binding (K_i)	DOR binding (K_i)	KOR/MOR selectivity	DOR/MOR selectivity
NTX	0.26 ± 0.02	5.15 ± 0.26	117.06 ± 8.94	20	450
NAP	0.37 ± 0.07	60.72 ± 5.58	277.51 ± 7.97	164	750
NAQ	0.55 ± 0.15	26.45 ± 5.22	132.50 ± 27.01	48	241

Table 3.2. Functional characterizations of the ligands in *in vitro* and *in vivo* studies.

Compounds	IC ₅₀	K _i	%tage efficacy of DAMGO	AD ₅₀ (mg/kg) for blocking nociception of morphine (95 % CL)
NTX	3.90 ± 2.96	1.85 ± 1.41	-	-
NAP	2.29 ± 0.15	1.09 ± 0.07	22.72 ± 0.84	4.51 (2.45, 8.26)
NAQ	5.42 ± 0.70	2.57 ± 0.33	15.83 ± 2.53	0.45 (0.27, 0.78)

**Figure 3.5.** Identified potent and selective MOR antagonists.

The elucidation of opioid crystal structures was a very significant development for this area of research. In light of this advancement, the objective of this project was to characterize binding modes of 6 α - (NAQ) and 6 β - (NAP) N-heterocyclic naltrexamine derivatives and to verify the plausible ‘address’ regions that can guide development of more selective antagonists.

3.2.2 Methods

3.2.2.a Sequence analysis

The amino acid sequences of human opioid and bovine rhodopsin receptors were obtained from Universal Protein Resource (UniProt)⁹⁴ (Entry code: P35372 (MOR), P41145 (KOR), P41143 (DOR) and P02699 (Bovine rhodopsin receptor). Sequence alignment analysis was done using ClustalX 2.0⁹⁵

3.2.2.b Receptor model

The X-ray crystal structures for MOR (4DKL), KOR (4DJH) and DOR (4EJ4) were retrieved from PDB Data Bank. Sybyl-X 2.0 was used to build each receptor model, hydrogen atoms were added, Gasteiger-Hückel charges were assigned, and hydrogen coordinates were then optimized by a 10,000 iteration minimization while holding all heavy atoms as an aggregate with the Tripos forcefield (TFF).

3.2.2.c Ligand Models

Sybyl-X 2.0 was used to sketch the chemical structures of the two lead MOR ligands (NAP and NAQ) as well as the non-selective ligand NTX, and their Gasteiger-Hückel charges were assigned before energy minimization (10,000 iterations) with the TFF.

3.2.2.d Ligand Docking

GOLD 5.1, a automated genetic algorithm based docking program was used to perform the docking studies with standard default settings, unless otherwise specified.⁹⁶ The binding site was defined to include all atoms within 10 Å of the γ -carbon atom of Asp^{3.32} (Ballesteros-Weinstein numbering, indicating a residue found 18 position towards the amino terminus from the most conserved residue found in TM3, numbered 50 by convention)⁹⁷ of the three opioid crystal structures. Distance constraints of 4 Å between the piperidine nitrogen of the ligands' morphinan nucleus and Asp^{3.32}, and between the ligands' tetrahydrofuran oxygen and the phenolic oxygen of Tyr^{3.33} were given, so as to model ionic interaction between the acidic receptor residue and quaternary nitrogen of the ligand and hydrogen bond interaction between hydrogen bond donor tyrosine and hydrogen bond acceptor tetrahydrofuran oxygen of the 'morphinan' skeleton. Based on the fitness scores and the binding orientation of each ligand within the binding cavity, the best 50 GOLD-docked solutions were selected and merged into the receptor. The interactions between ligand and receptor within the binding pocket were optimized; clashes and strain energy were removed by energy minimizing the combined receptor-ligand structures (1000 iterations under TFF). These optimized models were then subjected to hydrophobic analysis with the HINT program. HINT (Hydrophobic INTeractions) is

an empirical free energy scoring tool based on the experimental measurements of logP for 1-octanol and water, to estimate atomic level free energies associated with the non-covalent interactions.⁹⁸

3.2.2.e Conformational analysis

Conformational analysis was done in Sybyl-X 2.0 by running a short-term molecular dynamics simulation. The NAP and NAQ structures were solvated with a water box that was then energy minimized under conditions described previously (1000 iterations). A molecular dynamics simulation on the obtained system was then performed under NVT (constant number of atoms, volume and temperature at 300K) ensemble for 100 ns with periodic boundary conditions with a 2 fs time-step. The energy-minimized average for the last 10 ns frames of simulation were analyzed for both the ligands.

3.2.3 Results

3.2.3.a Sequence alignment analyses of three opioid receptors

Analysis of amino acid sequence alignment of all three opioid receptors along with bovine rhodopsin (Table 3.4 and Figure 3.6) reveals the following:

- 1) The three human opioid receptors share very high overall homology (over 60% sequence identity) with higher sequence identity for the putative ligand binding pockets formed primarily by transmembrane (TM) helices 2, 3, 5 and 6 (putative ‘message’ domain of the receptor)

- 2) An even higher identity (close to 90%) is seen for the intracellular loop (ICL) regions, which is consistent with the fact that the three opioid receptors share the same family of G-proteins ($G_{i/o}$) for signal transduction, and ICL is the primary region for G-proteins binding.
- 3) Much lower sequence identities were observed in the extracellular loop (ECL) regions, and for both N- and C termini. ECL3 is especially important because it is located directly above the ‘message’ region of the binding site and carried the lowest sequence identity of all domains. This further consolidates the argument for a potential ‘address’ domain defined in the original homology modeling based study.
- 4) In spite of the high sequence homology in the transmembrane region, two regions of variations were observed. At ‘site 1’, close to the top of TM6 and TM7, two spots of deviations were at 6.58 and 7.35 (Ballesteros-Weinstein numbering) positions. (Red colored numbering in Figure 3.6). At position 6.58, MOR had basic lysine, KOR had acidic glutamate, and DOR had aromatic tryptophan residue. While at position 7.35, MOR had aromatic tryptophan, KOR had aromatic tyrosine, and DOR had hydrophobic leucine residue. This residue was identified as potential address site in the previously reported homology modeling study. ‘site 2’ was defined by variations observed in regions close to the top of TM5 (blue colored numbering in Figure 2.6). At position 5.31, MOR has threonine, KOR has aspartate, and DOR has serine residues. While at position 5.35, KOR and DOR have acidic aspartate and MOR has a longer by one carbon, glutamate residue. (Table 3.3)

Table 3.3. The non-conserved amino acid residue composition of the two binding sites in the three opioid receptors.

Receptor	Site 1	Site 2
MOR	K303 ^{6.58} and W318 ^{7.35}	E229 ^{5.35} and T225 ^{5.31}
KOR	E297 ^{6.58} and Y312 ^{7.35}	D223 ^{5.35} and Y219 ^{5.31}
DOR	W284 ^{6.58} and L300 ^{7.35}	D210 ^{5.35} and S206 ^{5.31}

Table 3.4. Sequence identity among three opioid receptors.

Domain	Percent sequence identity		
	Delta/mu	Delta/kappa	Mu/kappa
TM1	69	62	62
TM2	95	86	82
TM3	90	95	100
TM4	43	57	33
TM5	85	77	77
TM6	73	64	73
TM7	78	82	86
EL1	73	67	67
EL2	52	52	30
EL3	21	13	21
IL1	90	90	100
IL2	91	95	91
IL3	86	81	86
N-terminus	28	33	18
C-terminus	40	32	35
Entire protein	62	61	57

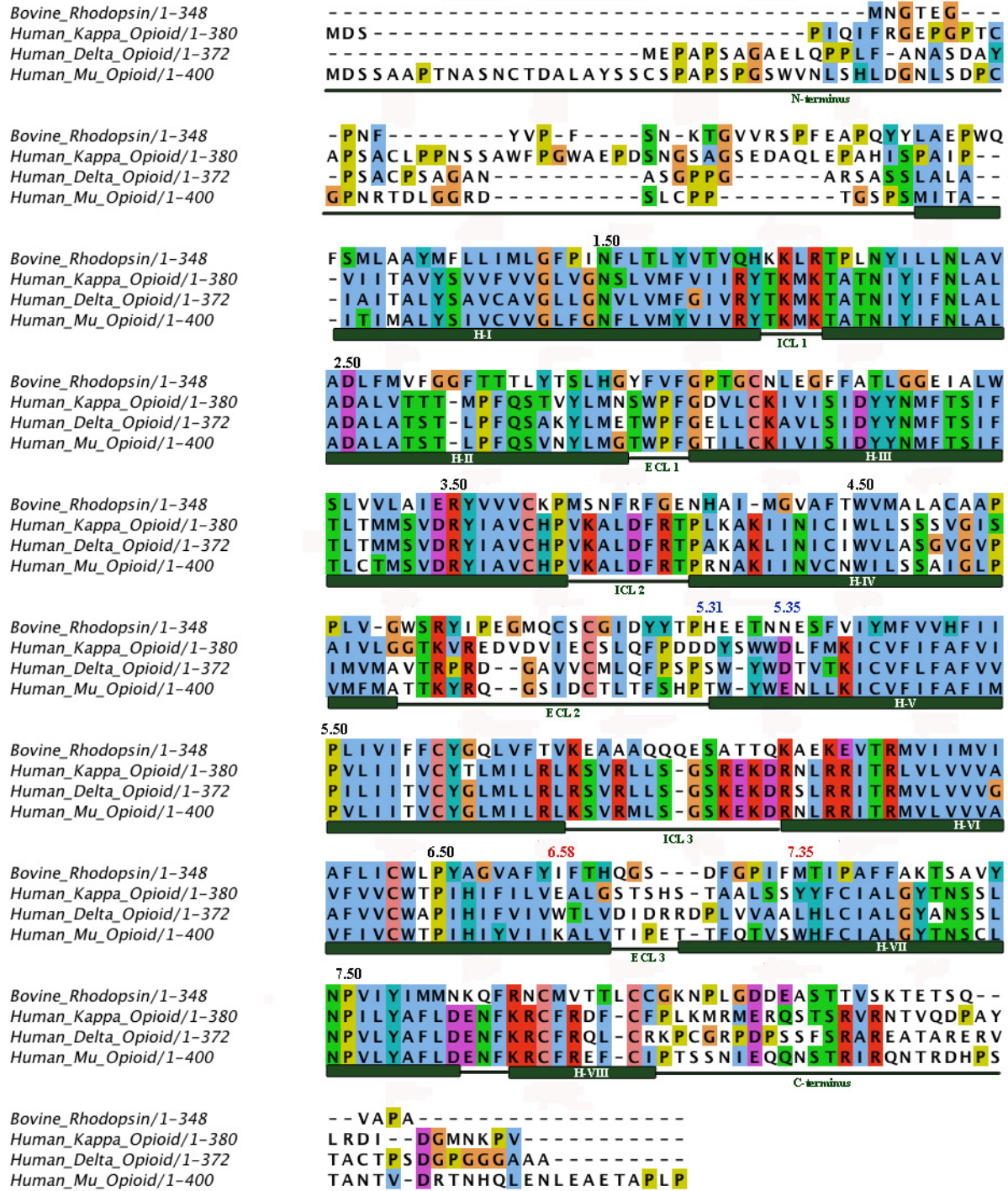


Figure 3.6. Sequence alignment of opioid receptors and bovine rhodopsin. Ballesteros-Weinstein numbers indicated for the most conserved residues in each trans-membrane (black), important residues for Site 1 (red), important residues for Site 2 (blue), TM indicated by broad green lines.

3.2.3.b Conformation analysis

Due to the partial double bond character of the amide linkage of the two compounds (NAP and NAQ), the ligands can adopt either ‘*anti*’ or ‘*syn*’ conformation, as represented for NAP (Figure 3.7A). The averaged conformations measured from the last 10 ns of 100 ns MD simulations conducted for NAP and NAQ within a periodic water box for both ligands, adopted a predominantly ‘*anti*’ conformation, and hence ‘*anti*’ conformer is expected to be thermodynamically more stable.

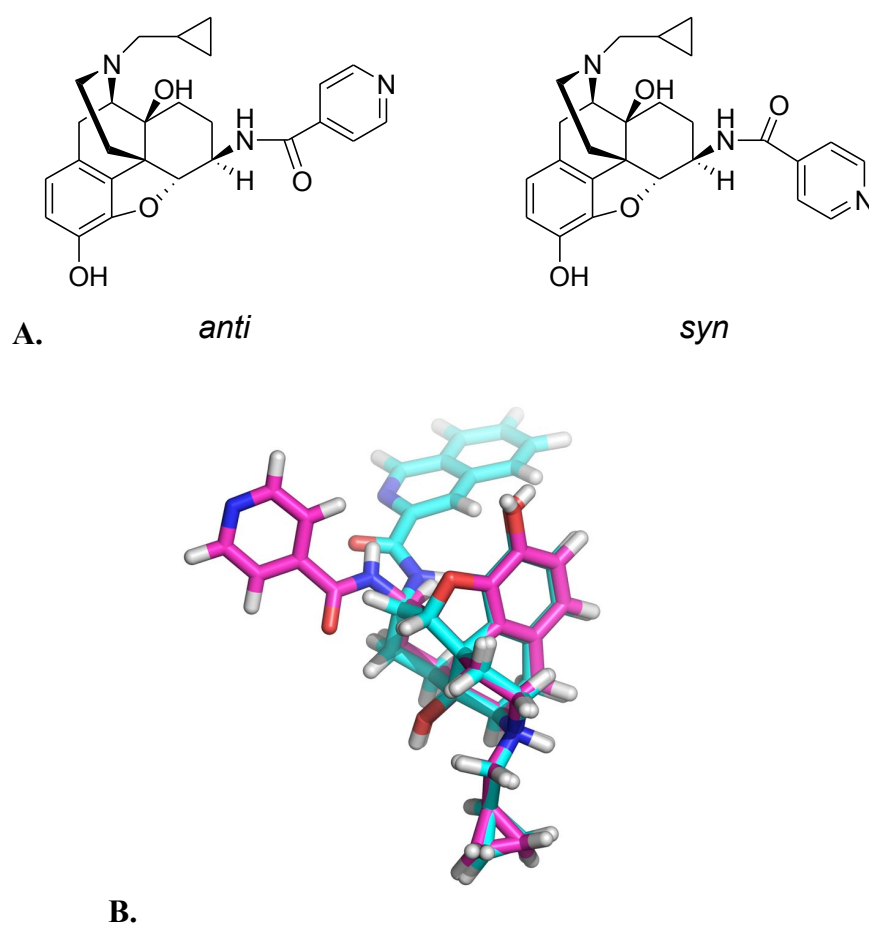


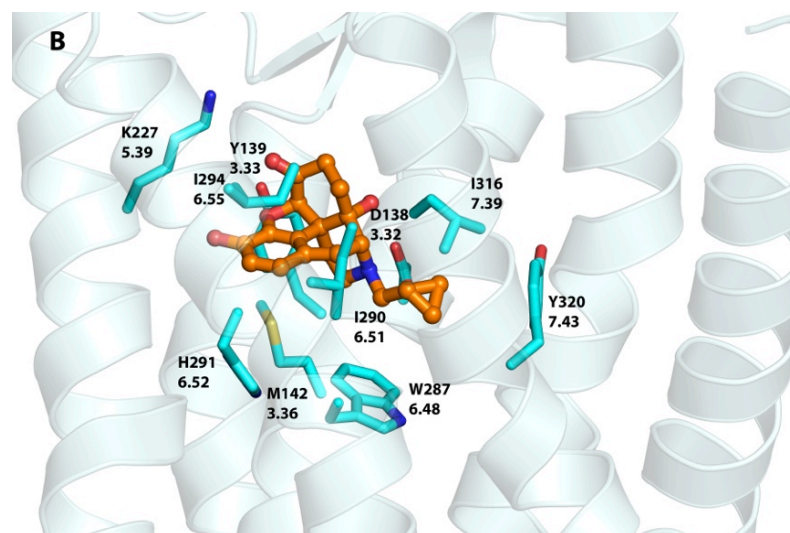
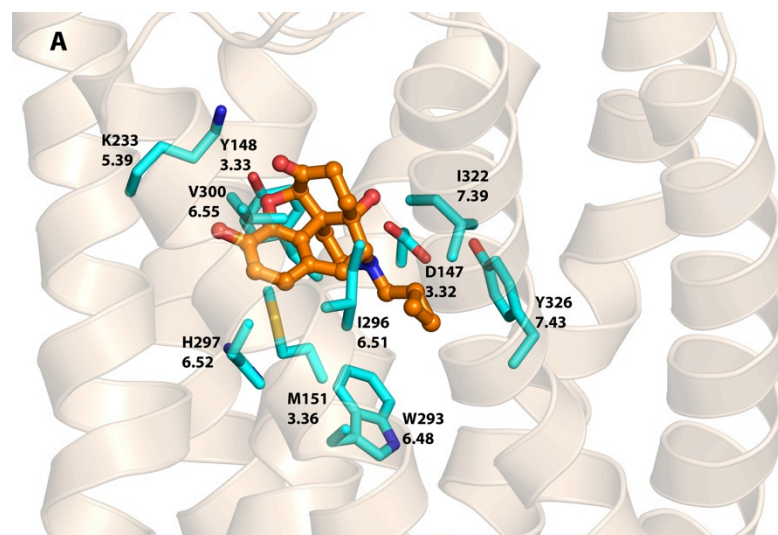
Figure 3.7. Conformational analysis of NAP inside a water box. A) Representation of “*anti*” and “*syn*” conformations for NAP. B) Conformational analysis results for NAP (magenta) and NAQ (cyan). Superimposed average structure for last 10 ns of a 100 ns NVT dynamic simulation inside a water box with PBC. Both NAP and NAQ preferred “*anti*” conformation over “*syn*”.

3.2.3.c Docking studies of the opioid universal antagonist NTX

NTX was used as a ‘probe’ to propose the ‘address’ binding domain within the MOR antagonist binding pocket in the original homology modeling studies of the three opioid receptors. NTX also shares a common core with the ligands bound in the crystal structures (β -funaltrexamine in the MOR, naltrindole in the DOR and JD_{Tic} in the KOR), so the conformations of the ligands co-crystallized with the receptors were used as reference for the docking studies. This modifies the docking experiment into a simpler issue of placing the 6-position substituents of NTX in the energetically favorable conformation. In the present study, the CHEM-PLP scoring function of GOLD program was used since it best replicated the docking solutions of NTX in a fashion similar to what is observed in each of the co-crystallized ligand within a pocket formed by helices 3, 6 and 7. The docking of NTX was followed by energy minimization to optimize the structure models for the ligand receptor complexes. Along with CHEM-PLP scoring function, which has been optimized for modeling steric complementarity between ligand and protein along with distance- and angle- dependent hydrogen bonding, the obtained poses were then rescored with HINT. Optimal docking poses for each NTX-receptor complex were chosen by the highest CHEM-PLP and HINT scores, which were, in this case, generally in agreement. (Table 3.5)

The residues observed to be involved in primary interactions of naltrexone were highly conserved among the three opioid receptors (Figure 3.8). Asp^{3.32} was involved in an ionic interaction with the 17-position tertiary amino group of the ligand, as constrained during the docking process. Tyr^{3.33} formed a hydrogen bond with the furanyl oxygen of the ‘morphinan’ core. The orientation of the 3-phenolic hydroxyl group also matches the orientation seen in MOR and KOR crystal structures indicating the likelihood of a hydrogen bonding interaction with

His^{6.52} through two water molecules. Lys^{5.39} may be involved in hydrogen bonding interactions with the 6-position carbonyl oxygen atom and Met^{3.36}, Trp^{6.48}, Ile^{6.51}, Val/Ile^{6.55}, Ile^{7.39} and Tyr^{7.43} formed a hydrophobic pocket to accommodate the morphinan skeleton of the molecule.



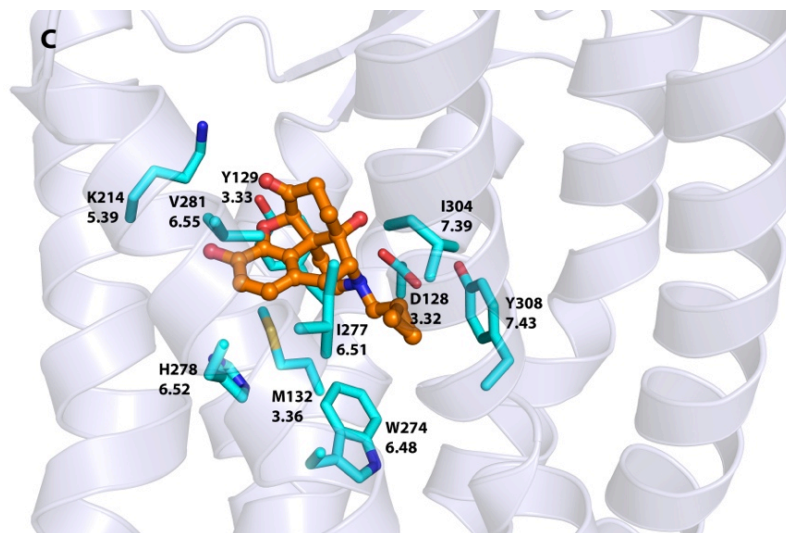


Figure 3.8. Docked poses of naltrexone (orange carbon atoms) inside three opioid receptor crystal structures: A) MOR B) KOR and C) DOR. Amino acid residue atoms: carbon (cyan), oxygen (red), nitrogen (blue), sulfur (yellow).

Table 3.5. Fitness scores for each docking modes of NTX, NAP and NAQ

Compounds	Docking pose	MOR		KOR		DOR	
		CHEM-PLP	HINT	CHEM-PLP	HINT	CHEM-PLP	HINT
NTX		80	1140	70	1009	85	1035
NAP	Site 1	86	1535	57	769	89	1263
	Site 2	89	1022	79	489	94	1034
NAQ	Site 1	81	1345	50	-344	76	465
	Site 2	83	1125	56	616	73	-10

3.2.3.d Analysis of the NAP and NAQ morphinan backbone binding site

All three opioid receptors share a very high degree of sequence similarity in the ‘message’ region of ligand-binding pocket. So expectedly the morphinan nucleus of NAP and NAQ were both docked within each receptor in a fashion similar to naltrexone. The ‘message’ component of the ligands occupied the practically identical ‘message’ domain in the receptors. While the ‘address’ component of the ligands, the amine-linked 6(C) side chain, were primarily clustered around two different binding loci in the three opioid receptors. Interestingly, the same sites were also identified in amino acid sequence analysis, where site 1 was located at the top of helix 6 and 7 (including part of ECL3) and site 2 was at the top of helix 5 and ECL2.

3.2.3.e NAP and NAQ in the MOR

As stated earlier the docked poses for NAP in the MOR were clustered around two high scoring poses related to the two suggested ‘address’ sites. For the first pose NAP adopted a ‘syn’ conformation with respect to the amide linkage. The pyridinyl sidechain of the ligand was oriented towards site 1 where the side chain could stack with Trp318^{7.35} with π - π interactions in addition to a plausible hydrogen bond. (Figure 3.9A) Furthermore, Lys303^{6.58} may also form a hydrogen bond with the pyridinyl nitrogen of NAP. For the second pose, the ligand adopted ‘anti’ conformation with respect to its amide linkage where the pyridinyl side chain is placed in a hydrophobic pocket (Site 2) at the top of helix 5 and near ECL2 (Figure 3.9B). However, lower HINT scores were observed owing to highly negative interactions due to presence of Glu229^{5.35} close to the pyridinyl side chain. Thus, it is postulated that NAP prefers site 1 as a ligand binding pose.

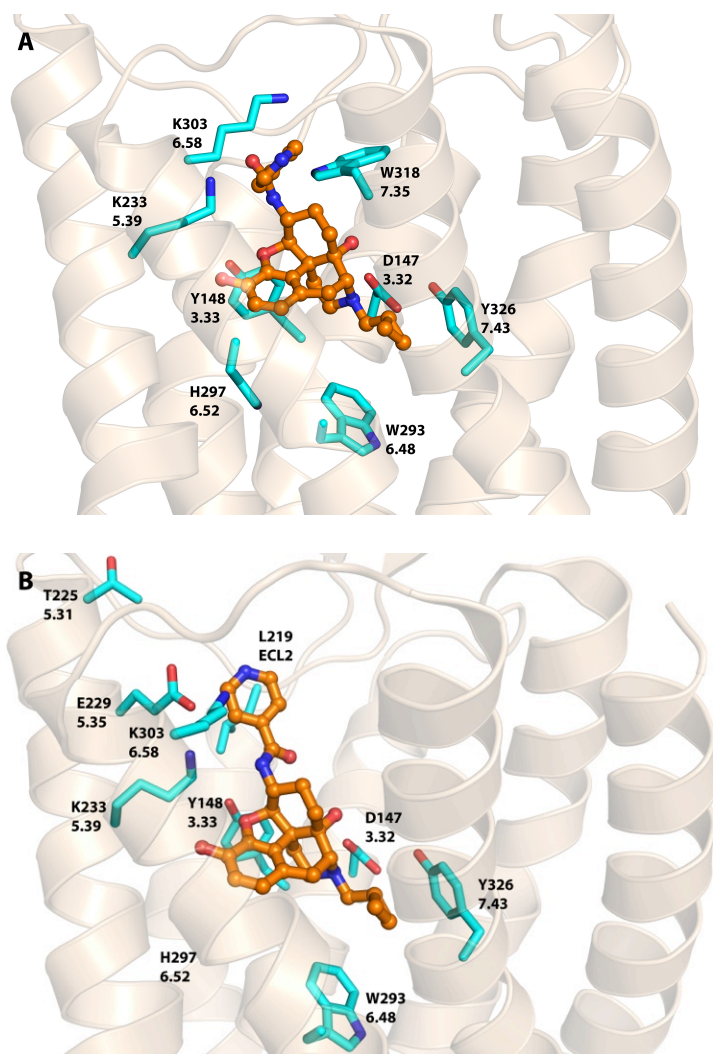


Figure 3.9. Docked poses of NAP in the mu opioid receptor. A) NAP in MOR binding Site 1. B) NAP in MOR binding Site 2. NAP atoms: carbon (orange); amino acid residue atoms carbon: (cyan), oxygen (red), nitrogen (blue).

NAQ follows a similar pattern in its docking solutions. However, for both the major binding solutions, the ligand adopted the ‘*syn*’ conformation. As observed in NAP docking mode at site 1, the quinolinyl side chain of NAQ appears to interact with Trp318^{7,35} with π - π stacking, while in site 2 (Figure 3.9C), the side chain has an unfavorable interaction with Glu229^{5,35} (Figure 3.9D). This again suggests Site 1 as a preferred site of interaction for NAQ.

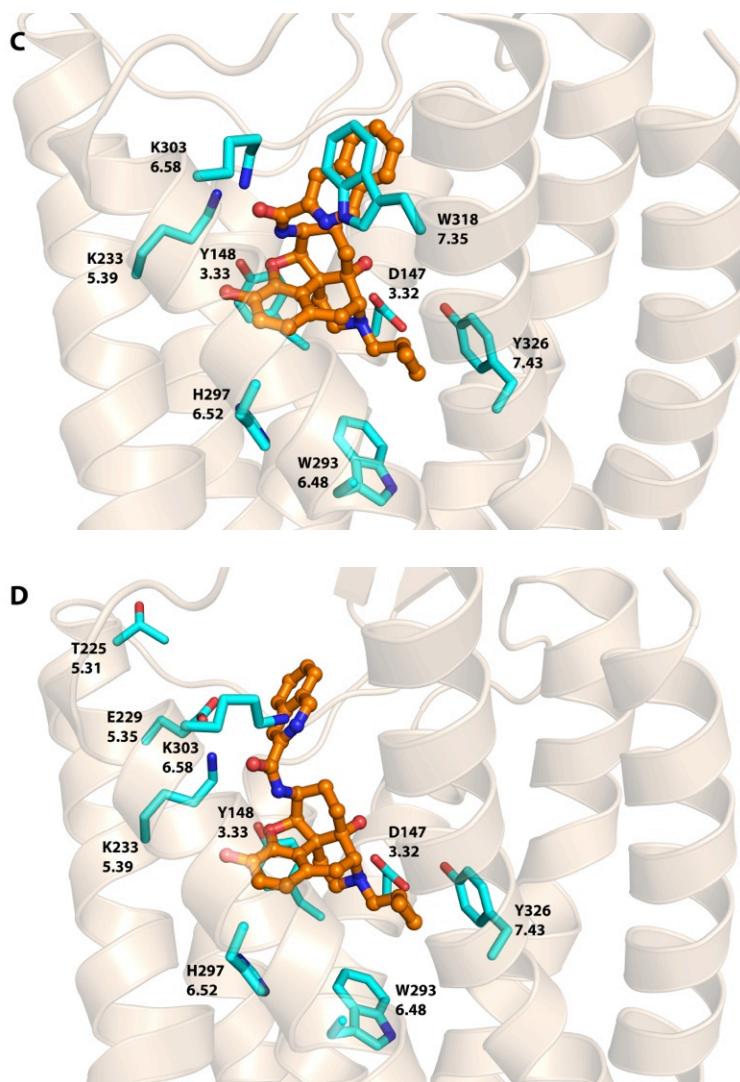


Figure 3.9. Docked poses of NAQ in the mu opioid receptor. C) NAQ in MOR binding Site 1. D) NAQ in MOR binding Site 2. NAQ atoms: carbon (orange); amino acid residue atoms carbon: (cyan), oxygen (red), nitrogen (blue).

3.2.3.f NAP and NAQ in the KOR

Docking of NAP in the KOR also gave two favorable binding poses that were identical to the results as described earlier for MOR. In both these binding sites for KOR the ligand adopted the ‘anti’ conformation, however GOLD and HINT scoring gave conflicting preference of docking

modes. (Table 3.3) At site 1 the aromatic side chain may interact with Tyr312^{7.35} with π - π interactions, which is similar to the interactions observed in MOR-ligand model. However, the presence of Glu297^{6.58} in place of Lys303^{6.58} of the MOR appears to cause deleterious interactions with the ligand side chain (as evidenced by lower HINT scores compared to MOR) (Figure 3.10A). In site 2 of the KOR decreased unfavorable interaction of the NAP side chain is expected because the presence of one carbon shorter Asp223^{5.35} residue compared to the analogous Glu229^{5.35} of the MOR. (Figure 8B). Moreover, the presence of Tyr219^{5.31} and Ser211 (ECL2) may result in more favorable hydrogen bonding interactions with the nitrogen atom of the side chain. However, according to HINT scores, site 1 was still found to be preferred, which is in contrast to the preference suggested by CHEM-PLP scores.

NAQ adopted a 'syn' conformation in both of its KOR docking poses (Figure 3.10 C, D). Even more significant hydrophobic incompatibility with Site 1 Glu297^{6.58} is expected for the larger hydrophobic group (quinolinyl side chain) of NAQ, probably negating the thermodynamically favorable aromatic π - π stacking interactions of that side chain with Tyr312^{7.35}. However, the HINT scores for NAQ binding in site 2 (Table 3.3) indicated no negative interactions with Asp223^{5.35}, also there is a possibility of hydrogen bonding between the side chain and Tyr219^{5.31} and/or Ser211 (ECL2). In this case both HINT and CHEM-PLP scores agreed about the preference of site 2 as a major binding pose for NAQ on KOR.

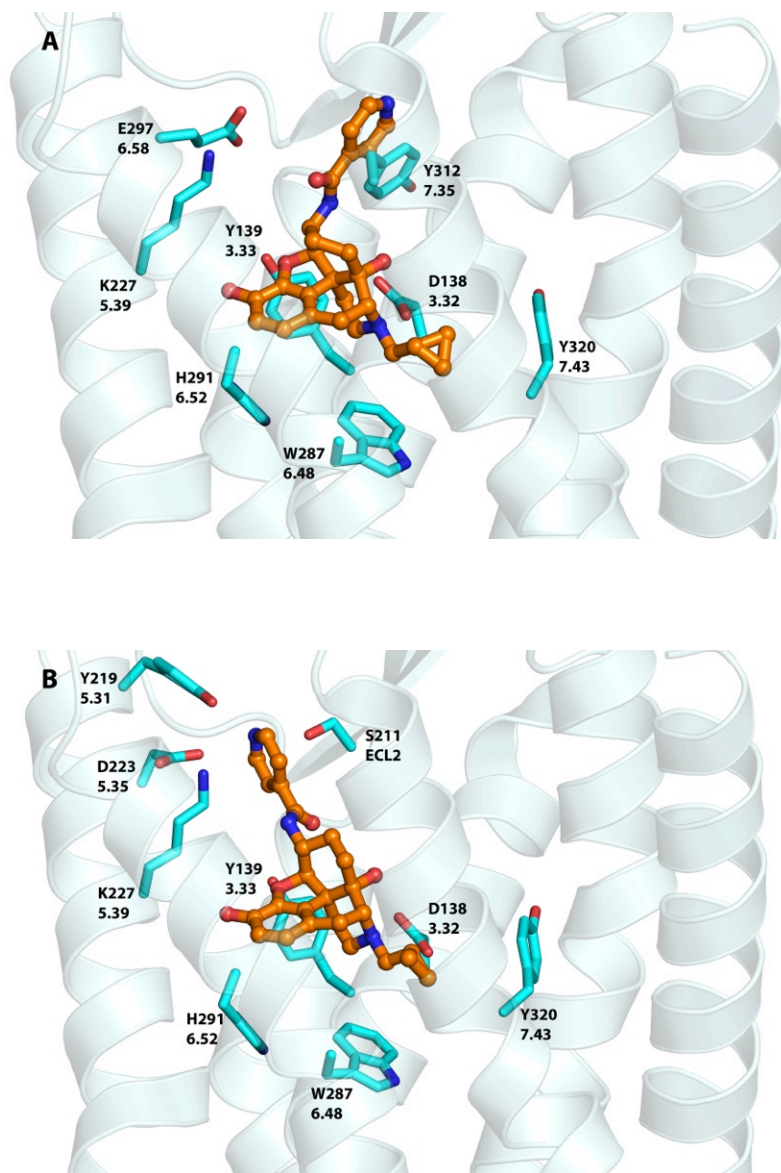


Figure 3.10. Docked poses of NAP in the kappa opioid receptor. A) NAP in KOR binding Site 1. B) NAP in KOR binding Site 2. NAP atoms: carbon (orange); amino acid residue atoms carbon: (cyan), oxygen (red), nitrogen (blue).

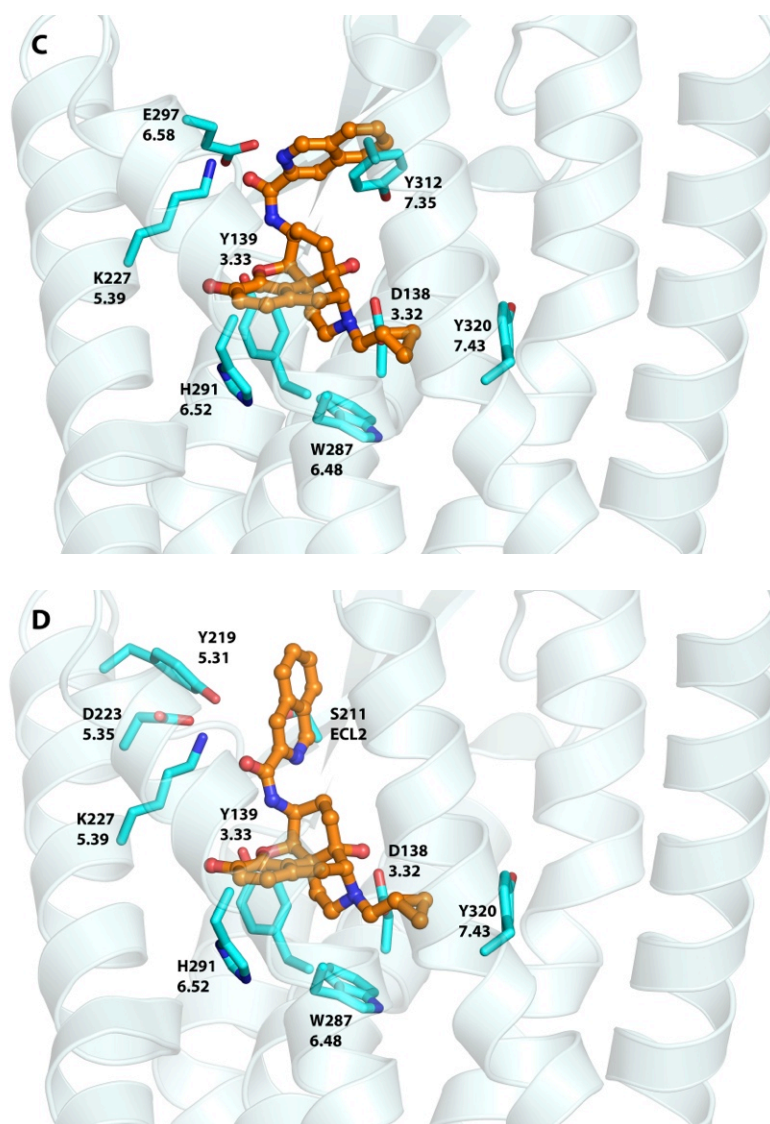
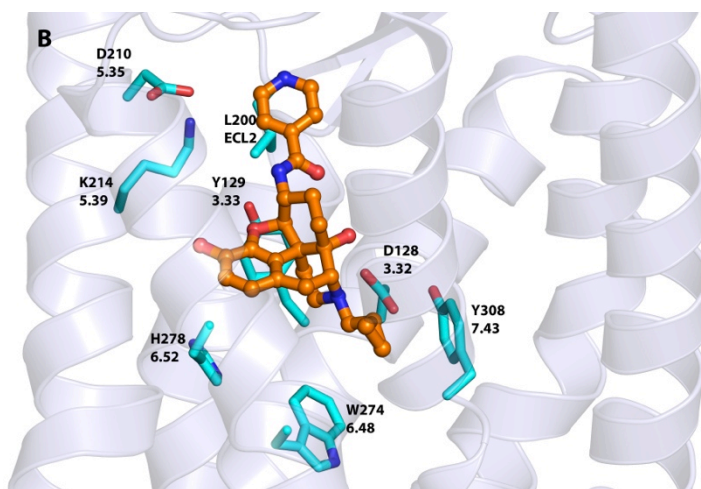
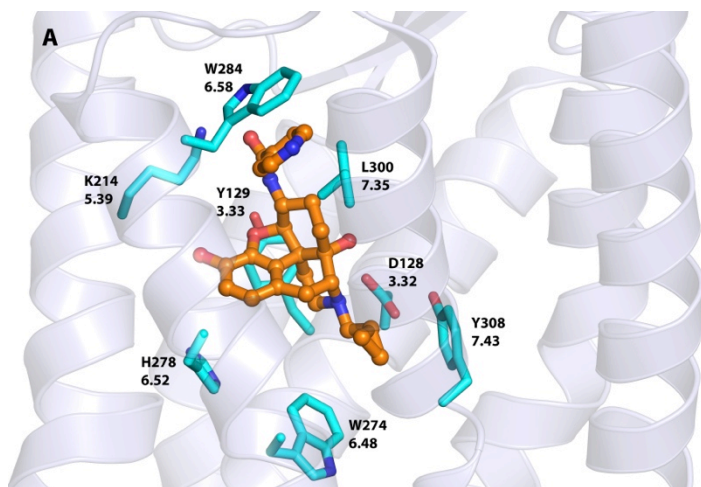


Figure 3.10. Docked poses of NAQ in the kappa opioid receptor. C) NAQ in KOR binding Site 1. D) NAQ in KOR binding Site 2. NAQ atoms: carbon (orange); amino acid residue atoms carbon: (cyan), oxygen (red), nitrogen (blue).

3.2.3.g NAP and NAQ in the DOR

The docked ligand adopted a ‘syn’ conformation in site 1 of the DOR with the side chain expectedly stacked in a hydrophobic pocket formed by Trp284^{6.58} and Leu300^{7.35} (Figure 3.11A).

While the pyridinyl side chain was placed in a hydrophobic pocket close to the top of helix 5 and ECL2 of site 2 in an ‘*anti*’ conformation. (Figure 3.11B). A preference for the ‘*syn*’ conformation was observed for NAQ, though it still adopted nearly identical binding poses to NAP. Notably, these putative interactions seen for DOR-ligand complex failed to replicate any of the hydrogen bonding interactions observed in the MOR and the KOR models, which offers a plausible understanding for the lower affinity of NAP and NAQ for the DOR.



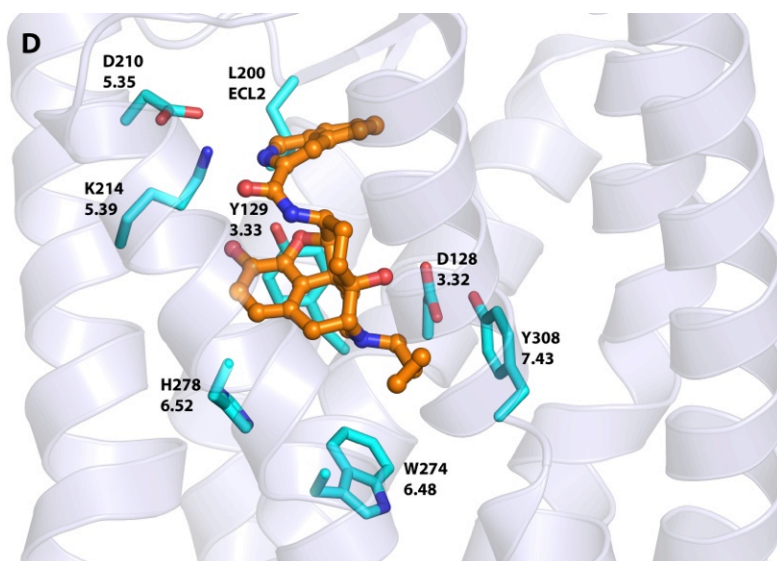
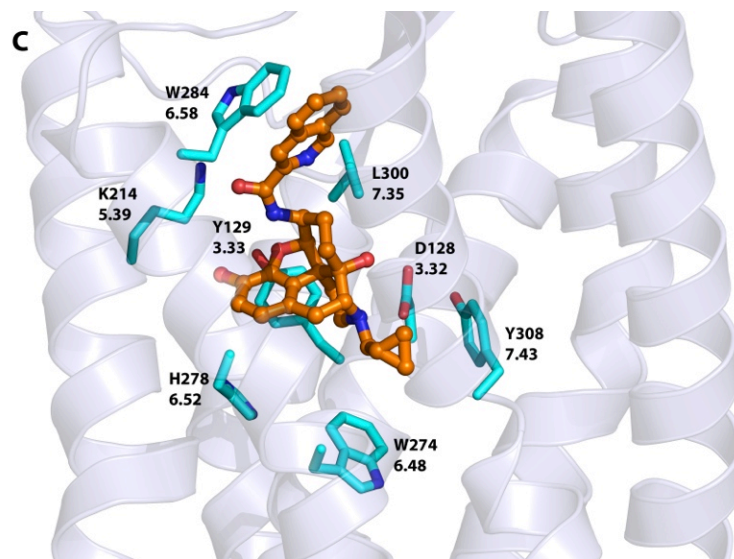


Figure 3.11. Docked poses of NAP and NAQ in the delta opioid receptor. A) NAP in DOR binding Site 1. B) NAP in DOR binding Site 2. C) NAQ in DOR binding Site 1. D) NAQ in DOR binding Site 2. NAP and NAQ atoms: carbon (orange); amino acid residue atoms carbon: (cyan), oxygen (red), nitrogen (blue).

3.2.3.h Validation of docking mode by site-directed mutagenesis studies

A verification for the binding modes responsible for MOR selectivity of NAP and NAQ was provided by a site-directed mutagenesis study with a transient Chinese hamster ovary (CHO) cell line transfected with wild type and mutated MORs. Either Trp318^{7,35} or Tyr210 in MOR were mutated to alanine and NTX was used as a control in these studies. (Table 3.6) A dramatic decrease was seen both in case of NAP and NAQ for mutant W318A, while both bound to the Y210A mutant with affinities comparable to those of wild type MOR. The binding affinities of the NTX control were largely unaffected for either mutated receptor compared to their wild types, agreeing with the unembellished nature of NTX. The preference of the aromatic NAP and NAQ side chains for π - π stacking and hydrogen bonding interactions with Trp318^{7,35} of the MOR in site 1 over Tyr210 (ECL 2) in site 2, as indicated by the docking scores, was also validated by this site-directed mutagenesis study. Overall, the above observations validated initial hypothesis that these two leads may recognize a distinct ‘address’ loci in the MOR to confer their selectivity for the mu over the delta and kappa opioid receptors.

Table 3.6. Binding of ligands to the site-directed mutated MORs.

Compound	Wild type MOR (nM) \pm SEM		Y210A MOR (nM) \pm SEM		W318A MOR (nM) \pm SEM	
	IC ₅₀	K _i	IC ₅₀	K _i	IC ₅₀	K _i
NTX	3.90 \pm 2.96	1.85 \pm 1.41	0.95 \pm 0.49	0.45 \pm 0.23	10.35 \pm 1.64	4.91 \pm 0.78
NAP	2.29 \pm 0.15	1.09 \pm 0.07	1.61 \pm 0.17	0.77 \pm 0.08	> 1000	ND ^a
NAQ	5.42 \pm 0.70	2.57 \pm 0.33	3.31 \pm 1.71	1.57 \pm 0.81	> 1000	ND

3.2.4 Conclusions

Comparison of the docking modes of naltrexone on the homology models of MOR, KOR and DOR, done previously, had indicated a plausible ‘address’ region on the MOR. This address loci was lined by the residues with aromatic character, along with two hydrogen bond donating moieties, Trp318 and Tyr210. A series of naltrexone derivatives were synthesized with substitutions capable of engaging both the aromatic and the hydrogen bond donating character of the region at 6(C) positions. The two novel naltrexamine derivatives, NAP and NAQ, were identified as MOR antagonists based on their *in vitro* and *in vivo* pharmacological profiles, which included high binding affinity and selectivity for the MOR over the DOR and KOR.

The docking studies of NAP and NAQ on the crystal structures of opioid receptors validated the original ‘address’ loci on the MOR albeit with certain alterations. The MOR address loci still had two hydrogen bond donating moieties; however, instead of aromatic Tyr210 residue the basic Lys303 residue was observed. This alteration is in agreement with the site-directed mutagenesis studies that showed dramatic loss of binding affinity for NAP and NAQ on Trp318 mutation but no such effect of mutating Tyr210 residue.

Furthermore, sequence alignment and ligand docking studies also revealed an alternate ‘address’ region on the MOR close to the top of TM5 and ECL2. In this alternate site the MOR has glutamate residue, while the KOR and the DOR have aspartate residue. The presence of one carbon longer acidic residue in MOR, can conceivably allow better interactions with the substituents of naltrexone derivatives. Thus, the ligands with groups interacting at this locus may show greater discrimination between the opioid receptors.

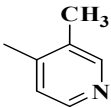
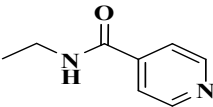
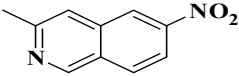
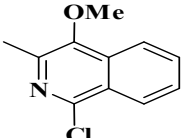
The modeling and the site-directed mutagenesis studies showed that NAP and NAQ preferred site 1, the region lined with the Trp318 and the Lys303 residues in MOR. However, NAP, NAQ and their cognate ligands may have dual binding modes. The equilibrium between the two binding modes may shift depending on the nature of substituents attached to the naltrexamine skeleton.

This model postulates that the hydrogen bond accepting groups on the pyridyl and isoquinolyl moieties would interact with the basic lysine residue at site 1 on MOR, and hence provide further selectivity. The ligand binding to site 1 of MOR could also benefit from the attachment of electron withdrawing groups to the N-heterocyclic aromatic moiety via increase in cation- π interactions between the N-heterocyclic aromatic group and solvent exposed Lys303.

Furthermore, ligand binding at site 2 could be improved by increasing the linker length between the morphinan skeleton and the N-heterocyclic moiety that would allow closer interactions with the glutamate residue at TM5 of MOR.

Based on this model and identification of NAP and NAQ as the lead molecules, a series of next generation derivatives have been synthesized and pharmacologically characterized. Some analogs are shown in Table 3.7. For NAP derivatives, addition of the electron donating methyl group had little improvement in selectivity over NAP. However, increase in the linker length between the N-heterocyclic aromatic moiety and the morphinan skeleton improved selectivity of the KOR. For NAQ derivatives, inclusion of the hydrogen bond acceptor nitro group to the isoquinolyl moiety decreased the MOR binding, probably due to decreased cation- π interactions between the basic Lys303 side chain and the heteroaromatic ring because of the strong electron withdrawing nature of the nitro group. In comparison with NAQ, the binding affinity of NCQ

Table 3.7 Second-generation naltrexamine derivatives. Radioligand binding and selectivity profile

Name	Cnf	Substituent	MOR binding (K _i)	KOR binding (K _i)	DOR binding (K _i)	KOR/MOR	DOR/MOR
NMP	β		0.58 ± 0.25	96.7 ± 12.2	273.6 ± 1.8	166	472
NGP	β		0.73 ± 0.59	203.2 ± 67.0	526.1 ± 78.3	278	719
NNQ	α		5.7±1.7	27.9±2.0	94.7±1.1	4.9	16
NCQ	α		0.55±0.01	22.2±2.1	33.9±0.5	40	62

remained unchanged towards the MOR and the KOR, however the binding improved for DOR, probably due to increase in the hydrophobic bulk.

The above examples illustrate the difficulty in designing of the selective opioid ligands. The combination of multiple plausible binding modes and multiple characteristics that a substitution can impart to the ‘address’ part of the ligand complicates the selectivity profile of a ligand. However, the modeling studies presented here guided the identification of lead

compounds selective for MOR. Further application of the “message–address” concept, in combination with molecular modeling studies, site-directed mutagenesis studies and guided synthesis, may help in designing more selective ligands for the MOR.

3.3 Modeling pharmacological profile switch from mu-opioid receptor selectivity to mu/kappa opioid dual selectivity of 14-position heteroaromatic substituted naltrexone derivatives

3.3.1 Introduction

Previous docking studies of naltrexone on homology models of MOR, KOR and DOR had indicated two plausible docking modes and hence two possible sites for addition of functionalized moieties – the 6th position of morphinan core (described earlier) and the 14 position of morphinan core. Both docking modes had implicated Trp318 and Tyr210 residues as a plausible ‘address’ site in MOR. (Figure 3.12) As described earlier for 6(C)-substituted naltrexone derivatives, a series of N-heterocyclic aromatic moieties were synthesized with 14-O substitution through an ester bond.^{99,100} (Figure 3.13) Various other groups have reported such 14th substituted naltrexone derivatives with limited selectivity towards MOR, including the irreversible antagonist clocinnamox.¹⁰¹⁻¹⁰⁴

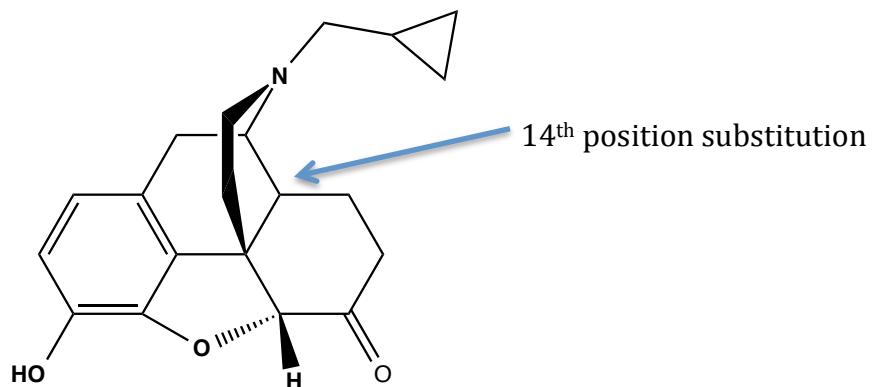


Figure 3.13. ‘Morphinan’ skeleton of Naltrexone indicating 14th position of substitution

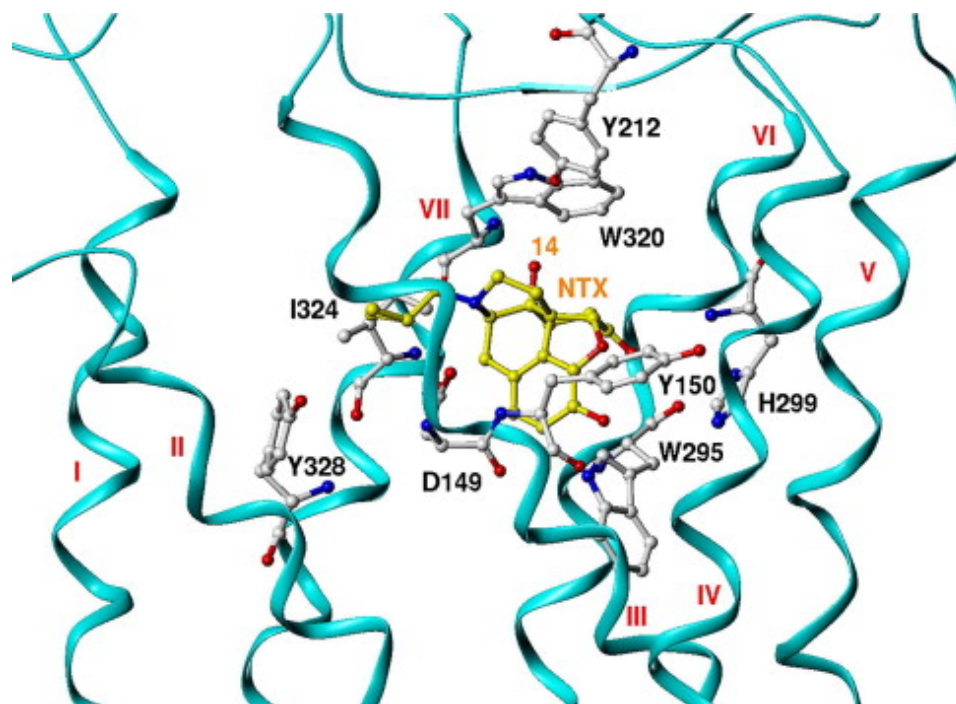


Figure 3.12. Second binding mode of naltrexone inside MOR homology model. Reprint from reference 99.

Broadly, 14-O derivatives of naltrexone showed selectivity towards MOR. However, the ester linkage is susceptible to hydrolysis and so was converted to its isoster amide in second generation of compounds.¹⁰⁵ However, the second generation of 14-substituted naltrexone derivatives indicated KOR/MOR dual selectivity (Table 3.8 and 3.9). The primary objective of this project was to model the selectivity profile of 14-O naltrexone derivatives in light of the newly crystallized opioid receptors, as well as to model subsequent the loss in selectivity for second generation of 14-N linked derivatives.

The receptor binding data obtained via radioligand binding studies for first generation (14-O) and second generation (14-N) of compounds is shown in Table 3.8 and 3.9. The following broad conclusions can be drawn from the given data –

1. Ester linked 14-substituted compounds were MOR selective, while amine linked compounds were dual KOR/MOR selective. Loss in selectivity was because of better binding of the N-linked derivatives to KOR. Binding towards DOR was also improved for second generation of compounds, especially biphenyl derivatives.
2. Among the O-linked first generation of compounds, the presence of nitrogen in the aromatic substitution improved binding. No such relationship was seen for the N-linked second generation derivatives.
3. Changing the linker length in second-generation compounds (third generation derivatives), which effectively changes the position of the functionalized moiety, does not have any effect on receptor selectivity.

Table 3.8. Opioid receptor binding affinity (from radioligand binding assays) and selectivity of first generation O-linked 14th substituted naltrexone derivatives.

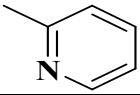
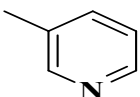
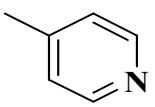
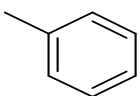
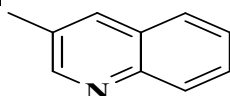
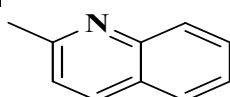
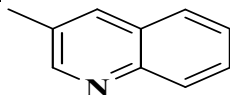
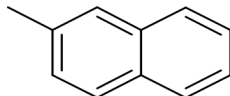
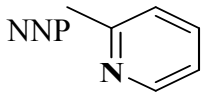
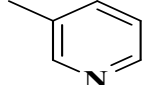
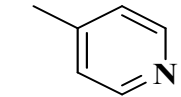
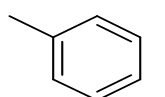
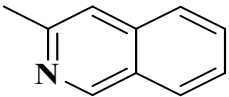
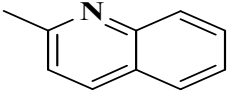
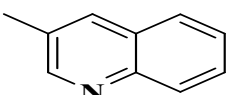
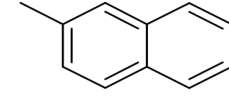
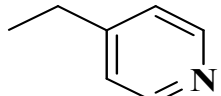
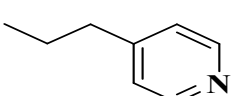
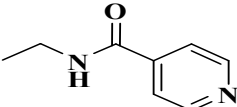
	K_i (nM) ± SEM			Selectivity Ratios		
	MOR (M)	KOR (K)	DOR (D)	K/M	D/M	D/K
NTX	0.20 ± 0.02	5.15 ± 0.26	117.0 ± 8.9	20	450	23
NOP 	0.14 ± 0.03	25.5 ± 6.5	117.4 ± 18.0	182	838	4.6
	1.59 ± 0.61	47.8 ± 8.5	170.3 ± 12.6	30	107	3.6
 paraNOP	5.58 ± 1.34	49.2 ± 20.4	405.3 ± 234.7	8.8	73	8.2
	123.2 ± 38.2	586.4 ± 32.4	>10,000.00	4.7	>81	>17
	68.4 ± 6.0	>10,000	>10,000	>146	>146	NA
	1.44 ± 0.32	67.2 ± 36.7	22.8 ± 19.5	47	16	0.34
	2.69 ± 0.72	148.2 ± 55.5	818.4 ± 507.2	55	304	5.5
	225.3 ± 46.6	46.6 ± 13.5	907.2 ± 193.0	0.21	4	19

Table 3.9. Opioid receptor binding affinity (from radioligand binding assays) and selectivity of second and third generation O-linked 14th substituted naltrexone derivatives.

	K_i (nM) ± SEM			Selectivity Ratios		
	MOR (M)	KOR (K)	DOR (D)	K/M	D/M	D/K
NTX	0.34 ± 0.03	0.90 ± 0.11	95.46 ± 6.09	2.6	281	106
NNP 	1.51 ± 0.34	0.36 ± 0.01	94.5 ± 6.5	0.24	63	263
	0.75 ± 0.28	0.16 ± 0.01	39.9 ± 0.5	0.21	53	249
paraNNP 	0.82 ± 0.33	0.33 ± 0.01	10.9 ± 1.3	0.4	13	33
	4.34 ± 0.70	0.12 ± 0.001	57.3 ± 4.3	0.03	13	717
	3.50 ± 1.87	0.27 ± 0.02	25.1 ± 1.8	0.07	7.2	93
	9.09 ± 4.94	0.26 ± 0.01	15.1 ± 0.6	0.03	1.7	58
	1.13 ± 0.25	0.13 ± 0.02	1.48 ± 0.05	0.12	1.3	11
	6.22 ± 4.01	0.33 ± 0.02	10.5 ± 1.4	0.05	1.7	32
	0.29 ± 0.04	0.19 ± 0.03	3.92 ± 0.12	0.66	14	14
	0.32 ± 0.04	0.17 ± 0.02	9.1 ± 0.5	0.53	29	29
	0.30 ± 0.01	0.14 ± 0.01	0.37 ± 0.04	0.47	1.2	1.2

3.3.2 Methods

To understand the loss of selectivity towards the MOR for second generation of compounds, the most selective first generation compound NOP and its second generation analog NNP were selected for molecular modeling analysis.

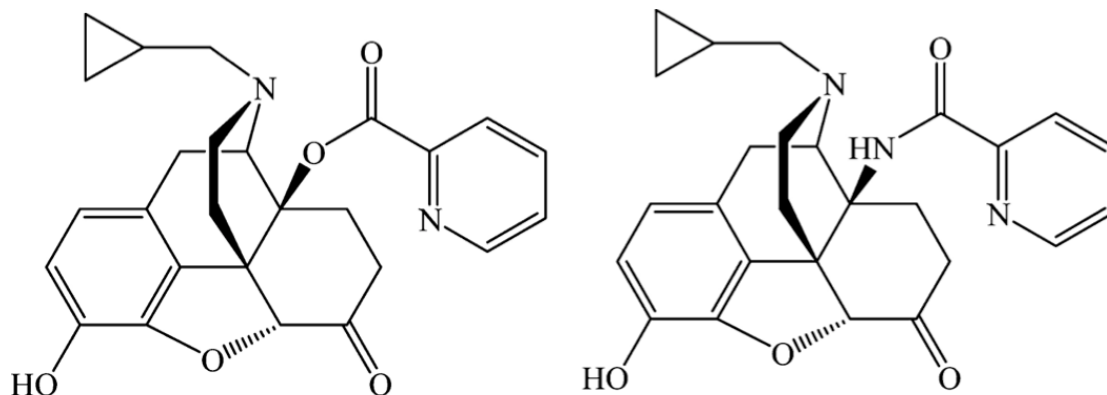


Figure 3.14. First generation (O-linked) NOP and second generation (N-linked) 14-substituted naltrexone derivatives.

1. Chemical structures of the ligands were sketched in Sybyl-X 2.0, and their Gasteiger-Hückel charges were assigned before energy minimization (10,000 iterations) with the TRIPOS force field (TFF).
2. The X-ray crystal structures for MOR (4DKL),⁴⁴ KOR (4DJH)⁵⁰ and DOR (4EJ4)⁵⁴ were retrieved from PDB Data Bank.

3. Automated docking on these retrieved receptor structures was done utilizing a genetic algorithm docking program GOLD⁹⁶ 5.1. The binding site was defined to include all atoms within 10 Å of the γ -carbon atom of Asp^{3.32} for the three opioid crystal structures along with a hydrogen bond constraint between the piperidine nitrogen of the ligands' morphinan nucleus and carboxylate of Asp^{3.32}. The best CHEM-PLP scored solutions were chosen for further analyses.

4. The 'morphinan type' docking pose, as observed in the respective crystal structures, was seen for both the ligands inside all the three receptors. The conserved residues of TM 3, 6 and 7 formed a hydrophobic pocket lined with Met3.36, Trp6.48 and Tyr7.43. Apart from a conserved ionic interaction between Asp3.32 and the basic nitrogen of morphinan skeleton, conserved hydrogen bonding interactions were also seen between Lys5.39 and 6th position carbonyl and Tyr3.33 and tetrahydrofuran oxygen. However the functionalized 'address' moiety i.e. heterocyclic ring also resided in a highly conserved region close to TM2 lined by Gln2.60.

5. On closer inspection of the receptor binding pockets a variant residue site was observed one α -helical turn above conserved Gln^{2.60}. In KOR and DOR this position (2.63) is occupied by Val and Lys, respectively while in MOR Asn occupies the site. A coordinates switch for side-chain terminal nitrogen and oxygen of Asn^{2.63} of MOR allowed a plausible hydrogen bonding interaction with the Gln residue present one turn below it.

6. After the 'switch' molecular dynamics (MD) simulations were performed in Sybyl-X 2.0 for 10 ps under NVT ensemble. All the residues outside a 15Å sphere radius of 14-position carbon of the ligand were defined as aggregates and MD simulations were run after assigning Gasteiger-Hückel charges and an initial temperature of 300 K. The average structure of the last 1ps of the simulation was again energy minimized after assigning Gasteiger-Hückel charges for the 1000 iterations. The above simulation was re-run under same conditions after replacing the ester O atom with an NH group.

3.3.3.Results

Interestingly, conformational changes observed for Gln2.60 of MOR, after the short term dynamic simulation, allowed for a possible hydrogen-bond interaction with the pyridyl nitrogen of the ligand. However, this conserved Gln residue among the three receptors was ill directed in both KOR and DOR (Figure 3.15A). One point of difference in an otherwise very well conserved docking pocket of the three receptors is at position 2.63, directly above Gln2.60. Based on our models here, we hypothesize that in MOR Asn2.63, present a helical turn above Gln2.60, helps to direct Gln2.60 towards the ligand with a greater possibility of hydrogen bonding. However, in KOR 2.63 this position is occupied by Val and the DOR 2.63 position is occupied by Lys. The Val of KOR does not have hydrogen bonding groups in its side chains, while Lys was directed outwards, interacting with the acidic residues present on the ECLs of KOR.

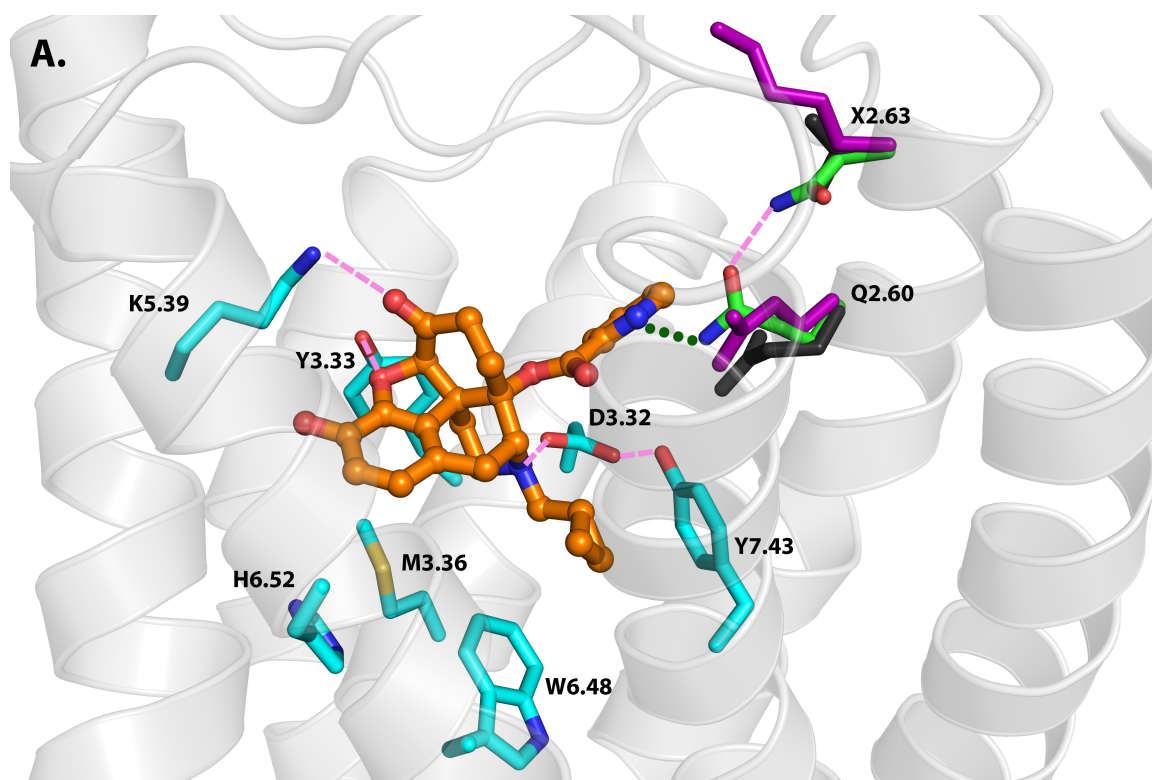


Figure 3.15A. Superimposed binding mode of NOP (orange balls and stick) in three opioid receptors: conserved residues (cyan), MOR residues (green), KOR residues (black), and DOR residues (purple). Pink dashes and green dots represent possible hydrogen-bonding interactions. Asn2.63 (MOR), but not Val2.63 (KOR) or Lys2.63 (DOR), facilitated the hydrogen-bonding interaction (green dots) between Gln2.60 and the pyridyl nitrogen atom. The hydrogen-bonding network yields the high MOR selectivity of NOP over the KOR and DOR.

However, the selectivity of ligands was lost for amide-linked second generation derivatives. To understand the possible conformational changes in residues around the binding pocket, the ester 'O' of the ligand was replaced with an amide 'NH' in the same docked pose of ligand. This was followed by a similar dynamic simulation experiment as described earlier. The resulting model suggests that, due to a possible internal hydrogen bond between amide NH and pyridyl N, the pyridyl N of ligand NNP prefers to stay close to the ligand amide. Thus it may be unavailable for the Gln2.60 linked hydrogen bond, which according to our model described earlier is responsible

for the selectivity. (Energy calculated for the NNP pose with internal H-bond was 12.5 kcal/mol lower than the pose without H-bond). Furthermore, the replacement of oxygen of ester, a hydrogen bond acceptor, with hydrogen bond donor –NH group close to conserved Asp^{3.32} increments a possibility of another beneficial interaction for all three receptors which results in the loss of selectivity.

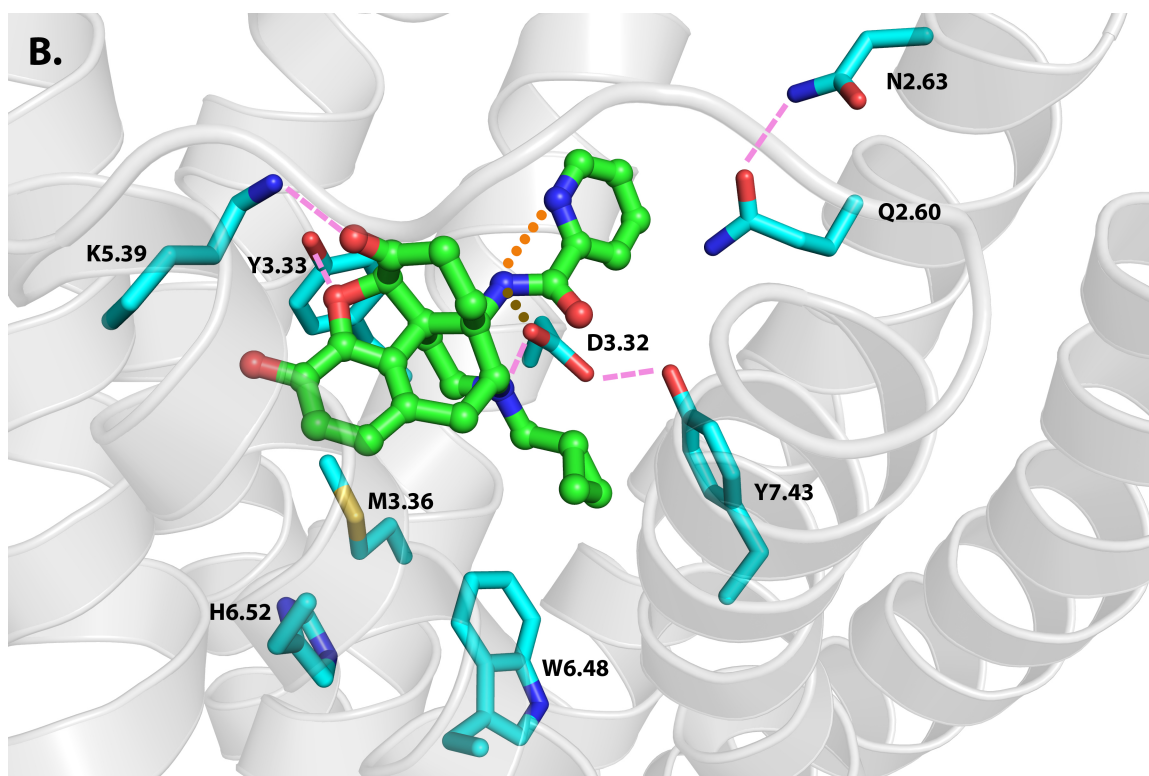


Figure 3.15B. The binding mode of ligand NNP (green balls and stick) in the MOR (cyan). Conserved hydrogen-bonding interactions, as seen for ligand 2, are shown in pink dashes. A potential internal hydrogen bond (orange dots) between the amide NH and the pyridyl nitrogen in ligand 10 disrupts the hydrogen-bonding network, as observed for ligand 2. Furthermore, a hydrogen-bonding interaction (brown dots) also formed between the amide NH and the conserved residue Asp3.32 in all three opioid receptors and thus enhanced the binding affinities of ligand 10 in all three opioid receptors.

Similar dynamics simulation experiments were also run for ligands with N in the 4-position of the hetroaromatic substitution of the derivatives. In the case of second generation derivatives (para-NNP), the γ -carbon of the Asp3.32 moved 1.2Å towards the linker, due to a possible interaction between the acidic Asp residue and the basic –NH linker (Figure 3.15C). A slight movement was also seen for Tyr7.43, and its hydroxyl was now directed towards the pyridyl ring (instead of being towards Asp3.32) that may also lead to hydrogen bonding interactions with the ligand.

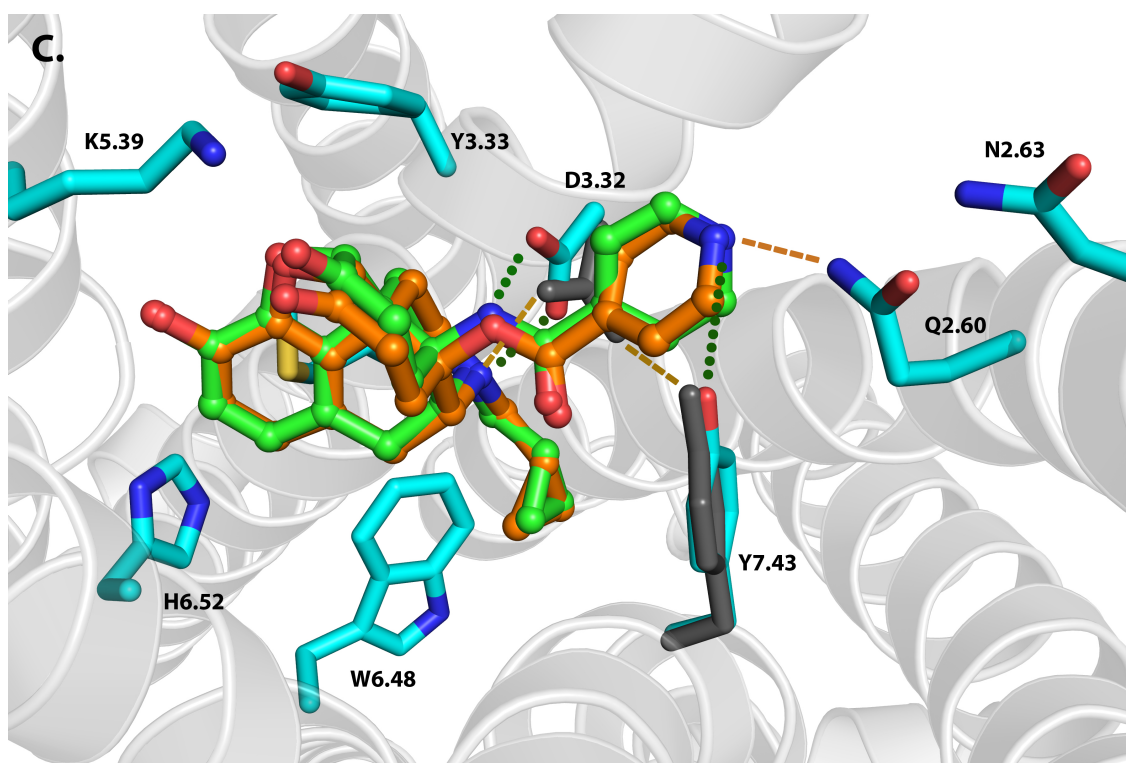


Figure 3.15C. Superimposed binding modes of ligand paraNOP (orange balls and sticks) and paraNNP (green balls and stick) in the MOR (cyan). Interactions, as seen for ligand paraNOP, are shown in brown dashes. paraNNP and MOR interactions are shown in green dots.

3.3.4 Conclusions

14-substituted naltrexone derivatives are reported to have discrepant structure-activity relationships with activity ranging from irreversible antagonism to agonism higher than morphine even for 17-N-substituted methylcyclopropyl morphinan ligands.^{102,106-108} 14-substituted ester linked N-heteroaromatic derivatives of naltrexone synthesized in our lab showed good selectivity towards MOR. However, this selectivity was lost due to the increased binding affinity towards both KOR and DOR.

Our model suggests that increased overall binding for all three receptors can be explained by replacement of the ester oxygen with an amide –NH group, which is capable of forming a hydrogen bond with the highly conserved acidic Asp^{3.32} present nearby. In absence of this –NH group, the ester oxygen interacts adversely with the acidic aspartate. However, presence of nitrogen in the functionalized substitution can help compensate for this negative interaction in MOR through hydrogen bonding with glutamate at position 2.60. This also explains importance of nitrogen in the ring for MOR binding in the first generation of compounds; importance of nitrogen was also lost in second generation derivatives. Although, the glutamate at position 2.60 is conserved in all three receptors, it is not directed towards the 14-functionalized substitution in the cases of KOR and DOR. The model indicates that this is because of directive effect of the non-conserved asparagine residue in MOR, a role that valine (in KOR) and lysine (in DOR) are unable to fulfill.

The model generated here represents a slight deviation from the ‘message-address’ strategy. Generally, in the application of the ‘message-address’ concept for the development of

the selective ligands, residues only in the immediate vicinity of the ligand are considered. However, this model suggests that instead of always relying on the 'address' sites composed of distinct residues for each receptor, other 'address' sites can be explored that are formed due to the conformational state of the conserved residue side chain in response to the changed microenvironment surrounding the conserved residue.

3.4 Characterization of the selectivity profile of NAQ derivatives

3.4.1 Introduction

As described earlier, NAQ, a C(6)-isoquinoline substitution naltrexone derivative, was designed to be selective for MOR on the basis of identification of ‘address’ sites in homology models of opioid receptors. NAQ has been reported to antagonize the effects of full agonist DAMGO (D-Ala²-MePhe⁴-Gly(ol)⁵) in the [³⁵S]GTPγS binding assay and effects of full agonist morphine in warm-water tail flick immersion assays in mice. NAQ itself shows low efficiency partial agonism in [³⁵S]GTPγS binding assay.^{109,92} Moreover, NAQ has shown better efficacy and less susceptibility to tolerance than naltrexone in reducing high concentration alcohol (30%) intake in mice.

NAQ’s encouraging results stimulated the need to explore its structure-activity relationship (SAR) with respect to its selectivity and efficacy. Docking studies, described previously, postulate two plausible docking modes for NAQ. In the first binding mode, the ‘address’ site on MOR was posited to be near the top of TM6 and TM7 where Trp318 and Lys318 were modeled to be involved in interactions. While in the second binding mode, Glu229, close to the top of TM5 and ECL2, can operate as ‘address’ site.¹¹⁰ To facilitate an SAR study, analogs of NAQ were synthesized based on the above model (as discussed in the section 3.2.4) and Craig’s plot¹¹¹ by incorporating substitutions on isoquinoline ring, distance between isoquinoline ring and epoxymorphinan skeleton, and the aromatic character of C(6) side chain. These compounds were then evaluated in radioligand binding competition, MOR [³⁵S]GTPγS binding, and behavioral tail flick immersion assays. NNQ, a 6-nitroisoquinoline analog of NAQ,

showed antagonistic activity towards MOR for DAMGO (full agonist), along with limited selectivity towards MOR (MOR \approx KOR < DOR).

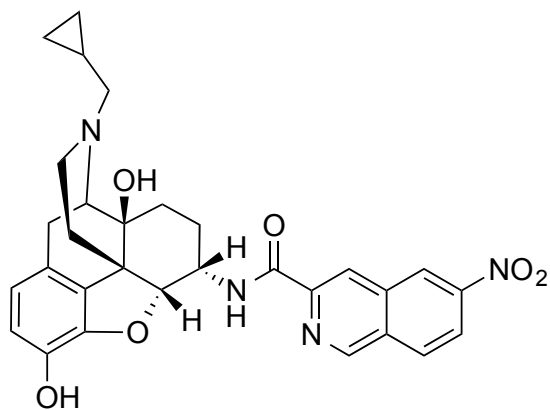


Figure 3.16. NNQ, 6-nitro derivative of NAQ

Table 3.10. Opioid receptor binding affinity, selectivity and [³⁵S]GTP γ S binding efficacy data for NNQ and NAP

Compd	K_i (nM)			Selectivity		MOR [³⁵ S]GTP γ S Binding	
	μ	κ	δ	κ/μ	δ/μ	EC ₅₀ (nM)	% E_{max} of DAMGO
NNQ	5.7 \pm 1.7	27.9 \pm 2.0	94.7 \pm 1.1	4.9	16	31.5 \pm 18.7	12.5 \pm 1.4
NAQ	0.55 \pm 0.15	26.45 \pm 5.22	132.50 \pm 27.01	48	241	15.83 \pm 2.53	

The objective of the following project was to model the selectivity profile of NNQ over opioid receptors. Previously described examples of 14-substituted naltrexone derivatives NOP and NNP had demonstrated the role of side chain conformations in the binding pocket. To enable more rigorous sampling of side chain conformation of the protein as well as for the ligand, long-term

molecular dynamic simulations were performed in ‘plasma membrane-like’ conditions and the resulting conformations were analyzed.

3.4.2 Methods

1. The molecular structure of the ligand (NNQ) was sketched in SYBYL-X 2.0, and energy minimization of the structure was performed after assigning Gasteiger–Hückel charges (10,000 iterations) with the Tripos force field (TFF).
2. The X-ray crystal structures for MOR (4DKL)⁴⁴, KOR (4DJH)⁵⁰ and DOR (4EJ4)⁵⁴ were retrieved from PDB Data Bank. SYBYL-X 2.0 was also used to prepare the obtained protein coordinates for ligand docking by extracting the crystallized ligand and the fusion protein at intracellular loop 3. However, crystallographic waters were preserved. This was followed by addition of hydrogen atoms and subsequent energy minimization of only the added hydrogen atoms.
3. GOLD5.2⁹⁶, a genetic algorithm-based automated docking program was employed to dock the ligand onto these “cleaned” receptor structures. The binding site was defined to include all atoms within 10 Å of the γ -carbon atom of Asp^{3.32} for the three opioid crystal structures, along with a hydrogen bond constraint between the basic nitrogen atom and the carboxylate group oxygen atoms of Asp^{3.32}. The best CHEM-PLP-scored solutions were chosen for molecular dynamics (MD) studies.

4. Gaps in the protein sequence including those due to incorporation of the fusion proteins in the crystal structure (Leu238-Arg253 in DOR, Leu259-Arg273 in MOR and Ser255-Arg263 in KOR) and gaps due to missing electron density in crystal structure of the receptors (e.g. ECL3 of KOR, Gly300-Ser305) were modeled and refined by MODELLER 9v10.¹¹²
5. Density functional theory (DFT) calculations at the 6-31G* level were employed to calculate partial atomic charges of the NNQ atoms using NWChem 6.0.¹¹³ Force field parameters and topology files for NNQ were generated utilizing SwissParam.¹¹⁴ The atomic charges obtained from NWChem were added to the ligand topology file. The topology and parameter files were further edited, accordingly.
6. Coordinates for the spatial arrangement of the receptors within the lipid bilayer were retrieved from the Orientations of Proteins in Membranes (OPM) database.¹¹⁵ OPM estimates arrangement of transmembrane protein inside the lipid bilayer by minimizing the transfer energy of the protein from water to the lipid membrane.
7. System preparation for MD simulation –
VMD 1.9.1¹¹⁶ was used to prepare the system for MD simulations. Coordinate (pdb) and connectivity files (psf) were generated for receptor-ligand complex using the psfgen module. The VMD membrane module was employed to create a lipid bilayer of POPC (1-Palmitoyl-2-oleoylphosphatidylcholine). This was followed by addition of 30 Å of water

layers to both sides of membrane at the vertical axis, using Solvate plugin. All the waters and POPC molecules at a distance of 0.65 Å or less from the receptor-ligand complex were then deleted followed by deletion of waters within the POPC membrane. The water system was then ionized to 0.15 M of NaCl by the Autoionize plugin. (Figure 3.17 representation of MOR-NNQ-lipid bilayer-ionized water system)

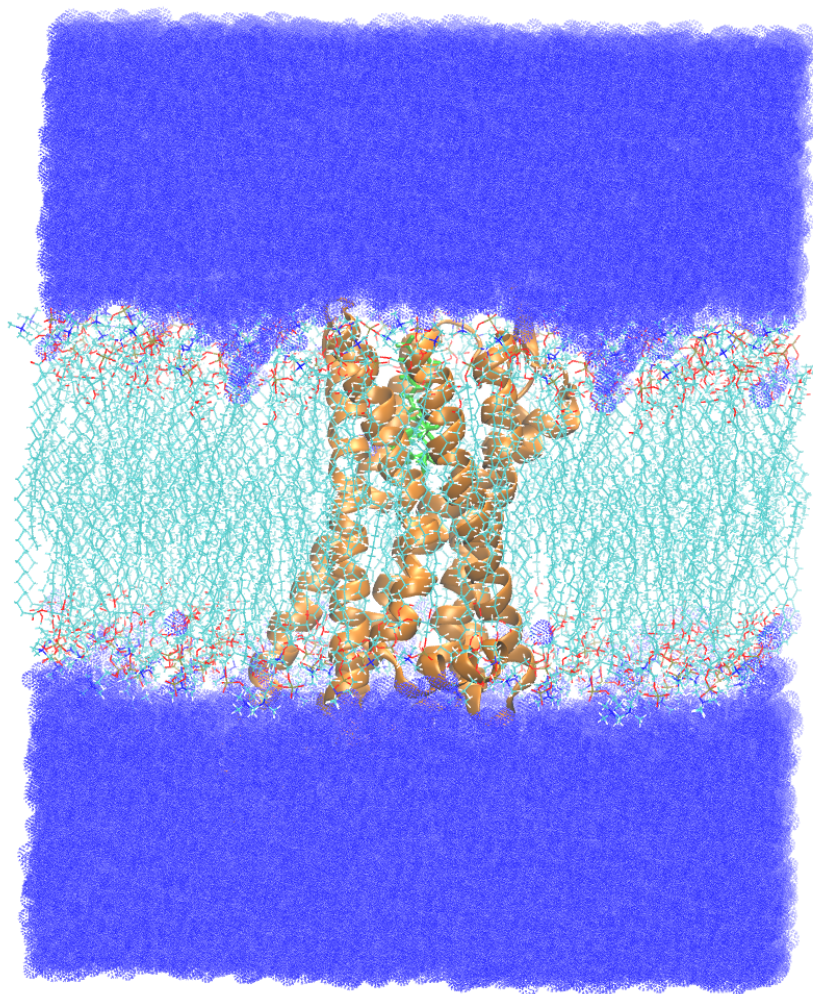


Figure 3.17. MOR(orange cartoon)-NNQ(green balls and stick)-lipid bilayer (cyan lines)-aqueous box (blue) representation. 83821 atoms, 66340 bonds, 78042 angles, 85254 dihedrals, 1137 impropers, 17837 residues, 17229 waters, 67 chloride and 49 sodium ions.

8. Melting Lipids –

All molecular modeling simulations were performed using NAMD 2.8.¹¹⁷ MD simulations were carried out in four stages. In the first stage, equilibration of the fluid-like lipid bi-layer was performed via minimization (1000 iterations) followed by NPT equilibration (pressure equilibration) of the lipid tails for a period of 0.5 ns. Simulations were carried out using the CHARMM^{118,119} force field with CHARMM22 parameters for protein, CHARMM27 parameters for lipids and CMAP corrections for proline, glycine and alanine dipeptides with a time-step of 2 femtoseconds (fs). Periodic boundary conditions were employed, and Particle Mesh Ewald (PME) summation was used to calculate long-range electrostatic interactions. Non-bonded interactions were calculated with a smooth cutoff between 10 to 12 Å with a frequency of 1 fs. Constant pressure and temperature at 310 K was maintained via Langevin dynamics.

9. Equilibration with constrained receptor-protein complex –

In the second stage, an NPT equilibration of the system was run for a period of 1 ns with harmonic constraints placed on protein, NNQ and crystallographic water atoms (5 kcal/(mol-Å)) while keeping all the parameters same as earlier.

10. Equilibration with constrained receptor-protein complex –

The harmonic restraint was released in stage 3 and the entire system was equilibrated using the NVT canonical ensemble for a further 1 ns.

11. Production Run –

The final production run was conducted using an NVT ensemble where the whole system was equilibrated for 15 ns.

12. Energy Analysis –

Energy landscape analysis was performed using the NAMD Energy 1.4 plug-in; non-bonded interaction analyses were performed at various distances with a dielectric constant of 6.5.¹²⁰ All the atoms, including protein and water molecules within a certain cutoff distance from the ligand, were included in the energy analyses. The binding modes with highest non-bonded interactions were selected for further analysis.

3.4.3 Results

Non-bonded interaction energies were calculated for NNQ-receptor complexes at four different distance cut-offs. (Table 3.11) In general, the choice of distance cut-off didn't impact non-bonded energy interactions, except at 5 Å for MOR- and KOR- receptor complexes. In the case of MOR-NNQ complex at 5 Å a decrease in Van der Waals (VDW) was observed, and for KOR-NNQ complex, a decrease in both Van der Waals (VDW) and electrostatic interactions was observed, when compared with larger distance cut-offs. For the DOR-NNQ complex the non-bonded interaction values were fairly constant.

Table 3.11. NNQ–receptor Interaction Energies (kcal/mol).

Radius ^a (Å)	MOR–NNQ			KOR–NNQ			DOR–NNQ		
	E ^b	VDW ^c	Total	E ^b	VDW ^c	Total	E ^b	VDW ^c	Total
10	-13.76	-71.64	-85.40	-22.52	-66.35	-88.87	-8.37	-63.49	-71.86
8	-14.69	-69.89	-84.58	-21.43	-66.04	-87.47	-8.18	-63.24	-71.42
6	-17.44	-67.83	-85.27	-23.00	-62.90	-85.90	-6.71	-63.82	-70.53
5	-16.45	-63.89	-80.34	-19.27	-58.52	-77.79	-11.70	-60.49	-72.19

^aDistance from the docked ligand NNQ; ^bE: Electrostatic interaction; ^cVDW: Van der Waals' interaction.

3.4.3.a Binding mode of NNQ in MOR

In the best scored non-bonded interaction pose for the NNQ-MOR complex the morphinan skeleton of the molecule agreed with the binding pose of the crystallographic ligand. (Figure 3.18) The morphinan core resided inside a hydrophobic pocket lined by Met^{3.36}, Trp^{6.48}, Ile^{7.39} and Tyr^{7.43}. The His^{6.52} conformation showed a plausible of hydrogen bond interaction with the phenoxy oxygen through a water molecule. Asp^{3.32} was involved in interactions with both the protonated nitrogen of the core and the 14-position hydroxyl. The amide linker also formed a hydrogen bond with backbone carbonyl of Ile^{6.51} through a water molecule. The nitro-isoquinoline group of the functionalized moiety was placed towards TM5, where its nitro group may form a water-mediated hydrogen bonding network with Glu^{5.35}. Notably, position 5.35 was one of the sites identified (site 2) as an alternative 'address' site for NAP and NAQ.

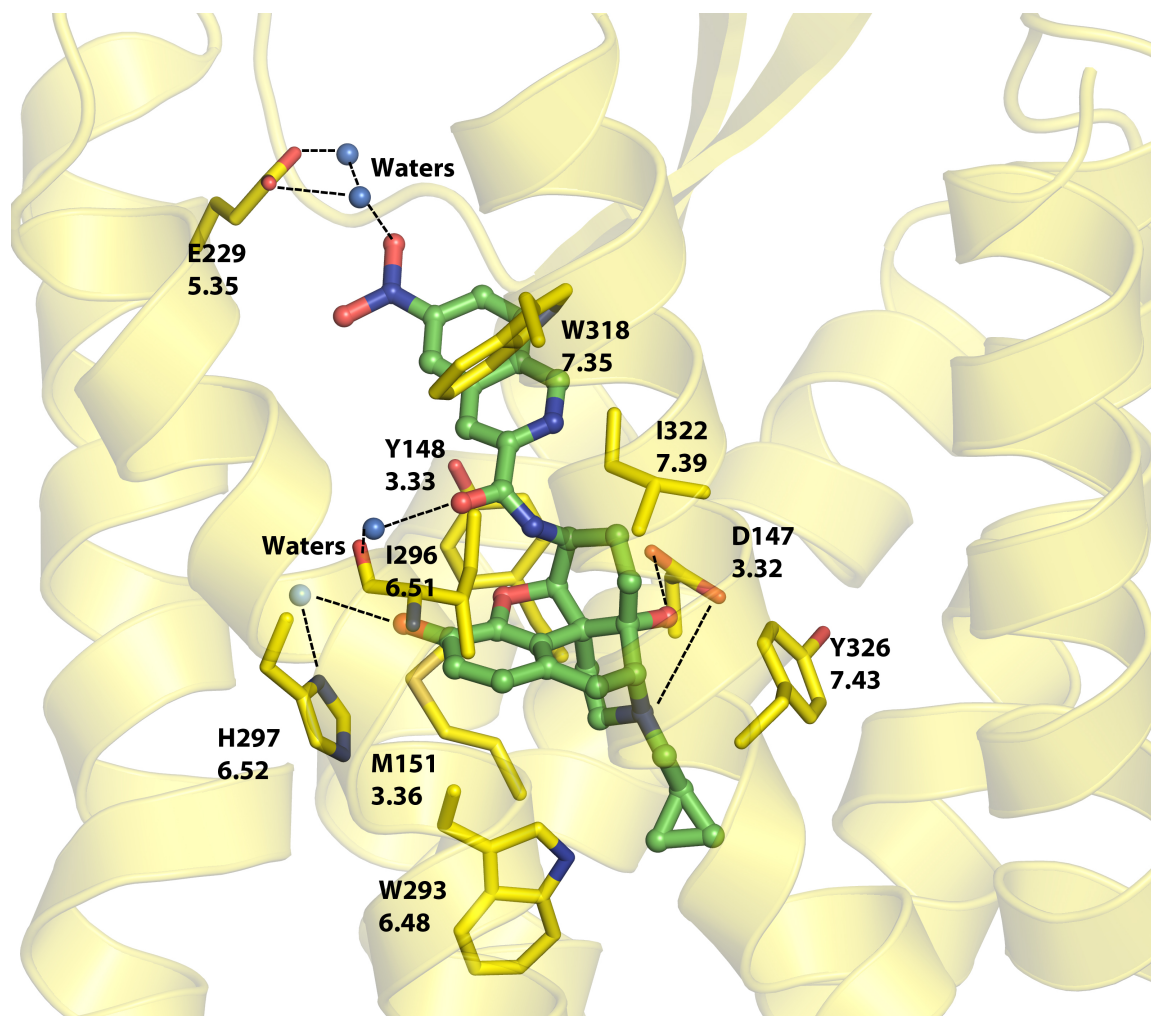


Figure 3.18. NNQ in green balls and sticks, interacting MOR residues in sticks (with both residue and Ballesteros–Weinstein indices), ionic interaction including hydrogen bonding interactions shown with black broken lines.

3.4.3.b Binding mode of NNQ in KOR

The morphinan docking pose inside KOR was similar to that observed in MOR. Met3.36, Trp6.48, Leu3.29 and Tyr7.43 formed a hydrophobic pocket surrounding the core skeleton. Asp^{3.32} also exhibited similar interactions with protonated amine and the 14-position hydroxyl, and His^{6.52} formed a hydrogen bonding network around the phenoxy oxygen through water

molecules. However, placement of the nitroisoquinoline moiety showed variation, instead of residing close to TM5, the functionalized moiety was placed between TM2, 3 and 7. The nitro group is involved in an interaction between backbone Ser210 (ECL2) and Gln^{2.60}. This binding mode was different than ‘address’ sites identified earlier as ‘site 1’ and ‘site 2’.

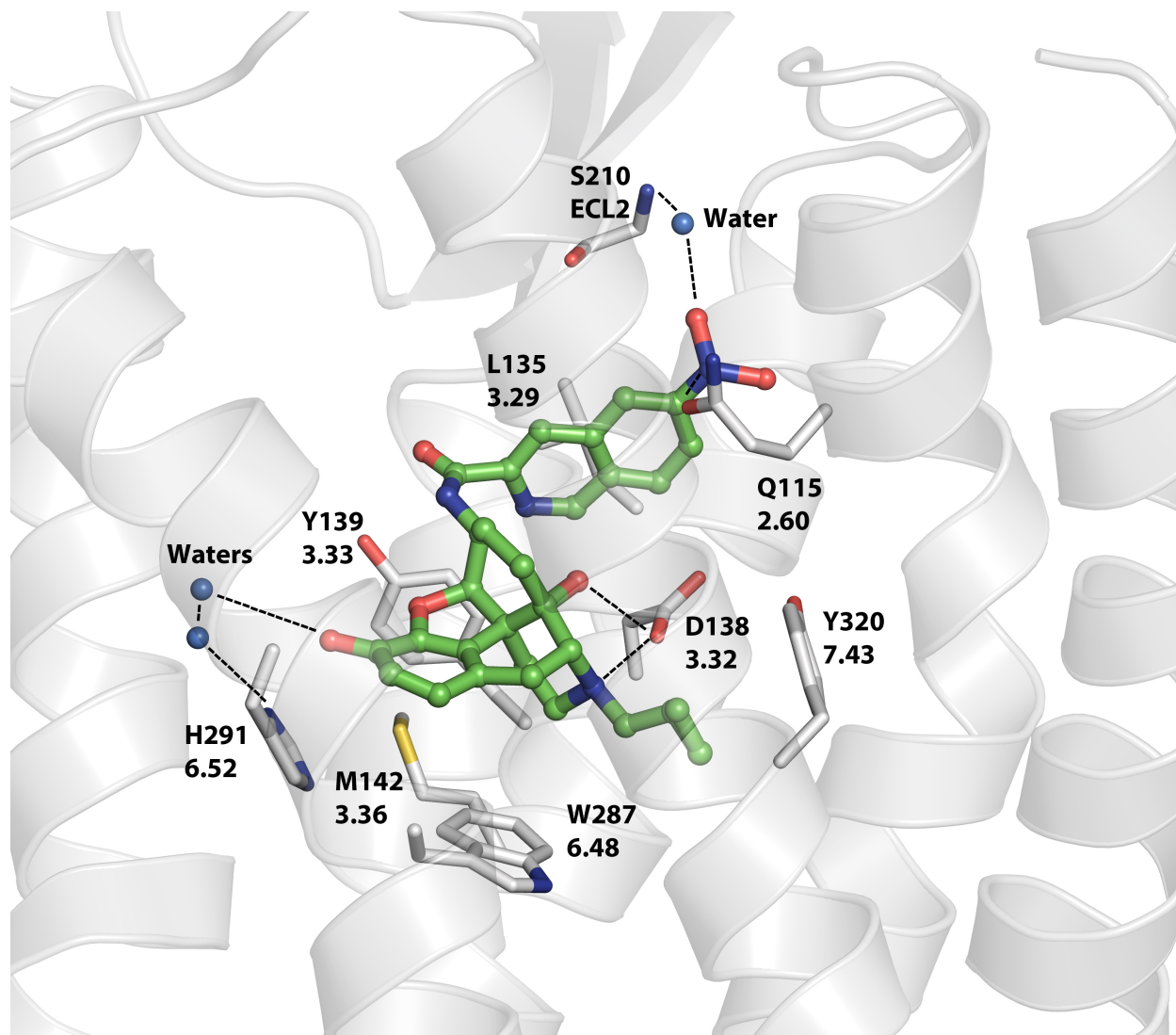


Figure 3.19. NNQ in green balls and sticks, interacting KOR residues in sticks (with both residue and Ballesteros–Weinstein indices), ionic interaction including hydrogen bonding interactions shown with black broken lines.

3.4.3.c Binding mode of NNQ in DOR

Although similar residues were involved in forming hydrophobic linings around the morphinan skeleton, there was an overall displacement of the core, with the nitroisoquinoline substituent directed towards TM7. In this binding mode, the nitro group can form interaction with the ECL3 arginine and TM7 His^{7.36}. Due to displacement of the morphinan skeleton, the conserved acidic Asp^{3.32} was now directed away from the protonated nitrogen. Hence, only one interaction (between Asp and 14-hydroxyl) is plausible, as evidenced by low electrostatic energy for DOR complexes.

Comparison between binding modes of NNQ on MOR, KOR and DOR

In MOR-NNQ complex the functionalized nitroisoquinoline moiety occupies the ‘address’ region identified as ‘Site 2’, where it forms hydrogen bonding interactions with Glu^{5.35} through waters. This glutamate residue is a non-conserved residue among the opioid receptors. In the KOR and the DOR this residue is replaced by one carbon shorter acidic residue, aspartate. According to the binding models generated here, interactions through water bridges may not be possible for DOR and KOR. Hence, NNQ adopts a different binding mode in the DOR and the KOR. In KOR, loss of ‘site 2’ interactions is compensated by interactions at TM7 and ECL2. However, in DOR it is also accompanied by loss of ionic bridge interactions between the protonated amine and the conserved aspartate.

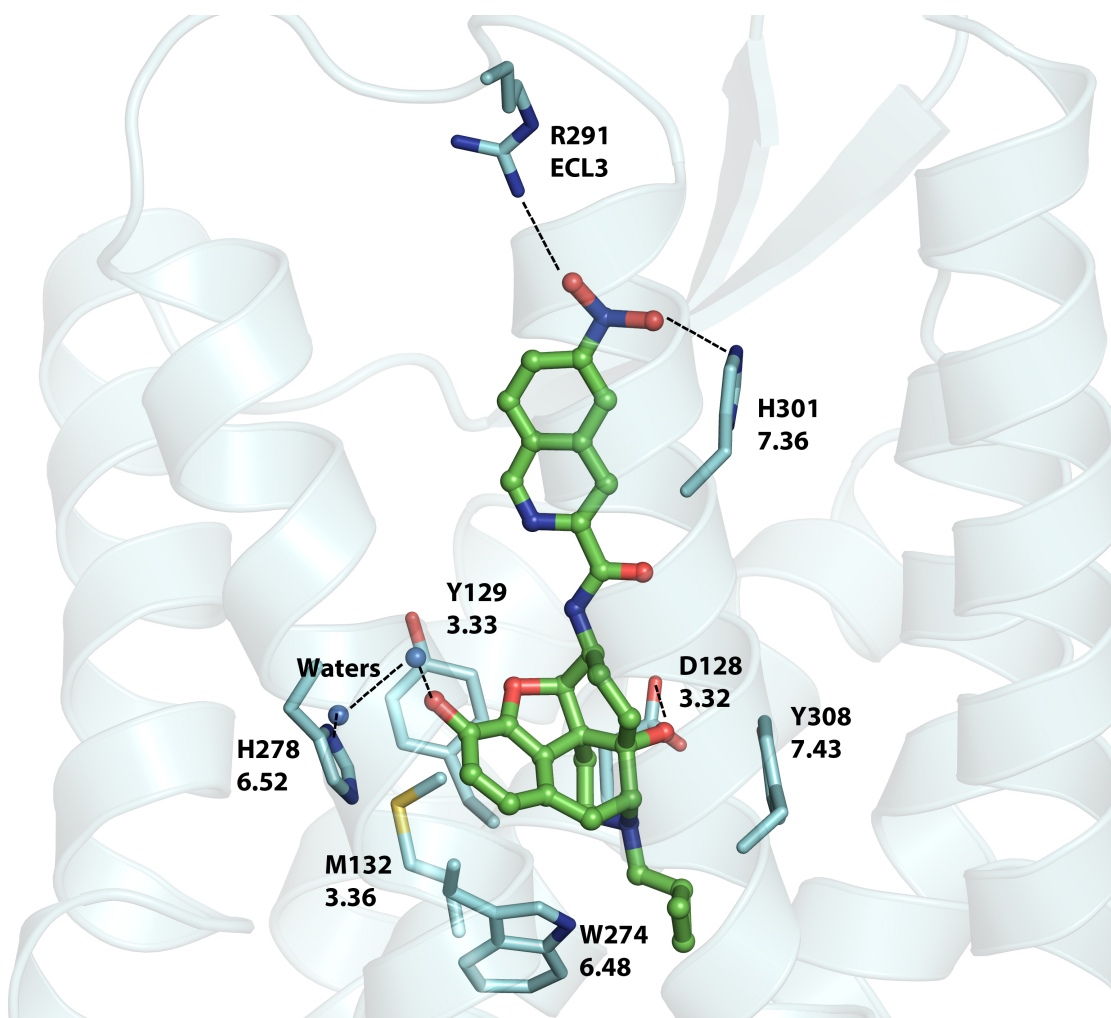


Figure 3.20. NNQ in green balls and sticks, interacting DOR residues in sticks (with both residue and Ballesteros–Weinstein indices), ionic interaction including hydrogen bonding interactions shown with black broken lines.

3.4.4 Conclusions

When compared to NAQ, NNQ shows a 10-fold decrease in selectivity towards MOR over KOR, and a 15-fold decrease in selectivity towards MOR over DOR. This decrease in selectivity is primarily due to the 10-fold loss of binding affinity of NNQ to MOR. According to the model

discussed earlier in the section 3.2.4, inclusion of the nitro group on the heteroaromatic substituent can have a dual effect on the MOR binding. The nitro group can act as a hydrogen bond acceptor towards the lysine residue at position 6.58 of site 1 in MOR. However, the cation- π interactions are expected to decrease due to the strong electron withdrawing character of the nitro group. The docking followed by a 15 ns equilibration study presented here indicates that the NNQ prefers site 2 ‘address’ instead. The interactions between the acidic glutamate residue at position 5.35 and the nitro group are mediated through water molecules.

The nitro group on the heteroaromatic substitution, according the previous model, is expected to decrease the KOR-NNQ binding due to the presence of an acidic glutamate residue at position 6.58 of site 1 in KOR. Possibly, the presence of aspartate instead of glutamate at position 5.35 in KOR hampers the interactions seen for the MOR at site 2 through a single water molecule bridge. However, the nitro isoquiniline substitution locates another ‘address’ region, the region identified earlier for the 14-substituted naltrexone derivatives where the nitro group interacts with the conserved glutamine residue at position 2.60 and with the Ser210 of the ECL2.

There is only a slight increase in DOR binding for NNQ with respect to NAQ, even after the addition of two new plausible interactions of the nitro group with hydrogen bond donors at helix 7 and ECL3. This may be because of dislocation of the ‘morphinan’ nucleus resulting in decreased interactions with the conserved acidic residue at position 3.32.

These results underline the possibility of multiple address regions in a receptor that a ligand can avail. A ligand itself can also have multiple binding modes and the equilibrium between those binding modes is a function of characteristics a substitution imparts to the ligand. The study also indicates the importance of including water molecules in modeling the selectivity

of opioid ligands. The tightly held water molecules on the surface of the protein may add exploitable features on the 'address' region of the receptor. So it may be advisable to incorporate dual functionalized substituent moieties to design further selective compounds.

3.5 Discussion

The development of MOR selective antagonists requires identification of distinct address sites on the MOR. Following the identification of the address loci on the receptor, suitable substitutions can be made on the universal antagonists that may help in discriminating among the opioid receptors. One such address loci was identified based on the homology models of the opioid receptors. The docking studies of the universal antagonist, naltrexone, suggested two plausible positions for substitutions to exploit the identified address loci in MOR – 6(C) and 14(C) of the naltrexone.

The docking studies on 6-position substituted naltrexone derivatives validated the address loci identified in the homology model. Furthermore, an alternate ‘address’ locus was identified by sequence alignment and docking studies on the 6-position substituted derivatives. The model suggested the presence of two address regions in the opioid receptors and the ligand could adopt conformations that allow interactions with either of the address loci.

The docking studies on 14-position substituted naltrexone derivatives indicated presence of a third address region, formed due to the conformation adopted by an otherwise conserved residue side chain.

The long term MD simulation studies of second generation NNQ, a 6(C)-substituted naltrexone derivative, inside the opioid receptors embedded in the lipid bilayer iterated the importance of address loci identified previously. However, the nature of the interactions between the address loci on the receptor and the substituents was different from the interactions conceived in the previous model, especially due to incorporation of water molecules in the model.

Furthermore, a functionalized moiety also improved the binding of NNQ to KOR and DOR via interactions to the regions identified earlier and the new regions respectively.

The ability of ligands to adopt different conformations and the presence of multiple ‘address’ sites on the opioid receptors complicates the directed design of selective opioid ligands based on the ‘message-address’ concept. The presence of multiple address sites suggests that more selective ligands can be developed with multiple functionalized moieties that may interact with more than one address region in one conformation or restrict the binding mode of the ligand to a single conformation.

Overall, the work presented here represents the progression of ligand-receptor interaction models from a simple homology modeling based model to a lipid embedded-crystal structure based model. Continued application of the ‘message-address’ concept based on identification of address site interactions can help in guided synthesis of MOR selective antagonists.

Reference:

- (1) Brownstein, M. J. Review A Brief History of Opiates, Opioid Peptides, and Opioid Receptors. *Proc. Natl. Acad. Sci. U. S. A.* **1993**, *90*, 5391–5393.
- (2) Serturmer, F. W. A. *J. Pharm. f. Arzte. Apoth. Chem.* **1806**, *14*, 47-93.
- (3) Serturmer, F. W. A. *Gilbert's Ann. d. Physik.* **1817**, *25*, 56-89.
- (4) Wright, C. R. A. On the action of organic acids and their anhydrides on the natural alkaloids. *J. Chem. Soc.* **1874**, *12*, 1031.
- (5) Weijlard, J.; Erikson, A. E. N-allylnormorphine. *J. Am. Chem. Soc.* **1942**, *64*, 869-870.
- (6) Unna, K. Antagonistic effect of N-Allyl-Norporphine upon morphine. *J. Pharmacol. Exp. Ther.* **1943**, *79*, 27-31.
- (7) Simon, E. J.; Hiller, J. M.; Edelman, I. Stereospecific Binding of the Potent Narcotic Analgesic [³H] Etorphine to rat-brain homogenate. *Proc. Natl. Acad. Sci. U. S. A.* **1973**, *70*, 1947–1949.
- (8) Pert, C. B.; Snyder, S. H. Opiate receptor: demonstration in nervous tissue. *Science* **1973**, *179*, 1011-1014.
- (9) Trenius, L. Characteristics of the "receptor" for narcotic analgesics in synaptic plasma membrane fraction from rat brain. *Acta. Pharmacol. Toxicol.* 1973, *33*, 377-384.
- (10) Pasternak, G. W.; Pan, Y. Mu Opioids and Their Receptors: Evolution of a Concept. *Pharmacol. Rev.* **2013**, *65*, 1257–1317.
- (11) Kosterlitz, H. W.; Waterfield, A. A. In vitro models in the study of structure-activity relationships of narcotic analgesics. *Annu. Rev. Pharmacol. Toxicol.* **1975**, *15*, 29-47.
- (12) Hughes, J.; Smith, T. W.; Kosterlitz, W.; Fothergil, L. A.; Morgan, B. A.; Morris, H. R. *Nature* **1975**, *258*, 577-579.
- (13) Erspamer, V.; Melchiorri, P.; Falconieri-Erspamer, G.; Negri, L.; Corsi, R.; Severini, C.; Barra, D.; Simmaco, M.; Kreil, G. Deltorphins: A Family of Naturally Occurring Peptides with High Affinity and Selectivity for Delta Opioid Binding Sites. *Proc. Natl. Acad. Sci. U. S. A.* **1989**, *86*, 5188–5192.
- (14) Goldstein, A; Fischli, W.; Lowney, L. I.; Hunkapiller, M.; Hood, L. Porcine Pituitary Dynorphin: Complete Amino Acid Sequence of the Biologically Active Heptadecapeptide. *Proc. Natl. Acad. Sci. U. S. A.* **1981**, *78*, 7219–7223.

- (15) Martin, W. R.; Eades, C. G.; Thompson, J. A.; Huppler, R. E.; Gilbert, P. E. *J. Pharmacol. Exp. Ther.* **1975**, *197*, 517-532.
- (16) Lord, J. A. H.; Waterfield, A. A.; Hughes, J.; Kosterlitz, H. W. *Nature* **1975**, *267*, 495-499.
- (17) Arsenal, E. Localization of the Antinociceptive Action of Morphine in Primate Brain. *Pharmacol. Biochem. Behav.* **1975**, *3*, 133-138.
- (18) Akil, H.; Mayer, D. J.; Liebeskind, J. C. Antagonism of Stimulation-Produced Analgesia by Naloxone. *Science* **1976**, *191*, 961-962.
- (19) Pasternak, G. W.; Snyder, S. H. Opiate receptor binding: effects of enzymatic treatments. *Mol. Pharmacol.* **1973**, *10*, 183-193.
- (20) Li, S.; Zhu, J.; Chen, C.; Chen, Y. W.; Deriel, J. K.; Ashby, B.; Liu-Chen, L. Y. Molecular Cloning and Expression of a Rat Kappa Opioid Receptor. *Biochem. J.* **1993**, *295*, 629-633.
- (21) Evans, C. J.; Keith, D. E.; Morrison, H.; Magendzo, K.; Edwards, R. H. Cloning of a Delta Opioid Receptor by Functional Expression. *Science* **1992**, *258*, 1952-1955.
- (22) Chen, Y.; Mestak, A.; Liu, J.; Hurley, J. A.; Yu, L. Molecular Cloning and Functional Receptor from Rat Brain Expression of a μ -Opioid Receptor from Rat Brain. *Mol. Pharmacol.* **1993**, *44*, 8-12.
- (23) Law, P.; Loh, H. H. Regulation of opioid receptor activities. *J. Pharm. Exp. Ther.* **1994**, *289*, 607-624.
- (24) Barchfeld, C. C.; Medzihradsky, A. Receptor-mediated stimulation of brain GTPase by opiates in normal and dependent rats. *Biochem. Biophys. Res. Commun.* **1984**, *121*, 641-648.
- (25) Minneman, K. P.; Iversen, L. L. Enkephalin and opiate narcotics increase cyclic GMP accumulation in slices of rat neostriatum. *Nature* **1976**, *262*, 313-314.
- (26) Taussig, R.; Iñiguez-lluhi, J. A.; Gilman, A. G.; Iniguez-lluhi, J. A. Inhibition of Adenylyl Cyclase by $G_{i\alpha}$. **1993**, *261*, 218-221.
- (27) Hsia, J. A.; Moss, J.; Hewlett, E. L.; Vaughans, M. ADP-Ribosylation of Adenylate Cyclase by Pertussis Toxin. *J. Biol. Chem.* **1984**, *259*, 1086-1090.
- (28) Wickman, K.; Clapham, E. Ion Channel Regulation by G Proteins. *Pharmacol. Rev.* **1995**, *75*, 865-876.

- (29) Sadjia, R.; Alagem, N.; Reuveny, E. Gating of GIRK Channels: Details of an Intricate, Membrane-Delimited Signaling Complex. *Neuron* **2003**, *39*, 9–12.
- (30) Ippolito, D. L.; Temkin, P. A.; Rogalski, S. L.; Chavkin, C. N-Terminal Tyrosine Residues within the Potassium Channel Kir3 Modulate GTPase Activity of G-alpha_i. *J. Biol. Chem.* **2002**, *277*, 32692–32696.
- (31) Zamponi, G. W.; Snutch, T. P. Modulation of Voltage-Dependent Calcium Channels by g proteins. *Curr. Opin. Neurobiol.* **1998**, *8*, 351–356.
- (32) Rusin, K. I.; Giovannucci, D. R.; Stuenkel, E. L.; Moises, H. C. Kappa-Opioid Receptor Activation Modulates Ca²⁺ Currents and Secretion in Isolated Neuroendocrine Nerve Terminals. *J. Neurosci.* **1997**, *17*, 6565–6574.
- (33) Chavkin, C.; McLaughlin, J. P.; Celver, J. P. Regulation of Opioid Receptor Function by Chronic Agonist Exposure: Constitutive Activity and Desensitization. *Mol. Pharmacol.* **2001**, *60*, 20–25.
- (34) Guo, J.; Wu, Y.; Zhang, W.; Zhao, J.; Devi, L. a; Pei, G.; Ma, L. Identification of G Protein-Coupled Receptor Kinase 2 Phosphorylation Sites Responsible for Agonist-Stimulated Delta-Opioid Receptor Phosphorylation. *Mol. Pharmacol.* **2000**, *58*, 1050–1056.
- (35) Pei, G.; Kieffer, B. L.; Lefkowitz, R. J.; Freedman, N. J. Agonist-Dependent Phosphorylation of the Mouse μ -Opioid Receptor: Involvement of G Protein-Coupled Receptor Kinases But Not Protein Kinase C. *Mol. Pharmacol.* **1995**, *48*, 173–177.
- (36) Al-Hasani, R.; Bruchas, M. R. Molecular Mechanisms of Opioid Receptor-Dependent Signaling and Behavior. *Anesthesiology* **2011**, *115*, 1363-1381.
- (37) Belcheva, M. M.; Vogel, Z.; Ignatova, E.; Avidor-Reiss, T.; Zippel, R.; Levy, R.; Young, E. C.; Barg, J.; Coscia, C. J. Opioid Modulation of Extracellular Signal-Regulated Protein Kinase Activity Is Ras-Dependent and Involves Gbetagamma Subunits. *J. Neurochem.* **1998**, *70*, 635–645.
- (38) Minden, A; Karin, M. Regulation and Function of the JNK Subgroup of MAP Kinases. *Biochim. Biophys. Acta* **1997**, *1333*, 85–104.
- (39) Tibbles, L. A; Woodgett, J. R. The Stress-Activated Protein Kinase Pathways. *Cell. Mol. Life Sci.* **1999**, *55*, 1230–1254.
- (40) Trescot, A. M.; Datta, S.; Lee, M.; Hansen, H. Opioid Pharmacology. *Pain Physician* **2008**, *1975*, 133–154.

- (41) Harrison, R. S.; Ruiz-Gómez, G.; Hill, T. A.; Chow, S. Y.; Shepherd, N. E.; Lohman, R.-J.; Abbenante, G.; Hoang, H. N.; Fairlie, D. P. Novel Helix-Constrained Nociceptin Derivatives Are Potent Agonists and Antagonists of ERK Phosphorylation and Thermal Analgesia in Mice. *J. Med. Chem.* **2010**, *53*, 8400–8408.
- (42) Dang, V. C.; Christie, M. J. Mechanisms of Rapid Opioid Receptor Desensitization, Resensitization and Tolerance in Brain Neurons. *Br. J. Pharmacol.* **2012**, *165*, 1704–1716.
- (43) Groer, C. E.; Schmid, C. L.; Jaeger, A. M.; Bohn, L. M. Agonist-Directed Interactions with Specific Beta-Arrestins Determine Mu-Opioid Receptor Trafficking, Ubiquitination, and Dephosphorylation. *J. Biol. Chem.* **2011**, *286*, 31731–31741.
- (44) Manglik, A.; Kruse, A. C.; Kobilka, T. S.; Thian, F. S.; Mathiesen, J. M.; Sunahara, R. K.; Pardo, L.; Weis, W. I.; Kobilka, B. K.; Granier, S. Crystal Structure of the M-Opioid Receptor Bound to a Morphinan Antagonist. *Nature* **2012**, *485*, 321–326.
- (45) Wu, B.; Chien, E. Y. T.; Mol, C. D.; Fenalti, G.; Liu, W.; Katritch, V.; Abagyan, R.; Brooun, A.; Wells, P.; Bi, F. C.; Hamel, D. J.; Kuhn, P.; Handel, T. M.; Cherezov, V.; Stevens, R. C. Structures of the CXCR4 Chemokine GPCR with Small-Molecule and Cyclic Peptide Antagonists. *Science* **2010**, *330*, 1066–1071.
- (46) Cherezov, V.; Rosenbaum, D. M.; Hanson, M. A.; Rasmussen, S. G. F.; Thian, F. S.; Kobilka, T. S.; Choi, H. J.; Kuhn, P.; Weis, W. I.; Kobilka, B. K.; Stevens, R. C. High-Resolution Crystal Structure of an Engineered Human beta2-Adrenergic G Protein-Coupled Receptor. *Science* **2007**, *318*, 1258–1265.
- (47) Palczewski, K. Crystal Structure of Rhodopsin: A G Protein-Coupled Receptor. *Science* **2000**, *289*, 739–745.
- (48) Cox, B. M. Recent Developments in the Study of Opioid Receptors. *Mol. Pharmacol.* **2013**, *83*, 723–728.
- (49) Van't Veer, A.; Carlezon, W. A. Role of Kappa-Opioid Receptors in Stress and Anxiety-Related Behavior. *Psychopharmacology* **2013**, *229*, 435–452.
- (50) Wu, H.; Wacker, D.; Mileni, M.; Katritch, V.; Han, G. W.; Vardy, E.; Liu, W.; Thompson, A. A.; Huang, X. P.; Carroll, F. I.; Mascarella, S. W.; Westkaemper, R. B.; Mosier, P. D.; Roth, B. L.; Cherezov, V.; Stevens, R. C. Structure of the Human K-Opioid Receptor in Complex with JD1c. *Nature* **2012**, *485*, 327–332.
- (51) Gendron, L.; Mittal, N.; Beaudry, H.; Walwyn, W. Recent Advances on the Delta Opioid Receptor: From Trafficking to Function. *Br. J. Pharmacol.* **2014**, 1–54.

- (52) Przewlocki, R. Opioid Abuse and Brain Gene Expression. *Eur. J. Pharmacol.* **2004**, *500*, 331–349.
- (53) Zhao, P.; Ma, M. C.; Qian, H.; Xia, Y. Down-Regulation of Delta-Opioid Receptors in Na⁺/H⁺ Exchanger 1 Null Mutant Mouse Brain with Epilepsy. *Neurosci. Res.* **2005**, *53*, 442–446.
- (54) Granier, S.; Manglik, A.; Kruse, A. C.; Kobilka, T. S.; Thian, F. S.; Weis, W. I.; Kobilka, B. K. Structure of the δ -Opioid Receptor Bound to Naltrindole. *Nature* **2012**, *485*, 400–404.
- (55) Fenalti, G.; Giguere, P. M.; Katritch, V.; Huang, X. P.; Thompson, A. A.; Cherezov, V.; Roth, B. L.; Stevens, R. C. Molecular Control of δ -Opioid Receptor Signalling. *Nature* **2014**, *506*, 191–196.
- (56) Zimmerman, D. M.; Leander, J. D. Selective Opioid Receptor Agonists and Antagonists: Research Tools and Potential Therapeutic Agents. *J. Med. Chem.* **1990**, *33*, 895–902.
- (57) Eguchi, M. Recent Advances in Selective Opioid Receptor Agonists and Antagonists. *Med. Res. Rev.* **2004**, *24*, 182–212.
- (58) Matthes, H. W.; Maldonado, R.; Simonin, F.; Valverde, O.; Slowe, S.; Kitchen, I.; Befort, K.; Dierich, A.; Meur, M.; Dolle, P.; Tzavara, E.; Hanoune, J.; Roques, B. P.; Kieffer, B. L. Loss of morphine-induced analgesia, reward effect and withdrawal symptoms in mice lacking the μ -opioid-receptor gene. *Nature* **1996**, *383*, 819–823.
- (59) Skoubis, P. D.; Matthes, H. W.; Walwyn, W. M.; Kieffer, B. L.; Maidment, N. T. Naloxone Fails to Produce Conditioned Place Aversion in Mu-Opioid Receptor Knock-out Mice. *Neuroscience* **2001**, *106*, 757–763.
- (60) Gavériaux-Ruff, C.; Kieffer, B. L. Opioid Receptor Genes Inactivated in Mice: The Highlights. *Neuropeptides* **2002**, *36*, 62–71.
- (61) World Drug Report 2012; Report from the United Nations Office on Drugs and Crime: New York, June, 2012; http://www.unodc.org/documents/data-and-analysis/WDR2012/WDR_2012_web_small.pdf.
- (62) Bart, G. Maintenance Medication for Opiate Addiction: The Foundation of Recovery. *J. Addict. Dis.* **2012**, *31*, 207–225.
- (63) Veilleux, J. C.; Colvin, P. J.; Anderson, J.; York, C.; Heinz, A. J. A Review of Opioid Dependence Treatment: Pharmacological and Psychosocial Interventions to Treat Opioid Addiction. *Clin. Psychol. Rev.* **2010**, *30*, 155–166.

- (64) Stotts, A. L.; Dodrill, C. L.; Kosten, T. R. Opioid Dependence Treatment: Options in Pharmacotherapy. *Expert Opin. Pharmacother.* **2009**, *10*, 1727–1740.
- (65) Isbell, H.; Vogel, V. H. The addiction liability of methadone (amidone, dolophine, 10820) and its use in the treatment of the morphine abstinence syndrome. *Am. J. Psychiatry* **1949**, *105*, 909–914.
- (66) Walsh, S. L.; Preston, K. L.; Stitzer, M. L.; Cone, E. J.; Bigelow, G. E. Clinical Pharmacology of Buprenorphine: Ceiling Effects at High Doses. *Clin. Pharmacol. Ther.* **1994**, *55*, 569–580.
- (67) Krupitsky, E.; Nunes, E. V.; Ling, W.; Illeperuma, A.; Gastfriend, D. R.; Silverman, B. L. Injectable Extended-Release Naltrexone for Opioid Dependence: A Double-Blind, Placebo-Controlled, Multicentre Randomised Trial. *Lancet* **2011**, *377*, 1506–1513.
- (68) Comer, S.; Sullivan, M. A.; Yu, E.; Rothenberg, J. L.; Kleber, H. D.; Kampman, K.; Dackis, C.; Brien, C. P. O. Injectable, Sustained-Release Naltrexone for the Treatment of Opioid Dependence. *Arch. Gen. Psychiatry* **2014**, *63*, 210–216.
- (69) Updating Estimates of the Economic Costs of Alcohol Abuse in the United States: Estimates, Update Methods, and Data; National Institute on Alcohol Abuse and Alcoholism: Bethesda, MD, 2000.
- (70) Kieffer, B. L.; Gavériaux-Ruff, C. Exploring the Opioid System by Gene Knockout. *Prog. Neurobiol.* **2002**, *66*, 285–306.
- (71) Contet, C.; Kieffer, B. L.; Befort, K. Mu Opioid Receptor: A Gateway to Drug Addiction. *Curr. Opin. Neurobiol.* **2004**, *14*, 370–378.
- (72) Gold, M. S.; Dackis, C. A.; Pottash, A. L.; Sternbach, H. H.; Annitto, W. J.; Martin, D.; Dackis, M. P. Naltrexone, Opiate Addiction, and Endorphins. *Med. Res. Rev.* **1982**, *2*, 211–246.
- (73) Gonzalez, J. P.; Brogden, R. N. A review of its pharmacodynamic and pharmacokinetic properties and therapeutic efficacy in the management of opioid dependence. *Drugs* **1988**, *35*, 192–213.
- (74) Soyka, M.; Roesner, S. New Pharmacological Approaches for the Treatment of Alcoholism. *Expert Opin. Pharmacother.* **2006**, *7*, 2341–2353.
- (75) Oslin, D. W.; Berrettini, W. H.; O'Brien, C. P. Targeting Treatments for Alcohol Dependence: The Pharmacogenetics of Naltrexone. *Addict. Biol.* **2006**, *11*, 397–403.

- (76) Anton, R. F. Naltrexone for the Management of Alcohol Dependence. *N. Engl. J. Med.* **2008**, *359*, 715–721.
- (77) Miotto, K.; Mccann, M.; Basch, J.; Rawson, R.; Ling, W. Naltrexone and Dysphoria : Fact or Myth? *Am. J. Addict.* **2002**, *11*, 151–160.
- (78) Ritter, A. J. Naltrexone in the Treatment of Heroin Dependence: Relationship with Depression and Risk of Overdose. *Aust. N. Z. J. Psychiatry* **2002**, *36*, 224–228.
- (79) Van Dorp, E. L. A.; Yassen, A.; Dahan, A. Naloxone Treatment in Opioid Addiction: The Risks and Benefits. *Expert Opin. Drug Saf.* **2007**, *6*, 125–132.
- (80) Niciu, M. J.; Arias, A. J. Targeted Opioid Receptor Antagonists in the Treatment of Alcohol Use Disorders. *CNS Drugs* **2013**, *27*, 777–787.
- (81) South, T.; Deng, C.; Huang, X. F. AM 251 and Beta-Funaltrexamine Reduce Fat Intake in a Fat-Preferring Strain of Mouse. *Behav. Brain Res.* **2007**, *181*, 153–157.
- (82) Ward, J.; Portoghese, P. S.; Takemori, E. Pharmacological characterization of *in vivo* of a novel opiate, β -Funaltrexamine. *J. Pharm. Exp. Ther.* **1982**, 494–498.
- (83) Broadbear, J. H.; Sumpter, T. L.; Burke, T. F.; Husbands, S. M.; Lewis, J. W.; Woods, J. H.; Traynor, J. R. Methocinnamox Is a Potent, Long-Lasting, and Selective Antagonist of Morphine-Mediated Antinociception in the Mouse: Comparison with Clocinnamox, Beta-Funaltrexamine, and Beta-Chlornaltrexamine. *J. Pharmacol. Exp. Ther.* **2000**, *294*, 933–940.
- (84) Schmidhammer, H.; Burkard, W. P.; Eggstein-Aeppli, L.; Smiths, C. F. C. Synthesis and Biological Evaluation of 14-Alkoxymorphinans. 2(-)-N-(Cyclopropylmethyl)-4,12-dimethoxymorphinan-6-one, a selective μ opioid receptor antagonist. *J. Med. Chem.* **1989**, 418–421.
- (85) Spetea, M.; Schüllner, F.; Moisa, R. C.; Berzetei-Gurske, I. P.; Schraml, B.; Dörfler, C.; Aceto, M. D.; Harris, L. S.; Coop, A.; Schmidhammer, H. Synthesis and Biological Evaluation of 14-Alkoxymorphinans. 21. Novel 4-Alkoxy and 14-Phenylpropoxy Derivatives of the Mu Opioid Receptor Antagonist Cyprodime. *J. Med. Chem.* **2004**, *47*, 3242–3247.
- (86) Kramer, T. H.; Shook, J. E.; Kazmierski, W.; Ayres, E. A.; Wire, W. S.; Hruby, V. J.; Burks, T. F. Novel Peptidic Mu Opioid Antagonists : Characterization in Vitro and in Vivo. *J. Pharmacol. Exp. Ther.* **1989**, 544–551.
- (87) Abbruscato, T. J.; Thomas, S. A; Hruby, V. J.; Davis, T. P. Blood-Brain Barrier Permeability and Bioavailability of a Highly Potent and Mu-Selective Opioid Receptor

- Antagonist, CTAP: Comparison with Morphine. *J. Pharmacol. Exp. Ther.* **1997**, *280*, 402–409.
- (88) Schwyzer, R. ACTH: a short introductory review. *Ann. N. Y. Acad. Sci.* **1977**, *297*, 3-26
- (89) Chavkin, C.; Goldstein, a. Specific Receptor for the Opioid Peptide Dynorphin: Structure-Activity Relationships. *Proc. Natl. Acad. Sci. U. S. A.* **1981**, *78*, 6543–6547.
- (90) Jones, R. M.; Hjorth, S. A.; Schwartz, T. W.; Portoghese, P. S. Communications to the Editor. **1998**, *41*, 0–3.
- (91) Portoghese, P. S.; Sultana, M.; Nagase, H.; Takemori, A. E. Applications of the message-address concept in the design of highly potent and selective non-peptide δ opioid receptor anatagonists. *J. Med. Chem.* **1988**, *31*, 1986–1987.
- (92) Li, G.; Aschenbach, L. C.; Chen, J.; Cassidy, M. P.; Stevens, D. L.; Gabra, B. H.; Selley, D. E.; Dewey, W. L.; Westkaemper, R. B.; Zhang, Y. Design, Synthesis, and Biological Evaluation of 6alpha- and 6beta-N-Heterocyclic Substituted Naltrexamine Derivatives as Mu Opioid Receptor Selective Antagonists. *J. Med. Chem.* **2009**, *52*, 1416–1427.
- (93) Yuan, Y.; Zaidi, S. A.; Elbegdorj, O.; Aschenbach, L. C. K.; Li, G.; Stevens, D. L.; Scoggins, K. L.; Dewey, W. L.; Selley, D. E.; Zhang, Y. Design, Synthesis, and Biological Evaluation of 14-Heteroaromatic-Substituted Naltrexone Derivatives: Pharmacological Profile Switch from Mu Opioid Receptor Selectivity to Mu/kappa Opioid Receptor Dual Selectivity. *J. Med. Chem.* **2013**, *56*, 9156–9169.
- (94) Magrane, M.; Consortium, U. UniProt Knowledgebase: A Hub of Integrated Protein Data. *Database (Oxford)* **2010**, *2011*, bar009.
- (95) Larkin, M. A.; Blackshields, G.; Brown, N. P.; Chenna, R.; McGettigan, P. A.; McWilliam, H.; Valentin, F.; Wallace, I. M.; Wilm, A.; Lopez, R.; Thompson, J. D.; Gibson, T. J.; Higgins, D. G. Clustal W and Clustal X Version 2.0. *Bioinformatics* **2007**, *23*, 2947–2948.
- (96) Hartshorn, M. J.; Verdonk, M. L.; Chessari, G.; Brewerton, S. C.; Mooij, W. T. M.; Mortenson, P. N.; Murray, C. W. Diverse, High-Quality Test Set for the Validation of Protein-Ligand Docking Performance. *J. Med. Chem.* **2007**, *50*, 726–741.
- (97) Ballesteros, J. A.; Weinstein, H. Integrated methods for the construction of three-dimensional models and computational probing of structure-function relations in G protein-coupled receptors. *Methods Neurosci.* **1995**, *25*, 366-428.
- (98) Eugene Kellogg, G.; Abraham, D. J. Hydrophobicity: Is LogP(o/w) More than the Sum of Its Parts? *Eur. J. Med. Chem.* **2000**, *35*, 651–661.

- (99) Li, G.; Aschenbach, L. C. K.; He, H.; Selley, D. E.; Zhang, Y. 14-O-Heterocyclic-Substituted Naltrexone Derivatives as Non-Peptide Mu Opioid Receptor Selective Antagonists: Design, Synthesis, and Biological Studies. *Bioorg. Med. Chem. Lett.* **2009**, *19*, 1825–1829.
- (100) Zhang, Y.; Elbegdorj, O.; Yuan, Y.; Beletskaya, I. O.; Selley, D. E. Opioid Receptor Selectivity Profile Change via Isosterism for 14-O-Substituted Naltrexone Derivatives. *Bioorg. Med. Chem. Lett.* **2013**, *23*, 3719–3722.
- (101) Lattanzi, R.; Spetea, M.; Schüllner, F.; Rief, S. B.; Krassnig, R.; Negri, L.; Schmidhammer, H. Synthesis and Biological Evaluation of 14-Alkoxymorphinans. 22.(1) Influence of the 14-Alkoxy Group and the Substitution in Position 5 in 14-Alkoxymorphinan-6-Ones on in Vitro and in Vivo Activities. *J. Med. Chem.* **2005**, *48*, 3372–3378.
- (102) Greiner, E.; Spetea, M.; Krassnig, R.; Schüllner, F.; Aceto, M.; Harris, L. S.; Traynor, J. R.; Woods, J. H.; Coop, A.; Schmidhammer, H. Synthesis and Biological Evaluation of 14-Alkoxymorphinans. 18. N-Substituted 14-Phenylpropyloxymorphinan-6-Ones with Unanticipated Agonist Properties: Extending the Scope of Common Structure-Activity Relationships. *J. Med. Chem.* **2003**, *46*, 1758–1763.
- (103) Rennison, D.; Moynihan, H.; Traynor, J. R.; Lewis, J. W.; Husbands, S. M. Structural Determinants of Opioid Activity in Derivatives of 14-Aminomorphinones: Effects of Changes to the Chain Linking of the C14-Amino Group to the Aryl Ring. *J. Med. Chem.* **2006**, *49*, 6104–6110.
- (104) Grundt, P.; Jales, A. R.; Traynor, J. R.; Lewis, J. W.; Husbands, S. M. Differential Effects on Opioid Receptor Binding and Functional Profiles. **2003**, 1563–1566.
- (105) Kourist, R.; Domínguez de María, P.; Bornscheuer, U. T. Enzymatic Synthesis of Optically Active Tertiary Alcohols: Expanding the Biocatalysis Toolbox. *ChemBiochem* **2008**, *9*, 491–498.
- (106) Nieland, N. P. R.; Moynihan, H. A.; Carrington, S.; Broadbear, J.; Woods, J. H.; Traynor, J. R.; Husbands, S. M.; Lewis, J. W. Structural Determinants of Opioid Activity in Derivatives of 14-Aminomorphinones: Effect of Substitution in the Aromatic Ring of Cinnamoylaminomorphinones and Codeinones. *J. Med. Chem.* **2006**, *49*, 5333–5338.
- (107) Moynihan, H.; Jales, a R.; Greedy, B. M.; Rennison, D.; Broadbear, J. H.; Purington, L.; Traynor, J. R.; Woods, J. H.; Lewis, J. W.; Husbands, S. M. 14 Beta-O-Cinnamoylnaltrexone and Related Dihydrocodeinones Are Mu Opioid Receptor Partial Agonists with Predominant Antagonist Activity. *J. Med. Chem.* **2009**, *52*, 1553–1557.

- (108) Nieland, N. P. R.; Rennison, D.; Broadbear, J. H.; Purington, L.; Woods, J. H.; Traynor, J. R.; Lewis, J. W.; Husbands, S. M. 14beta-Arylpropionylamino-17-Cyclopropylmethyl-7,8-Dihydronormorphinones and Related Opioids. Further Examples of Pseudoirreversible Mu Opioid Receptor Antagonists. *J. Med. Chem.* **2009**, *52*, 6926–6930.
- (109) Yuan, Y.; Li, G.; He, H.; Stevens, D. L.; Kozak, P.; Scoggins, K. L.; Mitra, P.; Gerk, P. M.; Selley, D. E.; Dewey, W. L.; Zhang, Y. Of Mu Opioid Receptor Selective Antagonists. **2011**, 346–351.
- (110) Zaidi, S. A.; Arnatt, C. K.; He, H.; Selley, D. E.; Mosier, P. D.; Kellogg, G. E.; Zhang, Y. Binding Mode Characterization of 6 α - and 6 β -N-Heterocyclic Substituted Naltrexamine Derivatives via Docking in Opioid Receptor Crystal Structures and Site-Directed Mutagenesis Studies: Application of the “Message-Address” Concept in Development of Mu Opio. *Bioorg. Med. Chem.* **2013**, *21*, 6405–6413.
- (111) Craig, P. N. Interdependence between Physical Parameters and Selection of Substituent Groups for Correlation Studies. *J. Med. Chem.* **1971**, *14*, 680–684.
- (112) Fiser, A.; Do, R. K.; Sali, A. Modeling of Loops in Protein Structures. *Protein Sci.* **2000**, *9*, 1753–1773.
- (113) Valiev, M.; Bylaska, E. J.; Govind, N.; Kowalski, K.; Straatsma, T. P.; Van Dam, H. J. J.; Wang, D.; Nieplocha, J.; Apra, E.; Windus, T. L.; de Jong, W. A. NWChem: A Comprehensive and Scalable Open-Source Solution for Large Scale Molecular Simulations. *Comput. Phys. Commun.* **2010**, *181*, 1477–1489.
- (114) Grosdidier, L.; Michielin, O.; Zoete, V.; Cuendet, M. A. SwissParam : A Fast Force Field Generation Tool for Small Organic Molecules. *J. Comput. Chem.* **2011**, *32*, 2359-2368.
- (115) Lomize, M. A.; Lomize, A. L.; Pogozheva, I. D.; Mosberg, H. I. OPM: Orientations of Proteins in Membranes Database. *Bioinformatics* **2006**, *22*, 623–625.
- (116) Humphrey, W.; Dalke, A.; Schulten, K. VMD: Visual Molecular Dynamics. *J. Mol. Graph.* **1996**, *14*, 33–38, 27–28.
- (117) Phillips, J. C.; Braun, R.; Wang, W.; Gumbart, J.; Tajkhorshid, E.; Villa, E.; Chipot, C.; Skeel, R. D.; Kalé, L.; Schulten, K. Scalable Molecular Dynamics with NAMD. *J. Comput. Chem.* **2005**, *26*, 1781–1802.
- (118) Feller, S. E.; Gawrisch, K.; MacKerell, A. D. Polyunsaturated Fatty Acids in Lipid Bilayers: Intrinsic and Environmental Contributions to Their Unique Physical Properties. *J. Am. Chem. Soc.* **2002**, *124*, 318–326.

- (119) Mackerell, A. D.; Feig, M.; Brooks, C. L. Extending the Treatment of Backbone Energetics in Protein Force Fields: Limitations of Gas-Phase Quantum Mechanics in Reproducing Protein Conformational Distributions in Molecular Dynamics Simulations. *J. Comput. Chem.* **2004**, *25*, 1400–1415.
- (120) Kukic, P.; Farrell, D.; McIntosh, L. P.; García-Moreno E, B.; Jensen, K. S.; Toleikis, Z.; Teilum, K.; Nielsen, J. E. Protein Dielectric Constants Determined from NMR Chemical Shift Perturbations. *J. Am. Chem. Soc.* **2013**, *135*, 16968–16976.

CHAPTER 4

UNDERSTANDING OPIOID RECEPTOR ACTIVATION MECHANISM THROUGH MOLECULAR DYNAMICS SIMULATIONS

4.1 Introduction

4.1.1 GPCR conformational diversity and crystallized GPCR agonist complexes

The canonical ternary complex model of GPCR signaling suggests a unidirectional response of the agonist-activated receptor through heterotrimeric G proteins. However, it is now accepted that upon binding of endogenous or synthetic agonists a receptor exhibits a far more complex signaling and regulatory profile. During the receptor activation, conformational changes in the transmembrane and cytosolic parts of the receptor provide an interaction surface for the incoming G protein. Most GPCRs also provide specific signaling through localized conformational changes at the carboxy terminus via interactions with various factors present close to the plasma membrane. Recently, signaling through intracellular compartments such as endosomes has also been reported.¹ Many GPCRs also exhibit basal (i.e. constitutive) activity, and agonists are known to modulate this activity by increasing (full agonist), partially increasing (partial agonist) or decreasing (inverse agonist) the G protein coupling response. The exact

molecular mechanisms involved in the receptor response upon ligand binding remains to be elucidated; however, recent advances in structural biology, particularly in the field of meso crystallization, have provided significant insights.

In some of the pioneering studies of the late 1990s, before determination of first the GPCR crystal structure, the importance of TM movement for receptor signaling was revealed. Sheikh and co-workers engineered a metal binding site close to the cytosolic part of TM3 and TM6 by mutating wild type residues to histidine in rhodopsin and β_2 adrenergic receptors (β -AR).^{2,3} The mutant receptors were able to stimulate G protein binding in response to an agonist. However, this ability was lost in the presence of metal ions, indicating that the cytosolic part of TM3 and TM6 lie in close proximity and a change in their conformational orientation is likely to be involved in receptor activation. Structural confirmation of the proximity of TM3 and TM6 came from the resolution of the first X-ray crystal structure of rhodopsin in the inactive ‘dark’ state in complex with covalently bound 11-*cis* retinal. In this structure, Arg^{3.50} of TM3 forms ionic interactions with Tyr^{6.30} of TM6, which was later named as ‘ionic lock’ that preserves the receptor in the inactive state.⁴ Twenty four more structures of rhodopsin have been crystallized since, which represents about one-third of all the crystallized GPCRs available in the Protein Data Bank (PDB).⁵

A large majority of rhodopsins crystallized are of bovine origin (21) and represent multiple states of receptor activity – ‘dark’ state (10), bathorhodopsin (1), lumirhodopsin (1), deprotonated intermediate (1), and meta II rhodopsin/meta rhodopsin III (8). Only low resolution electron density maps of meta I rhodopsin intermediate are available. All of the intermediate and active forms of rhodopsin are either photo-activated or were crystallized while soaked in the all-

trans active form of retinal and intermediates were stabilized by adjusting temperature or the pH.⁵

The availability of experimentally determined atomic coordinates for rhodopsin in multiple receptor conformations has delivered insights into the structural changes associated with receptor activation. With respect to the ‘dark’ state, only local rearrangements in retinal binding site are seen in intermediate states. While transiting from lumirhodopsin to meta I rhodopsin, small scale changes were observed that include a slight rotation of TM6 and movement of TM5 away from TM3.^{6,7} However, compared to the inactive form large scale deviations were observed in the activated form of the receptor, in both photo-activated and all-*trans* co-crystallized structures regardless of the presence or absence of interacting C-terminus residues of transducin (G protein cognate of rhodopsin).⁸⁻¹⁰ In the activated opsin form TM6 is tilted outwards by 6-10 Å due to rotation and not due to hinge movement, while TM5 extends a few turns into the intracellular region and also moves 2-3 Å closer to TM6. In the extracellular part, an opening is created between TM5 and TM6, and between TM1 and TM7, and displacement of ECL2 is observed that probably allows retinal to escape from the receptor following hydrolysis of the covalent linkage. Rearrangements in the conserved E(D)RY sequence of TM3 and NPxx(Y)F of TM7 are also observed. The ‘ionic lock’ between Glu247^{6,30} and Thr251^{6,34}, and Arg135^{3,50} of the DRY sequence is broken. Tyr223^{5,68} moves towards inter-helical region to stabilize Arg135^{3,50}, which in turn also interacts with the C-terminus of transducin.^{9,10} Increased localized bends at TM2 due to Gly89^{2,56} and Gly90^{2,57} are observed in batho- and lumirhodopsin structures; however, they again relax in meta II structures.⁵

Although the resolution of the crystal structures is limited, electron density reflecting water networks were observed indicating regional constraints binding the waters. In the inactive state of rhodopsin, the interconnected water network begins at Trp265^{6.48}, Asp83^{2.50}, Ser298^{7.45} and Asn302^{7.49} (of NPxxY domain), and ends at a ‘hydrophobic barrier’ formed due to leucine and methionine residues of TM1, TM2, TM3 and TM6. The water-mediated link between Trp265^{6.48} and Ser298^{7.45} is broken in the active state. However, Ser298^{7.45}, Asn55^{1.50}, Asp83^{2.50}, and Asn302^{7.49} continue to stabilize Pro303^{7.50} kink. Rotation of the TM6 opens up a ‘hydrophobic barrier’, allowing Tyr223^{5.58} and Tyr306^{7.53} into the inter-helical region. These residues form an extensive hydrogen bond network through waters linking the DRY motif of TM3 and helix 8, which in turn also interacts with transducin. Thus, rotation of Trp265^{6.48} and movement of TM6 results in a water network connecting residues close to the ligand binding pocket and residues interacting with transducin.¹⁰

Perhaps the most studied GPCR in terms of receptor activation is β_2 -adrenergic receptor (β_2 -AR), which also serves as the prototypical aminergic receptor. Crystallization of the β_2 -AR was made possible by two differing approaches for the same problem of conformational instability of ICL3. In the first approach, the receptor was crystalized in complex with a Fab antibody that recognizes ICL3 residues as epitopes. In the second strategy, the ICL3 loop was replaced by a well-structured T4-lysozyme subunit.¹¹ By employing the T4L-fusion method, crystal structures for agonist-bound β_2 -ARs were elucidated in complex with the G_s protein substitute nanobody (Nb80)¹² and with nucleotide-free G_s protein¹³. Similar conformations were observed for both the structures (RMSD \sim 0.6 Å) and they were also remarkably similar to the activated opsin structures. When compared to the inverse agonist-bound receptor structure, the

largest difference can be seen at the cytoplasmic surface where TM6 swings outwards by 11 Å or 14 Å. As seen in opsin structures, this outward movement is enabled by clockwise rotation of TM6 at a helix turn preceding Pro^{6.50} due to interruption of its hydrogen bonding with the proline residue, which is associated with repacking of Phe^{6.44}. The ‘ionic lock’ is also broken, allowing Arg^{3.50} to interact with the co-complexed Nb80 or G_{αS} subunit. The unstructured ICL2 loop of the inactive phase receptor forms a two-turn α-helix in the active phase receptor. An extension of seven residues into the cytoplasm is observed for TM5 in the G_S co-crystallized structure. The quality of electron density for the cytoplasmic half is better than for the extracellular part, indicating more variability of conformation in the ligand binding region, where only subtle changes were observed. An inward bulge centered at Ser^{5.46} (a turn above Pro^{5.50}) is seen, along with slight inward movement of extracellular part of TM6 and TM7.

By employing the T4-lysozyme fusion with¹⁴ or without¹⁵ thermostabilizing point mutations, agonist bound adenosine A_{2A} receptor structures have also been solved. The overall architecture of the activated state receptor closely matches previously described activated structures including a 2 Å bulge at TM5 (a turn above Pro^{5.50}), distortions and a 2 Å shift along TM3, inward movement of extracellular half of TM6 and TM7, and large scale displacement at cytoplasmic ends of TM5, TM6 and TM7. However, TM6 is displaced by only 3-4 Å, where it partially occludes the G protein binding site, which has led to suggestions that the observed structures may represent an intermediate state.

An agonist bound crystal structure of M₂ muscarinic receptor in complex with Nb9-8 camelid nanobody has also been reported with some departures from previously ascertained ‘active-like’ conformations. The extracellular half of TM5, TM6 and TM7 moves inward, while

no movement or bulge is seen in TM3. Also unlike modest changes in orthosteric ligand-binding sites of previously described receptors, a large scale inward movement of TMs closes the ligand binding site and occludes the agonist from extracellular solvent. Incorporation of a positive allosteric modulator in the crystal structure had no significant effect on the overall architecture of the receptor.¹⁶

The receptor may couple with alternative interactions partners, the most commonly studied being β -arrestin, which may result in different conformations for the receptor. The crystal structures for 5-HT_{2B} and 5-HT_{1B} are available, and are very interesting primarily because of the nature of the co-crystallized ligand, ergotamine.¹⁷ Ergotamine has a highly β -arrestin biased function on 5-HT_{2B} and less so on 5-HT_{1B}. 5-HT_{1B}-ergotamine complex shows active-state like changes characteristic of activation via G proteins at the TM3 bulge, and TM6 rotation and displacement along with a broken ionic salt bridge ‘lock’ between the DRY sequence of TM3 and the bottom of TM6. However, in the 5-HT_{2B}-ergotamine complex, TM6 rotation is not observed, but its TM7 movement and the location of the NPxxY sequence is more ‘active-like’ than in 5-HT_{1B}. These observations have led to speculations demarcating conformational changes in the receptor with functional selectivity of the ligand.

4.1.2 GPCR micro-switches

Micrco-switches are defined as a group of highly conserved residues having substantially different conformations in active and inactive states of the GPCR such that alternate in conformations of these residues help in stabilizing active, inactive or intermediate states of the receptor.

i) CWxP global toggle switch

This toggle switch was proposed to reconcile the apparent opposing movement of extracellular and cytoplasmic regions of TM6 relative to the remainder of TM helical bundle. The tryptophan residue at the position 6.48 was proposed to have ‘active’ and ‘inactive’ rotameric states and the presence of a conserved proline residue below the tryptophan would transduce the rotameric shift into a large cytoplasmic TM6 movement.¹⁸ However, no such ‘toggle’ mechanism has been observed in crystal structures and mutagenesis studies have demonstrated activation of GPCRs in the absence of the Trp^{6.48}.¹⁹ However, due to its proximity to other highly conserved network of residues it may play a physiologically relevant role in hydrophobic packing and disruption of water networks.

ii) DRY motif

This highly conserved motif is present at the intracellular part of TM3, where Asp^{3.49} stabilizes Arg^{3.50}; Arg^{3.50} in turn forms a salt bridge with the acidic Glu/Asp at position 6.30, thus ‘locking’ the receptor in the inactive state (Figure 4.1A). While in the active state, the ionic lock is broken, which allows displacement of TM6. Arg^{3.50} then interacts with ICL2 and the G α protein. However, this Glu is conserved in only 25% of class A GPCRs, and is not present in chemokine and opioid receptors.²⁰

iii) NPxxY motif

Tyr^{7.53} of this TM7 motif moves toward the inter-helical bundle and forms a water network that bridges its interactions with the Tyr^{5.58} residue in the active state (Figure 4.1B). This displacement has been observed in all the crystallized ‘active’ state GPCRs.

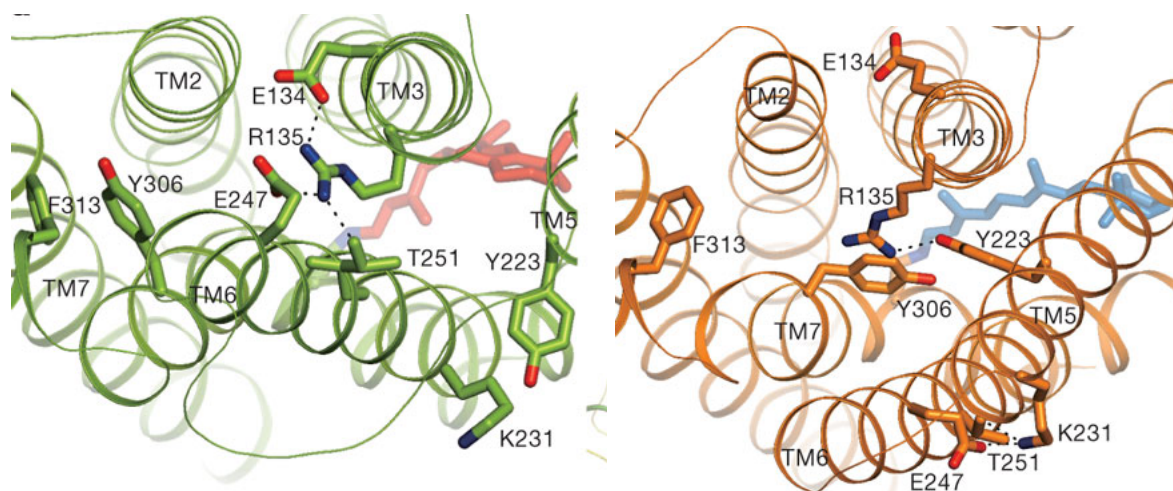


Figure 4.1. A. DRY motif ‘ionic-lock’ in inactive state **B.** NPxxY motif rearrangement in ‘active-state’. Reprint from reference 8.

iv) P-I-F motif

This motif is composed of the clustered residues Pro^{5.50}, Ile^{3.40} and Phe^{6.44}. The TM3 bulge observed in most active state receptor crystals is close to Pro^{5.50}, causing the residue to move slightly inwards. Concomitantly, the rotation of TM6 is correlated with a clockwise shift of Phe^{6.44} (as viewed from the extracellular side), and its ‘inactive-state’ position is taken by an alternate rotamer of Ile^{3.40}. Interestingly, in the 5-HT_{2B}-β arrestin biased ligand complex structure, clockwise rotation of Phe^{6.44} is not observed, while it is seen in the 5-HT_{1B}-unbiased ligand complex structure where the characteristic placement of P-I-F motif is observed. (Figure

4.2) This suggests that rotation of TM6 may be responsible for functional selectivity through G protein recruitment.¹⁷

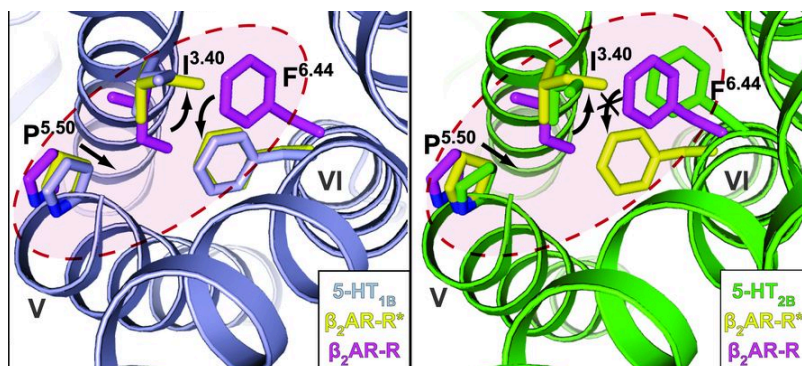


Figure 4.2. Movement in P-I-F motif in response to co-crystallization with ergotamine (dashed red elliptical) B. Alignment between 5-HT_{1B} (gray), inactive β_2 -AR (magenta) and active β_2 -AR (yellow), 5-HT_{1B} shows characteristic P-I-F movements seen in active form of β_2 -AR. C. Alignment between 5-HT_{2B} (green), inactive β_2 -AR (magenta) and active β_2 -AR (yellow), 5-HT_{2B} shows incomplete P-I-F movements in response to β -arrestin biased ligand (ergotamine). Reprint from reference 17.

4.1.3 Bimodal and multimodal models for GPCR activation

GPCRs are now known to exhibit functional versatility owing to its interactions with G proteins, β -arrestins, G protein receptor kinases (GRKs), and various other signaling proteins. This functional versatility should be a product of structural plasticity. The GPCR population in a given system can be described as an ensemble of discrete conformations whose energetics is influenced by ligand binding, signaling and regulatory proteins, pH, membrane lipids, ions, transmembrane voltage gradient and oligomerization. Under this model an ‘activation switch’ could be described as a shift in receptor sub-population in response to factors enumerated above, and there could be more than one ‘activated’ state of GPCR, each of which is biased towards a certain signaling profile.²¹

Rhodopsin, so far a prototypical GPCR for agonism studies, may not fit into the above model. Rhodopsin is unique in its high sensitivity and fidelity, and extremely fast ‘switching’ time. In its inactive ‘dark’ state, the rhodopsin receptor is covalently bound to 11-*cis* retinal, which is a highly efficient inverse agonist that ensures rhodopsin exhibits no basal activity. Isomerization of 11-*cis* retinal to the all *trans* form following photoactivation provides about 35 kcal/mol for transition from bathorhodopsin to meta II rhodopsin²² through a series of extremely short-lived intermediates. The meta II rhodopsin is capable of interacting with transducin within milliseconds, and each rhodopsin can activate hundreds of transducins, which makes the receptor system highly efficient.²¹ Moreover, all photoactivated rhodopsins proceed to the active meta II form even in the absence of transducin, as evidenced by crystallization of the activated meta II form without co-crystallization with transducin. Furthermore, the intermediates are too short lived to interact with other proteins and have a signaling profile of their own. This supports a ‘bimodal’ model of GPCR activation for rhodopsin, where rhodopsin population can be represented by two major discrete conformations and intermediate conformations are elaborate switching mechanisms between the two major populations.

This ‘on-off’ model is in contrast to ‘multimodal’ model for other GPCRs that are known to exhibit varying levels of basal activity, varying levels of ligand efficiency, interactions with more than one kind of G protein, interactions with β arrestins and other G protein independent signaling factors. β_2 -AR is one such example of a versatile but inefficient signaling machine. Adrenaline binds with relatively low affinity with β_2 -AR in the absence of G_s ($\sim 1 \mu\text{M}$) and each binding event generates ~ 8.2 kcal/mol energy for activation.²¹ The ‘activated’ receptor crystal structures of β_2 -AR could only be obtained in the presence of G protein or a G protein mimic.

This suggests even agonist bound β_2 -AR has high conformational heterogeneity and only in presence of another stabilizing factor (G protein) can somewhat homogenous 'crystallizable' populations be detected.

Figure 4.3 represents these two models. For rhodopsin, the inactive 'dark' state has the lowest energy conformation, and photoactivation of the receptor increases the energy of the 'dark' conformation, resulting in conversion to the activated meta II state. In case of the β_2 -AR, a heterogenous conformational population is observed due to the lesser difference between energy states of different forms of the receptors. Agonist binding further reduces the difference and stabilizes the ligand specific active form of the receptor, especially in the presence of G protein.

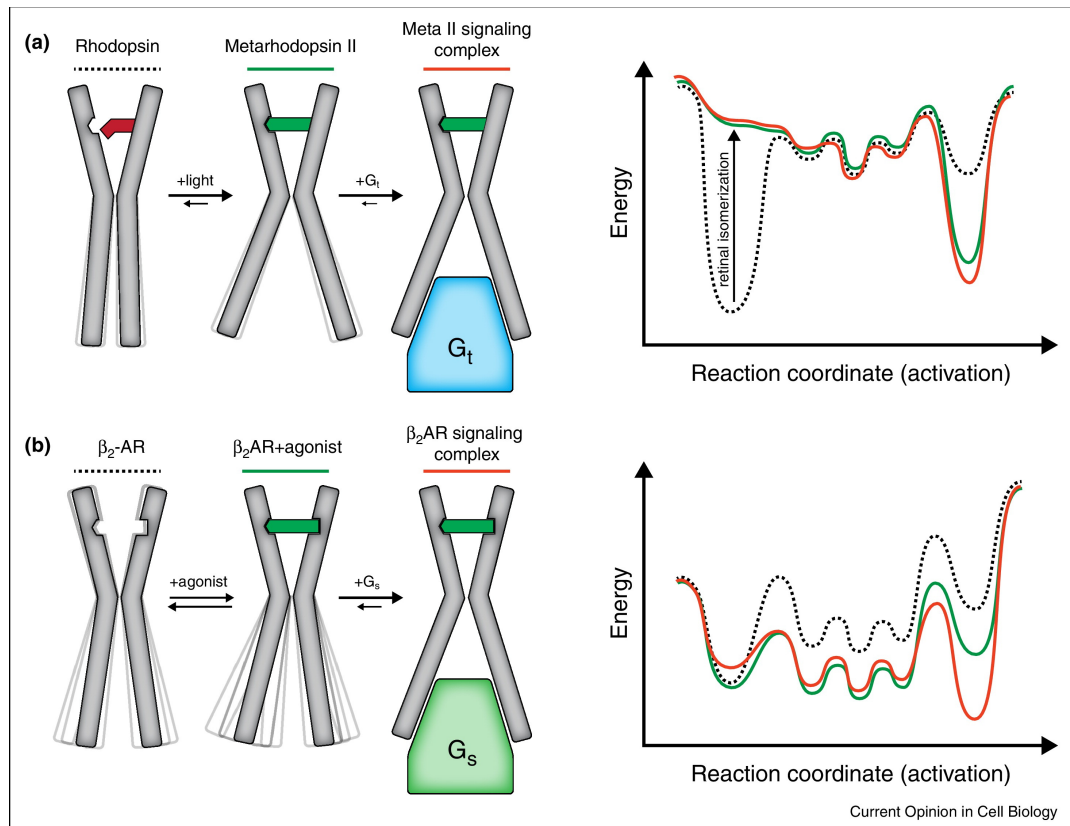


Figure 4.3. Bimodal and multimodal GPCR activation models (a) Equilibrium between rhodopsin, metarhodopsin II and metarhodopsin II-signalling complex. Energy profile of dark state (dotted line), metarhodopsin II (green) and metarhodopsin II transducin complex (red). (b) Equilibrium between, β_2 -AR and β_2 -AR-signalling complex. Energy profile of inactive β_2 -AR (dotted line), agonist bound β_2 -AR (green) and agonist bound β_2 -AR- G protein complex (red). Reprint from reference 21.

4.1.4 Unified GPCR activation model

The presence of highly conserved residues in seemingly varied GPCRs and identification of constitutively active mutants have played a major role in generating hypotheses regarding the GPCR activation mechanism. These hypotheses were further substantiated by various biophysical studies. Furthermore, structural elucidations of active and inactive forms of receptors have provided the ‘active’ and ‘inactive’ end points for the conformational spectrum of the

receptors. Different researchers have interpreted questions regarding the sequence of events leading to the activation ‘switch’ varyingly. Standfuss and co-workers, the group that crystallized the active form of rhodopsin, proposed that rotation and movement of TM6 causes disruption of water mediated interactions of Trp^{6.48} to Asp^{2.50}, Asn^{7.49} and Ser^{7.45}. This movement of Trp^{6.48} disrupts the hydrophobic barrier, enabling water present inside the helical region to form a hydrogen bonding network between Tyr^{5.58} and Tyr^{7.53}. Rasmussen and co-workers crystallized the active form of β_2 -AR, and have proposed a different sequence of events. They contend that ligand binding causes an inwards movement of TM5 in and around Pro^{5.50}. This movement disrupts the network of interactions between Pro^{5.50}, Ile^{3.40}, Phe^{6.44} (P-I-F motif) and Asn^{7.45}. This network disruption also causes rotation of TM6 around Phe^{6.44} and consequential outward movement of TM6.

Tehan *et al.* have recently published a consensus mechanism based on superimposition of active and inactive crystal structures identifying common movements - inward movement of TM5, slight rotation and upward movement of TM3, rotation of TM6, and inward movement of TM7 and TM1.²³ The central thesis is that the activation is effected by rearrangement of hydrophobic residues between TM3 and TM6 that hinders the water channel observed in active states. The hydrophobic hindering groups consist primarily of Leu^{3.43}, Phe^{6.44}, X^{6.41} (hydrophobic residue, Val for KOR). In the inactive state, the position of Leu^{3.43} is anchored to the top by Phe^{6.44} and X^{6.41}. Disruption of this network allows upward movement of TM3, rotation of TM6, and inward movement of TM5. (Figure 4.4.A and B) Upward movement of TM3 also pushes Leu^{3.43} towards Leu^{2.46} (Figure 4.4.C), whose inactive state position is now occupied by Asn^{7.49}. (Figure 4.4.D) Upward and inward movement of Asn^{7.49} allows Tyr^{7.53} to move across to the

interhelical region where it forms hydrogen bond with Tyr^{5.53} through a water molecule. (Figure 4.4.E) These gross movements in TM3 and TM6 would break the ionic salt bridge, if present, and opening of a water channel at the intracellular side stabilizes the resulting conformation.

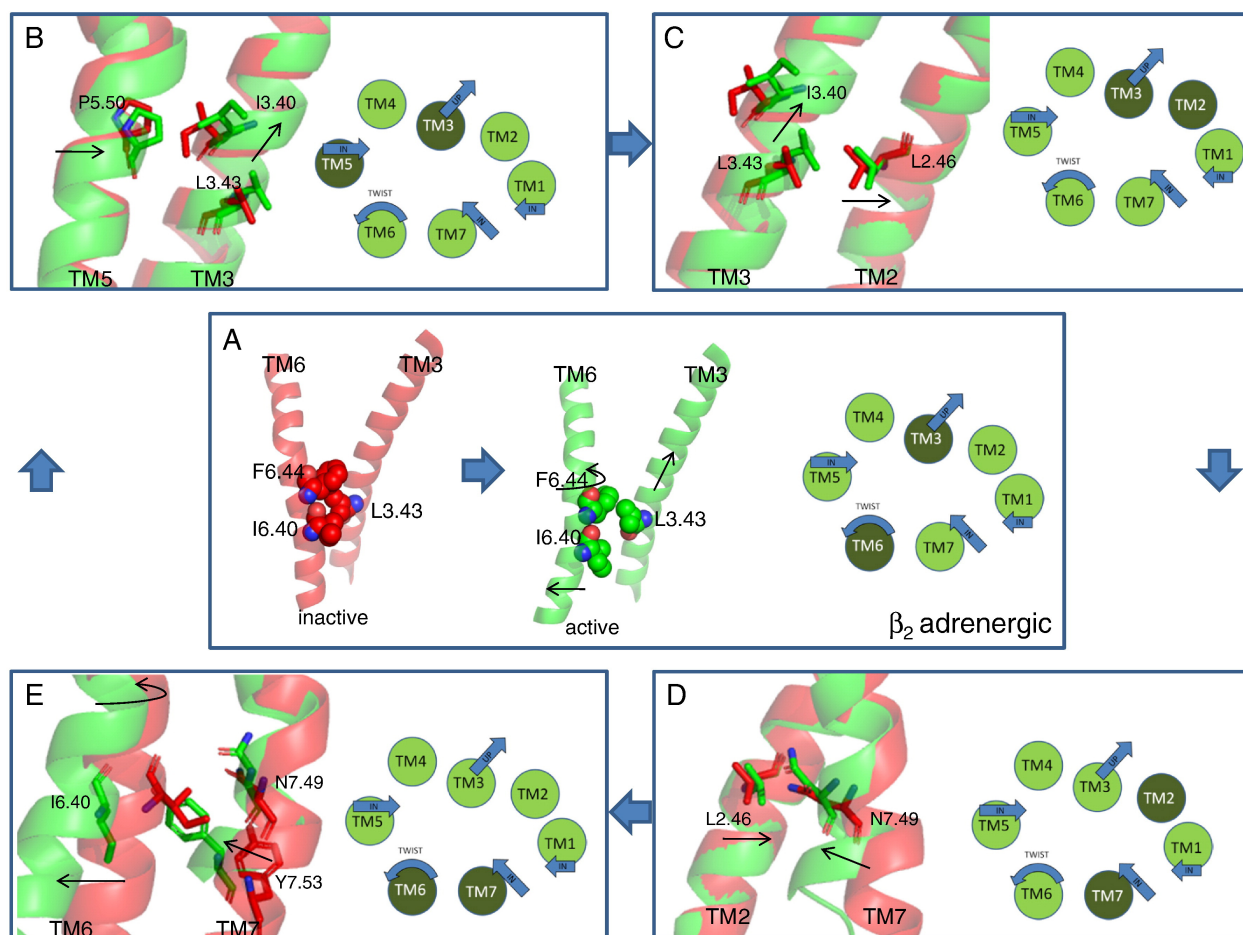


Figure 4.4. Proposed GPCR activation mechanism. Red TM (inactive conformation); green TM (active conformation). Inserts represent schematic overview of conformational changes in highlighted helices. A. Rotational movement of Phe^{6.44} and upward movement of TM3 (Leu^{3.43}). B. Inward movement of Pro^{5.50} C. Displacement of Leu^{2.46} due upward movement in TM3. D. Replacement of position previously occupied by Leu^{2.46} by Asn^{7.49}. E. Movement of Tyr^{7.53} to position previously occupied by TM6. Reprint from reference 23.

4.1.5 Modeling active state receptor for KOR

Salvinorin A (Figure 4.5) is one of the most potent naturally (active constituent of plant *Salvia divinorum*) occurring hallucinogens. Screening studies against an array of receptors, ion channels and transporters, followed up by functional assays and mouse receptor knockout studies revealed salvinorin A to be a selective KOR agonist.^{24,25} High binding efficiency of salvinorin A lends itself for development of pharmacological tools and ligands with novel pharmacological profile and therapeutic potential. In an effort to advance such exploration, irreversible agonists based on salvinorin A skeleton were designed. Substituted-cysteine accessibility method (SCAM) studies demonstrated the presence of free cysteine (not involved in a disulphide bond) in the solvent accessible region.²⁶ Modeling studies suggested the presence of Cys315 close to the putative salvinorin A binding pocket²⁶⁻²⁸; furthermore, the 22-position on salvinorin A was identified for inclusion of electron withdrawing groups to improve electrophilicity of this carbon, and such ligands were synthesized. 22-thiocyanatosalvinorin A (RB-64) displayed high selectivity, affinity and potency for KOR (Table 4.1) and a model for the RB64-KOR receptor complex was proposed.²⁹

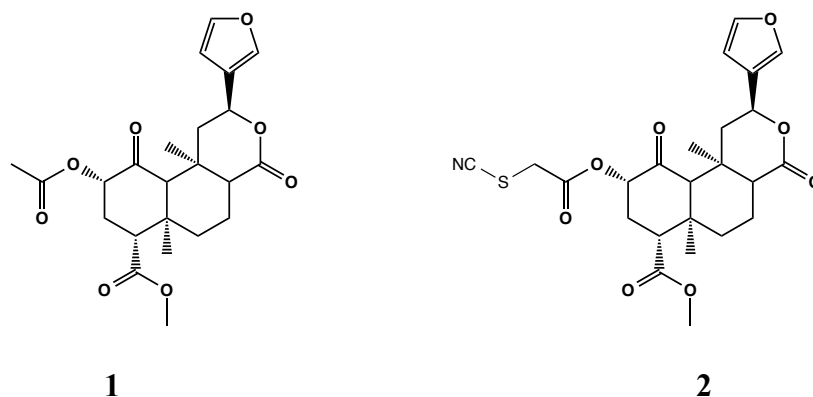


Figure 4.5. Salvinorin A (**1**) and RB-64 (22-thiocyanatosalvinorin A, **2**)

Table 4.1 Pharmacological profile of salvinorin A and its C-22 derivative RB-64.²⁹

Compounds	K_i (nM)	K_i (nM)	EC ₅₀	Relative E _{max} (%)
Salvinorin A	1.8 ± 1.4	21 ± 11	17 ± 6	100
RB-64	0.59 ± 0.21	39 ± 11	0.077 ± 0.016	95 ± 2

This chapter reports molecular dynamics (MD) experiments performed on the lipid bilayer-embedded KOR-RB64 complex model. The obtained trajectory of KOR–RB64 complex was then analyzed to determine a plausible KOR-agonist (RB–64) complex model and KOR protein activation switch. Similar MD simulations were also performed on the recently crystallized JDTic–KOR receptor complex³⁰. These latter simulations were performed as a ‘control’ in MD experiments.

Sodium is known to modulate GPCR receptor binding to G protein; inhibitory effects of sodium to G protein binding have also been reported for opioid receptors.³¹ In the recently crystallized high resolution structure of DOR, an allosteric sodium site was observed. KOR and DOR share very high sequence similarity in the TM region, so an allosteric sodium site was modelled on the KOR crystal structure, and similar MD simulation studies were performed.

Proteins show dynamic character at several scales – bond vibrations at femtosecond (fs) timescales, side chain rotation at picosecond (ps) to nanosecond (ns) timescales, and large scale domain motions at microsecond (μs) to millisecond (ms) timescale. The GPCR microswitches involve movements of the side chains as well as larger scale TM movements such as displacement and rotation. To achieve a higher degree of conformational sampling at nanosecond levels an accelerated molecular dynamic approach was used.

4.1.6 Accelerated molecular dynamics

Molecular dynamics is a widely used computational technique based on integration of Newton's equations of motion. It is fairly simple algorithmically and has the ability to accurately sample the conformational space of a molecular system, thus allowing time-dependent behavior and evolution studies. Accurate representation of a molecular system's potential energy landscape and the easily calculable thermodynamic and kinetic properties provide a special advantage while studying local motion and conformational changes of proteins, DNA and other biological systems. However, biological systems under study are usually large, hence simulation time has traditionally been limited to around the nanosecond time scale.

As previously stated, a sufficient study of protein dynamics would usually require at least milli- to microsecond time scales sampling to simulate large-scale conformational motions. Moreover, for most biological systems, the energy landscape has multiple minima or potential energy basins. These potential energy basins may have high free energy barriers. Dynamic evolution from one basin to another would require sampling of series of rare events. A number of MD methods have been introduced to approach this problem, such as conformational flooding, replica exchange, umbrella sampling, hyperdynamics, metadynamics and the adaptive biasing force method. However, they require prior knowledge of the potential energy landscape or require an end point conformation.

Accelerated MD (aMD) has the advantage that it can simulate infrequent events without any advance knowledge of the locations of either the potential energy barriers or potential energy basins. The basic idea behind aMD is represented in Figure 4.6. In aMD, a threshold energy (E) is defined, and at any time during the simulation if the true potential energy $V(r)$ is below the

threshold energy (E), a non-negative boost $\Delta V(r)$ is provided to the system so that there is a new modified potential, $V^*(r) = V(r) + \Delta V(r)$. The boost is defined by an acceleration factor α , where small values for α represent faster acceleration.³²

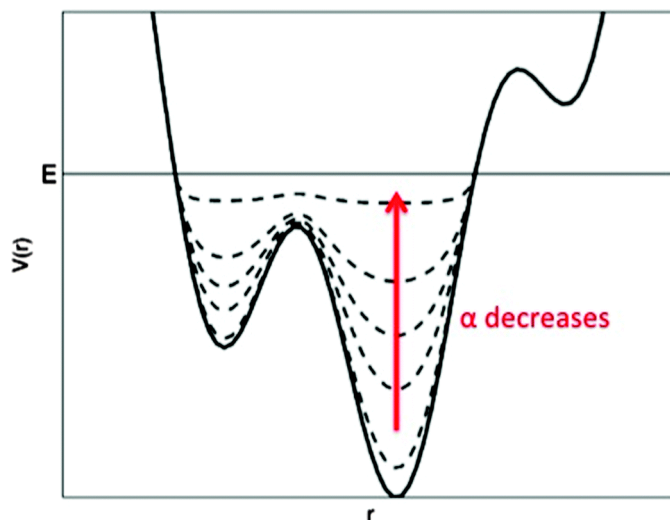


Figure 4.6. Schematic representation of the accelerated MD. Normal potential (black line), biased potential (dashed lines).

$$V^*(r) = V(r), V(r) \geq E$$

$$V^*(r) = V(r) + \Delta V(r), V(r) < E$$

$$\Delta V(r) = (E - V(r))^2 / (\alpha + E - V(r))$$

where, $V^*(r)$ = boosted potential

$V(r)$ = actual potential

E = threshold energy

$\Delta V(r)$ = boost potential

α = acceleration potential

Generally, during conventional molecular dynamics simulations of biological systems, extensive conformational sampling is done around a local minimum without adequately sampling other

conformations. In contrast, the biased potential provides an increased escape rate from a local minimum and subsequent evolution from one state to another occurs at an accelerated rate. This provides highly enhanced sampling over a period of time and hence can be used to study protein dynamics. The aMD method is reported to sample events with as little as 2000 times lesser timescales than conventional MD (cMD)³³ and is being increasingly implemented to study biological systems.

4.2 Methods

4.2.1 Generation of receptor models

The RB-64-KOR complex model (KOR–Agonist model) was adopted from the model proposed previously by Yan *et al.*²⁹ Substituted–Cysteine Accessibility Method (SCAM) and molecular modeling studies suggested Cys315^{7,38} to be the plausible site of irreversible binding to the KOR protein. The model proposes covalent bonding of RB-64 to the thiol group of Cys315^{7,38} via a disulfide bond. The preference for a disulfide linkage was demonstrated by mass spectrometric studies following incubation of RB–64 with a synthetic peptide (Ac-YFCIALGY) to mimic the covalent linkage between RB–64 and the KOR protein. Figure 4.7 represents the adopted model demonstrating the site of RB–64 linkage on TM7 along with the crystallographic waters adapted from KOR–JDTic crystal structure.³⁰

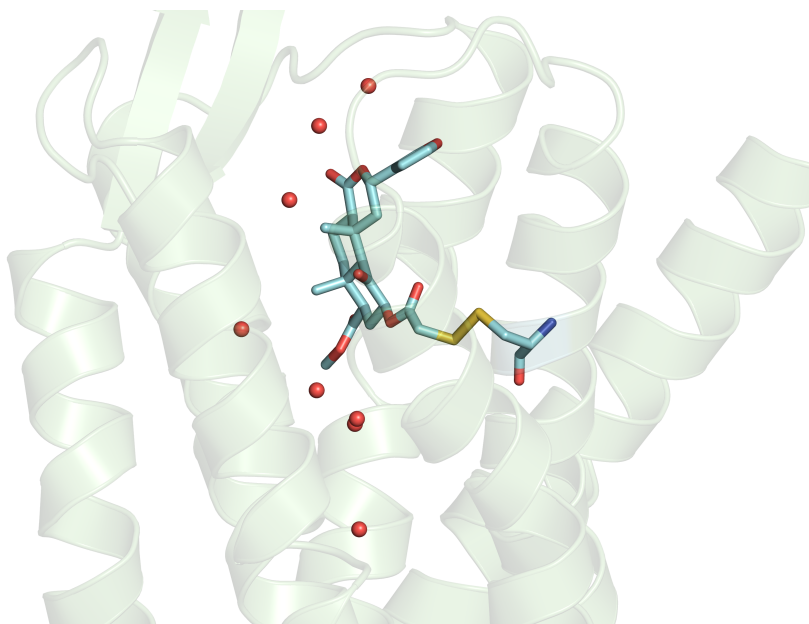


Figure 4.7. Cartoon representation of KOR demonstrating the point of linkage of RB-64 (sticks representation) at TM7 through a disulfide bond. Crystallographic waters are shown as red spheres.

The KOR–JDTic model (KOR-antagonist) was retrieved from PDB RCSB server (PDB ID: 4DJH)³⁰. The receptor–antagonist model was prepared in Sybyl-X 2.0 by expunging all substructures except for the KOR sequence, JDTic and crystallographic waters. Figure 4.8 represents placement of JDTic inside KOR protein as observed in the crystal structure.

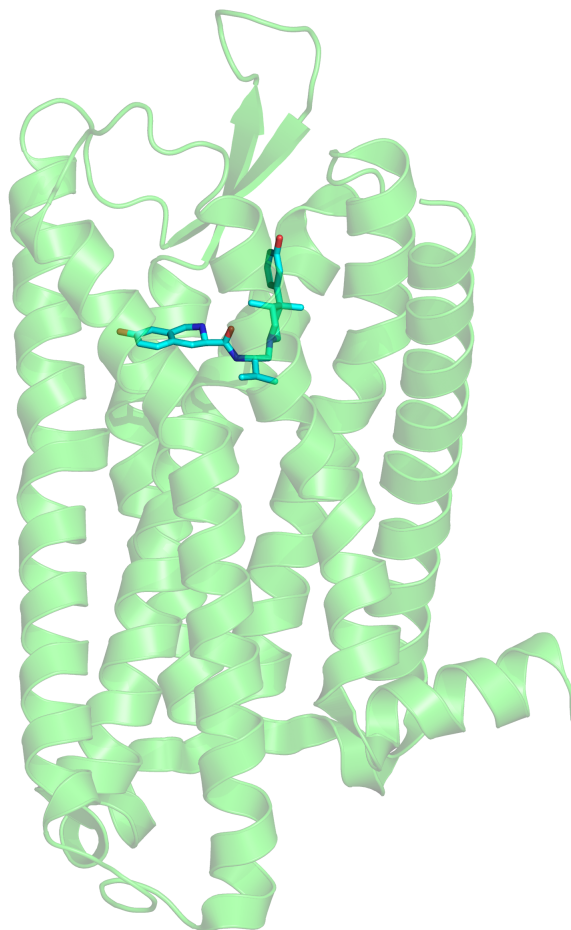


Figure 4.8. Placement of JDtic inside KOR as observed in the KOR crystal structure.

To explore the ‘sodium effect’ on KOR, the coordinates for sodium and the surrounding water molecules were adapted from recently crystallized high resolution (1.8 Å) complex of human DOR co-crystallized with naltrindole (PDB ID: 4E1Y)³⁴ following overlap with the KOR protein substructure of KOR–JDtic crystal structure. A local minimization was done on amino acid side chains at 10 Å radius from the sodium of the obtained KOR-sodium model (SybylX 2.0, 500 iterations, Gasteiger–Hückel charges, Tripos force field). Figure 4.9 represents the obtained

sodium site model. Owing to the high sequence similarity between KOR and DOR, identical interactions were observed.

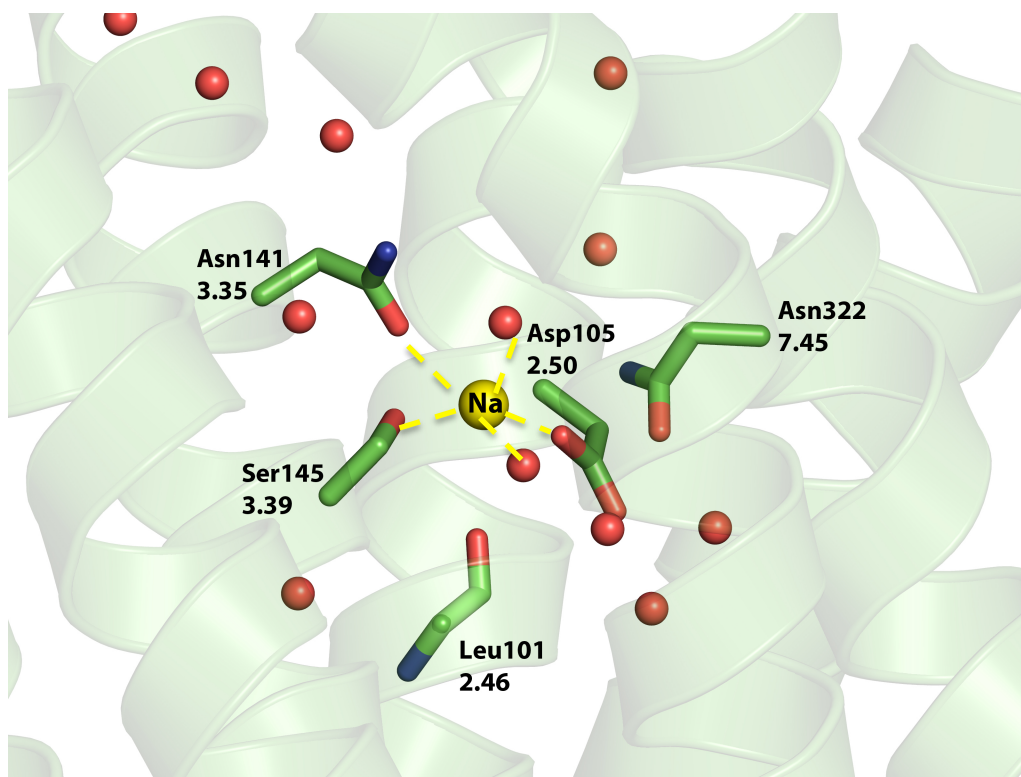


Figure 4.9. Position of sodium inside KOR. Sodium (yellow), waters (red spheres), Side chains of Asp105, Ser145, Asn141 and Asn322, and backbone chain of Leu101 (sticks) are shown.

By expunging all the substructures except the KOR protein and crystallographic waters from the JDTic-KOR crystal structure, the apoprotein-KOR model was generated. Gaps in the protein sequence due to removal of the T4-lysozyme sequence and the non-resolution of ECL3 in the crystal structure were modeled and refined using MODELLER 9v10³⁵.

4.2.2 Generation of topology and parameter files

Density functional theory (DFT) calculations at the 6-31G* level were employed to calculate partial atomic charges of the JD_Tic and RB64–Cys315 atoms using NWChem 6.0.³⁶ The CHARMM force field parameter and topology files for the ligands (JD_Tic and RB-64) were generated utilizing SwissParam.³⁷ The atomic charges obtained from NWChem were added to the ligand topology file. The default CHARMM topology and parameter files for proteins (CHARMM22)³⁸, lipids (CHARMM27)³⁹ including CMAP⁴⁰ corrections were further edited to include topology and parameters for the ligands.

4.2.3 Generation of lipid embedded receptor complex

VMD 1.9.1⁴¹ was used to prepare the system for MD simulations. Coordinate (pdb) and connectivity (psf) files were generated for the receptor–ligand complexes as well as for the apoprotein KOR and apoprotein KOR–sodium complex using the psfgen module. The VMD membrane module was employed to create a lipid bilayer of POPC (1-Palmitoyl-2-oleoylphosphatidylcholine). Coordinates for the spatial arrangement of the receptor within the lipid bilayer were retrieved from the Orientations of Proteins in Membranes (OPM) database.⁴² OPM estimates arrangement of transmembrane protein inside the lipid bilayer by minimizing the transfer energy of the protein from water to the lipid membrane. This was followed by the addition of 30 Å of water in layers to both sides of membrane, using the VMD solvate plugin. All the waters and POPC molecules at a distance of 0.65Å or less from the receptor–ligand complex were then deleted followed by deletion of waters within the POPC membrane. The water system was then ionized to 0.15 M of NaCl by the VMD autoionize plugin.

4.2.4 Conventional molecular dynamics run

All molecular modeling simulations were performed using NAMD 2.8.⁴³ The initial cMD simulations were carried out in four stages, as described below:

i) Melting lipids

In the first stage, equilibration of the fluid-like lipid bilayer was performed via minimization (1000 iterations) followed by NPT equilibration (pressure equilibration) of the lipid tails for a period of 0.5 ns. Simulations were carried out under the CHARMM force field with CHARMM22 parameters for protein, CHARMM27 parameters for lipids and CMAP corrections for proline, glycine and alanine dipeptides and parameters for ligands (if present) with a time-step of 2 femtoseconds (fs). Periodic boundary conditions were employed, and Particle Mesh Ewald (PME) summation was used to calculate long-range electrostatic interactions. Non-bonded interactions were calculated with a smooth cutoff between 10 to 12 Å with a frequency of 1 fs. The constant pressure and temperature at 310 K was maintained via Langevin dynamics.

ii) Equilibration with constrained receptor–protein complex

In the second stage, an NPT equilibration of the system was run for a period of 1 ns with harmonic constraints placed on the protein, the ligand (if present), the allosteric site sodium (if present) and crystallographic water atoms (5 kcal/(mol-Å)), while keeping all the parameters the same as earlier.

iii) Unrestrained equilibration of receptor–protein complex

The harmonic restraint was released in stage 3 and the entire system was equilibrated using the NVT canonical ensemble for a further 1 ns.

iv) Production run

The final production run was conducted using an NVT ensemble where the whole system was simulated for 20 ns.

4.2.5 Accelerated molecular dynamics run

Accelerated MD simulations were also performed under NAMD 2.8.⁴⁴ The dual boost method was implemented for aMD, where boosts were provided for both potential energy and dihedral energy. Threshold energy (E) and acceleration factor (α) were calculated by the following formula:

a) Potential energy

$$E_{\text{potential}} = V_{\text{potential_avg}} + 0.3 \times N_{\text{atoms}}$$

$$\alpha_{\text{potential}} = 0.3 \times N_{\text{atoms}}$$

where $V_{\text{potential_avg}}$ = average potential energy for 20 ns of conventional MD and N_{atoms} = total atoms in the system

b) Dihedral energy

$$E_{\text{dihedral}} = V_{\text{dihedral_avg}} + \lambda \times N_{\text{atoms}},$$

$$\alpha_{\text{dihedral}} = (\lambda \times V_{\text{dihedral_avg}})/5$$

where $V_{\text{dihedral_avg}}$ = average dihedral energy for 20 ns of conventional MD and N_{atoms} = total atoms in the system, λ = adjustable acceleration.

aMD simulations were run for all four systems under the same conditions as the production run of conventional MD.

4.3 Analysis

4.3.1 Stability of the accelerated system

The obtained trajectories for all four systems were examined for system stability. Long-term MD simulations, particularly accelerated MD simulations, can result in disruption of secondary structures such as helices. In lipid embedded systems, disorganization of lipid bilayers may occur. To verify integrity of the system during the simulation, the final trajectory was checked for quality of secondary structures (α -helicity) and stability of the POPC bilayer. (Table 4.2)

Table 4.2 Summary of Conventional MD (cMD) and Accelerated MD (aMD) simulations

System	α -helicity of the crystal structure (%)	Length of cMD run (ns)	α -helicity after cMD run (%)	Length of aMD run (ns)	α -helicity after aMD run (%)	Lipid layer thickness after aMD run (Å)	Surface area per unit lipid head P (Å ²)
KOR-JDTic	83.55(79.55)	20	83.58	70	73.72	50.73	22.43
KOR-RB64		20	79.70	80	74.73	55.26	23.46
ApoKOR-Na		20	82.81	60	78.94	50.40	22.87
Apo-KOR		20	81.00	80	82.32	51.50	23.06

The helicity of the secondary structure was calculated using STRIDE.⁴⁵ The helicity measure of the crystal structure is 83.55% or 79.55% (excluding and including unresolved amino acid residues, respectively). 20 ns of the cMD run had no apparent effect on the helicity of the protein. There was some decrease in helicity after the aMD run; however closer inspection of the

trajectory revealed that unwinding of helix was confined to small regions. Furthermore, thickness and density of the lipid bilayer remained fairly constant. This indicates that integrity of the system was maintained through both conventional and accelerated MD runs.

4.3.2 Trajectory analysis

To simplify analysis of the trajectories, only the C α atoms of KOR protein backbone were mapped. These C α trajectories were then fitted progressively (frame 2 onto frame 1, frame 3 onto frame 2, etc.), to discount any translational or rotational motion of whole protein molecule during the simulation. Principal components analyses were performed on the obtained C α coordinates.

4.3.2.a Analysis of KOR-JDTic lipid embedded complex (Receptor-Antagonist system)

Gromacs 4.4.3 utility tools were employed to analyze the obtained trajectories. Principal component analysis (PCA) was performed using the g_covar utility. This utility calculates and diagonalizes the covariance matrix to determine principal components describing the direction (eigenvector) and associated amplitude (eigenvalue) of receptor (C α atoms) motion. (Figure 4.10)

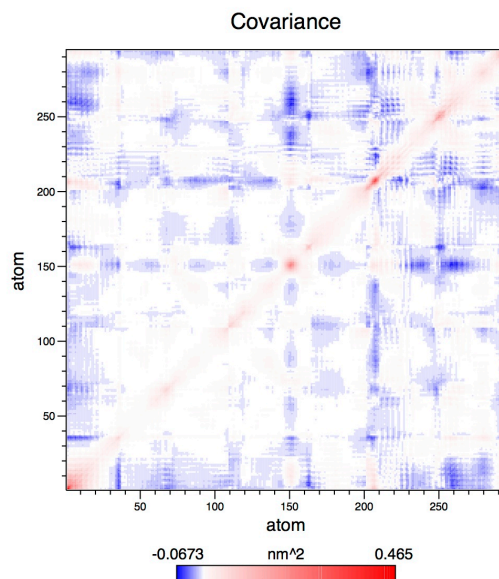


Figure 4.10. Co-variance matrix for aMD trajectory of KOR-JDTic system. Both X and Y axis define residue number (C α atoms) Red color indicates positive covariance, blue denotes negative covariance.

Figure 4.11 shows the eigenvalues for first ~ 33 principal components (PC) of ~ 800 components calculated in PCA of KOR-JDTic system trajectory. The eigenvalues suggest that first two principal components (PC1 and PC2) provide largest contribution to the covariance matrix and hence can be used to represent overall fluctuations in the receptor trajectory.

Eigenvalues of the covariance matrix

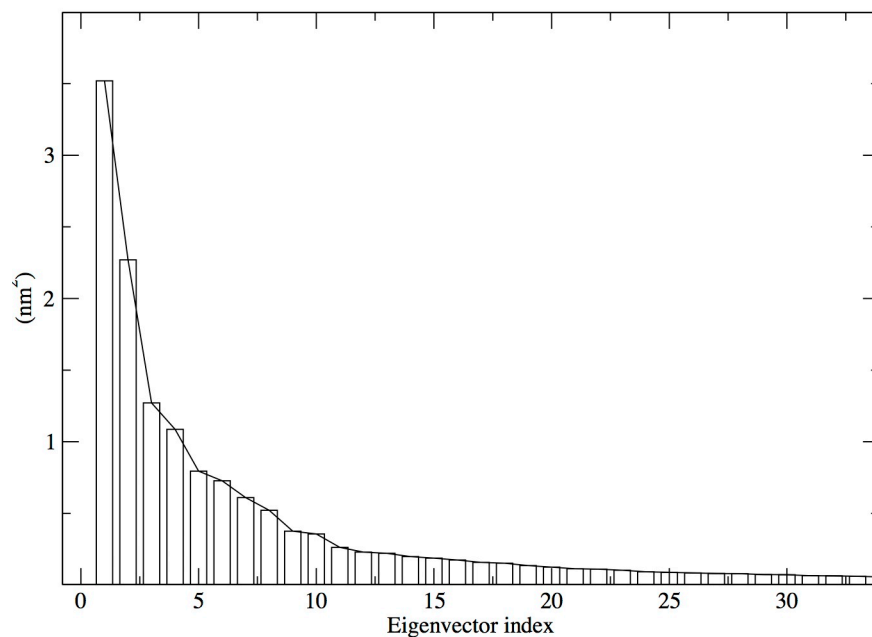


Figure 4.11. Eigenvalues (Y axis) associated with principal components (X axis) for KOR–JDTic system

The ensemble of simulated conformations of the receptor ($C\alpha$ atoms) was then projected two-dimensionally (PC1 and PC2) by utilizing the `g_anaeig` tool. (Figure 4.12a) Red circles show projections for the conformations simulated during the trajectory, while the projection for the crystal structure is shown by a black triangle. This analysis reveals that a varied receptor conformational space was explored during the simulation and the conformation for the crystal structure was well within the conformational space sampled. Population analysis to detect more probable conformations *i.e.* the conformations that were visited the most during the simulation, was done using the `g_sham` module. (Figure 4.12b)

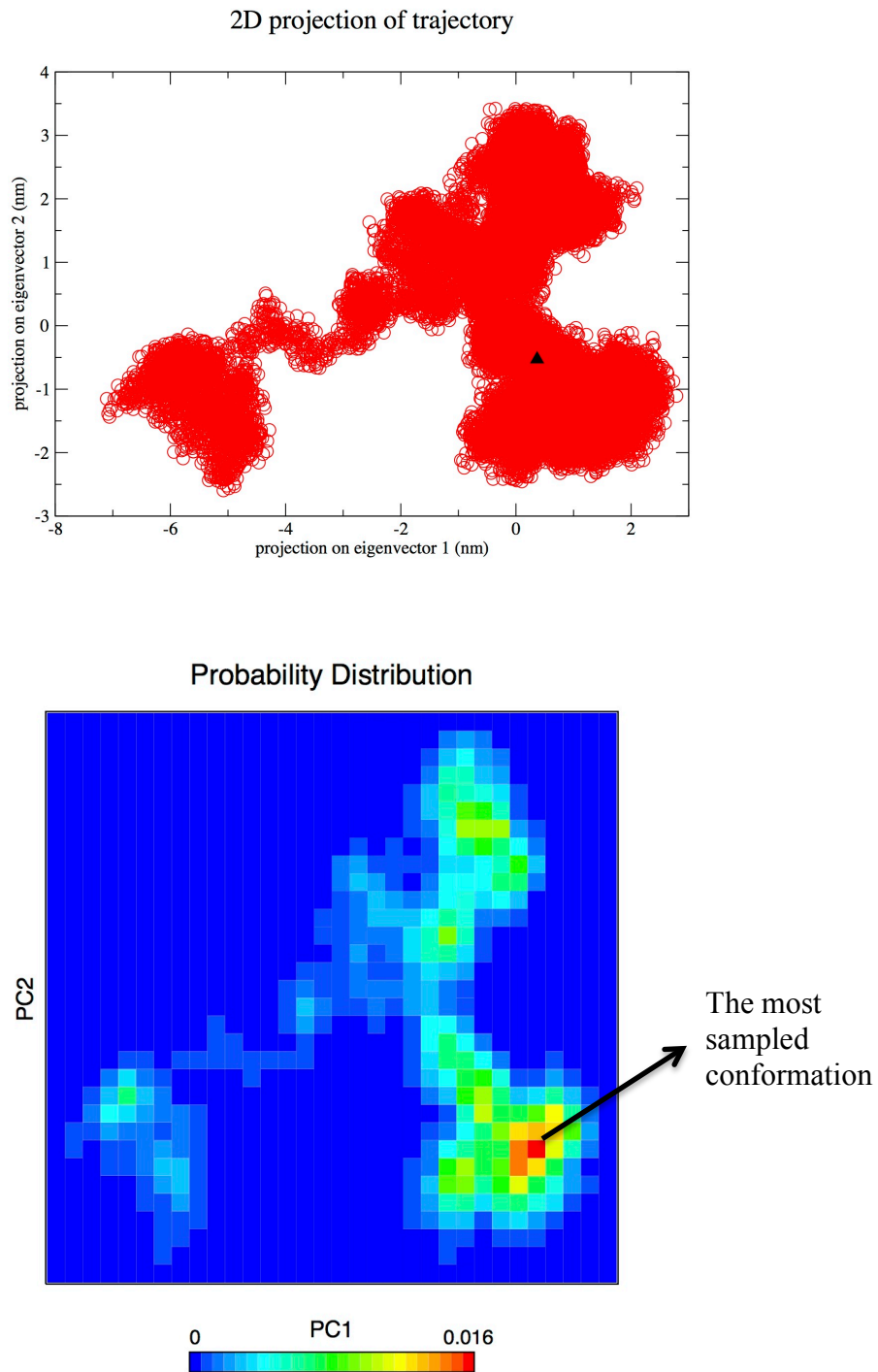


Figure 4.12. A. Projection of the receptor conformational space onto the two most significant principal components. B. Sampling probabilities of the projection.

The ‘heat map’ generated by g_sham module shows a spectrum of conformational occupancies where the most highly sampled conformations are indicated by red and the least sampled conformations are indicated by blue color. The most sampled conformations were found near the projection for the antagonist bound crystal structure of KOR (black triangle in Figure 4.11A), which suggests that the receptor is stabilized by JD_{Tic} (antagonist) in its inactive form. Root mean squared deviation (RMSD) of the C α atoms between a representative of the most sampled occupancy (KOR–JD_{Tic}–rep) and the crystal structure was found to be 2.814 Å, Figure 4.13 shows the overlapped aligned helices for the crystal structure (red) and KOR–JD_{Tic}–rep (yellow).

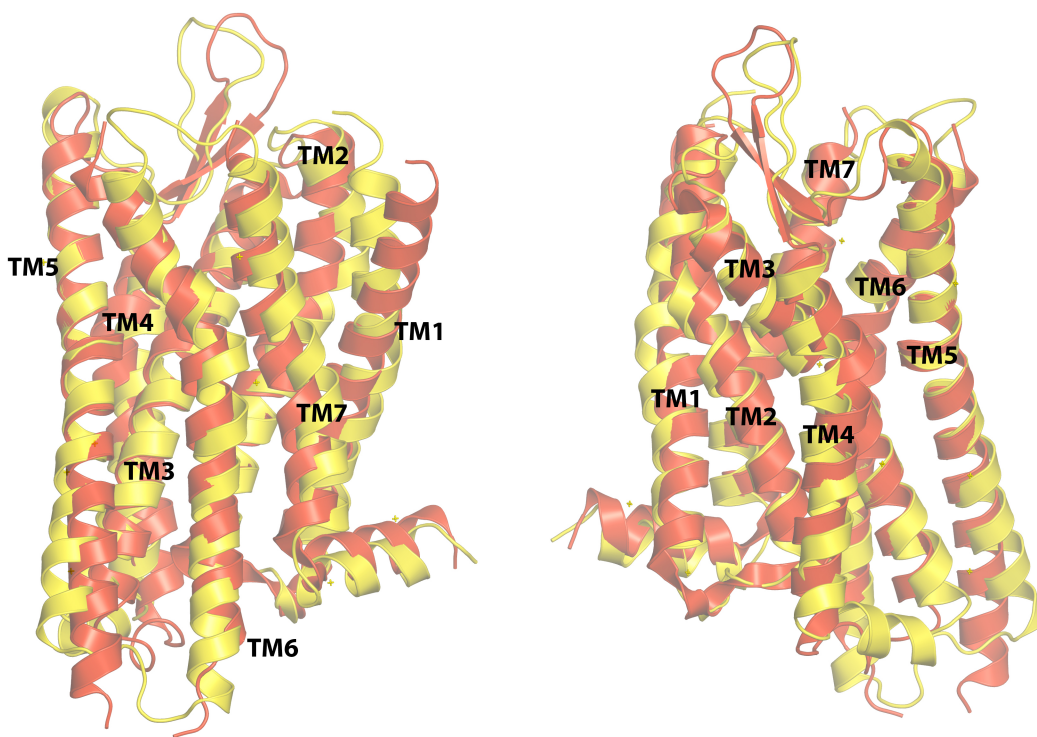


Figure 4.13. Overlaid and aligned conformations for crystal structure (red) and representative structure of most sampled conformation during the simulation (RMSD = 2.814 Å)

The alignment of KOR–JDTic–rep and KOR crystal structure showed limited deviations for $C\alpha$ atom positions and some changes in secondary structure, such as loss of the β -sheet in ECL2 and the formation of 2-turn α -helix at ICL2. However, the overall architecture remained the same and limited secondary structure variations have also been observed among the crystallized GPCRs, particularly the presence of ICL2 α helix. Importantly, this analysis demonstrated that subjecting the KOR–JDTic–lipid bilayer system to aMD maintained the integrity of the protein and highly sampled conformations showed little deviation from the structure elucidated from KOR–JDTic co-crystallization.

4.3.2.b Analysis of KOR–RB–64 lipid embedded complex (Receptor–Agonist system)

Similar procedures were also followed for analyzing the KOR–RB64 complex. Figure 4.14 shows the diagonalized co-variance matrix obtained from the $C\alpha$ trajectory and Figure 4.15 shows eigenvalues associated with the principal components calculated for KOR–RB–64 complex simulations from the co-variance matrix.

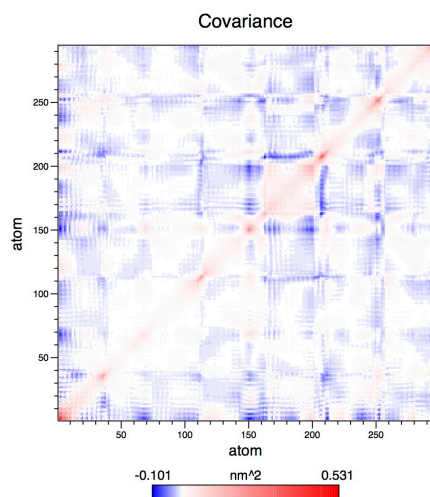


Figure 4.14. Co-variance matrix for aMD trajectory of KOR–JDTic system. Both X and Y axis define residue number ($C\alpha$ atoms). Red color indicates positive covariance, blue denotes negative covariance.

Eigenvalues of the covariance matrix

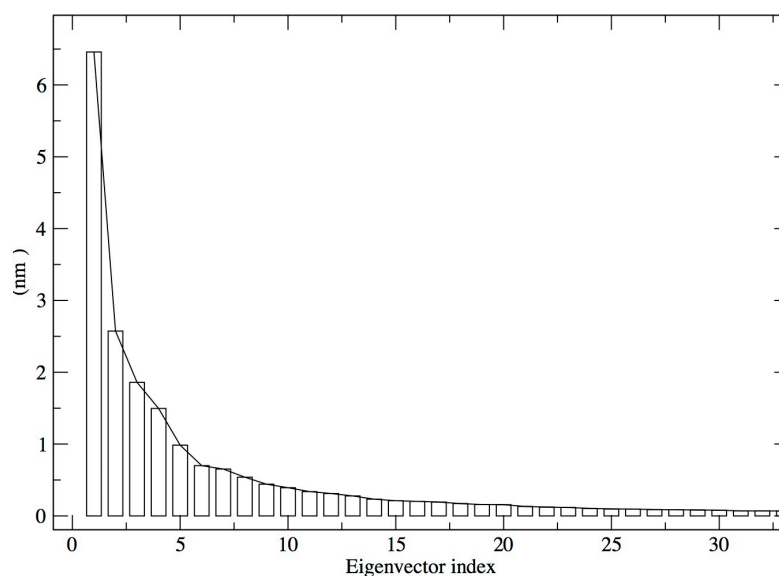


Figure 4.15. Eigenvalues (Y axis) associated with principal components (X axis) for KOR-RB64 system.

The simulated trajectory was then projected based on the two principal components with the highest contribution, PC1 and PC2. (Figure 4.16A) Red circles again denote the conformations sampled during the simulation and the projection for KOR-JDTic crystal structure is indicated by a black triangle. For this simulation, conformations with projections close to the crystal structure projection were *weakly* sampled. The population analysis for the obtained projections was done by probability sampling (refer to Figure 4.16B); as described earlier red denotes higher occupancy for a conformation and blue indicates low occupancy. In this simulation, two major distant clusters of high occupancy conformational projections were seen. The first three most occupied projections were close to each other, while the fourth most occupied projection was closer to the crystal structure projection. This suggested an apparent

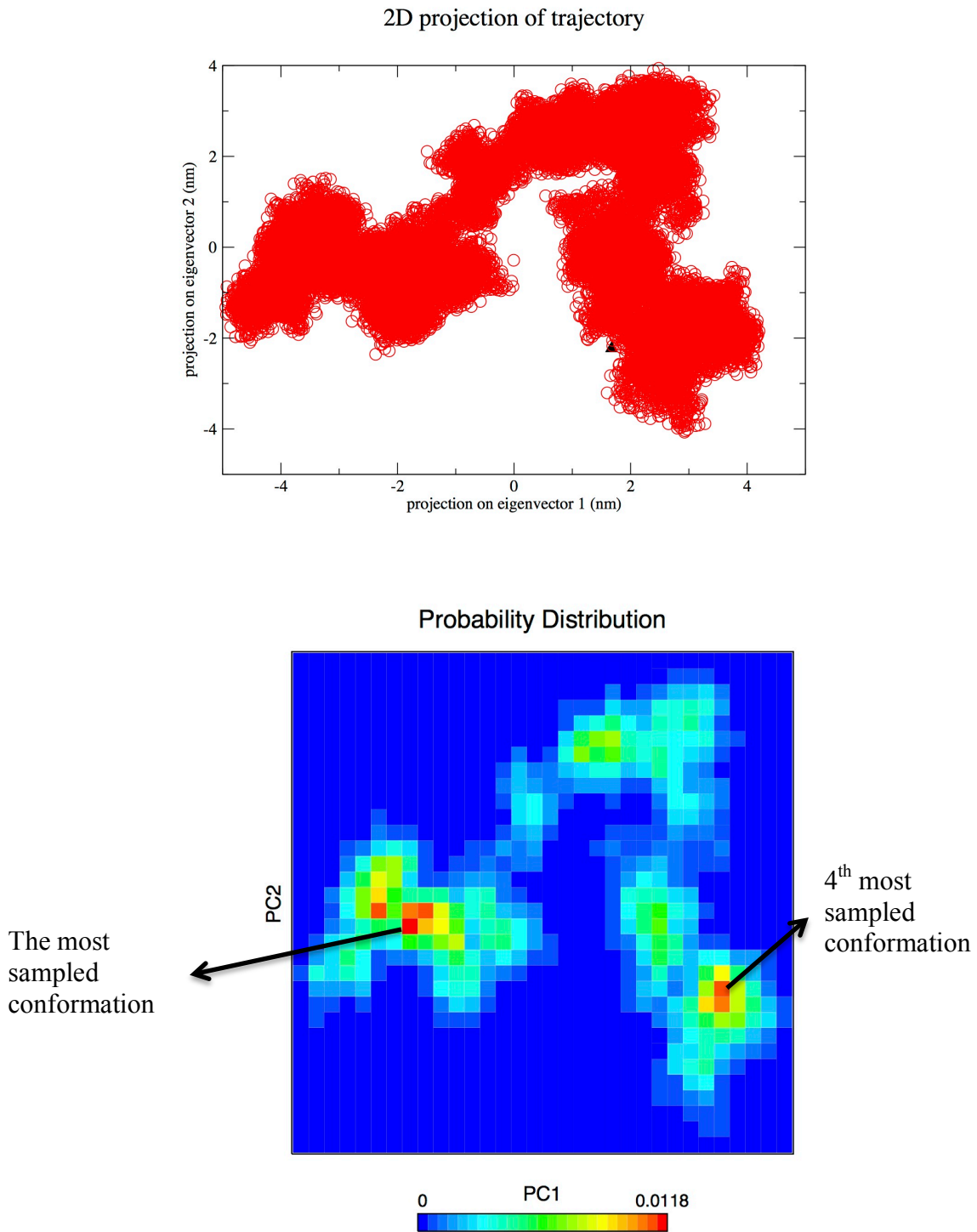


Figure 4.16. A. Projection of the receptor conformational space onto the two most significant principal components. B. Sampling probabilities of the projection.

transition in the receptor geometry projection were seen during early phase of the trajectory, while the most occupied projection's conformations start to appear around 58 ns (transition time). The RMSD calculated between a representative conformation of the highest occupied (KOR-RB64-rep-1) and the fourth highest occupied projections (KOR-RB64-rep-4), and the KOR-JDTic crystal structure was 3.678 Å and 4.447 Å, respectively.

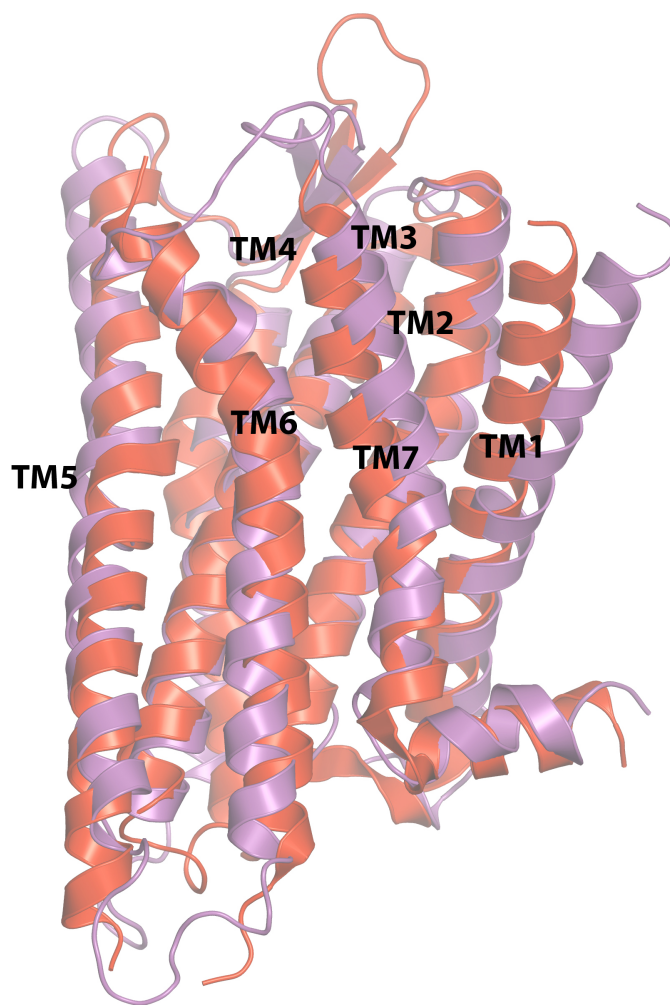


Figure 4.17. Overlaid and aligned conformations for crystal structure (red) and representative structure of fourth most sampled conformation during the simulation (magenta), RMSD = 3.678 Å.

Figure 4.17 shows the overlaid conformation for the fourth most sampled conformation and the conformation observed in the crystal structure. KOR–RB64-rep-4 has a similar conformation to that of the most populated conformation of KOR–JDTic system, except that β -sheet character of ECL2 is maintained for KOR–RB64-rep-4. Since projections for both the conformation lie close to the projection of the antagonist bound crystal structure, these conformations do not reflect sufficient departure from the antagonist ‘inactive’ state of the receptor.

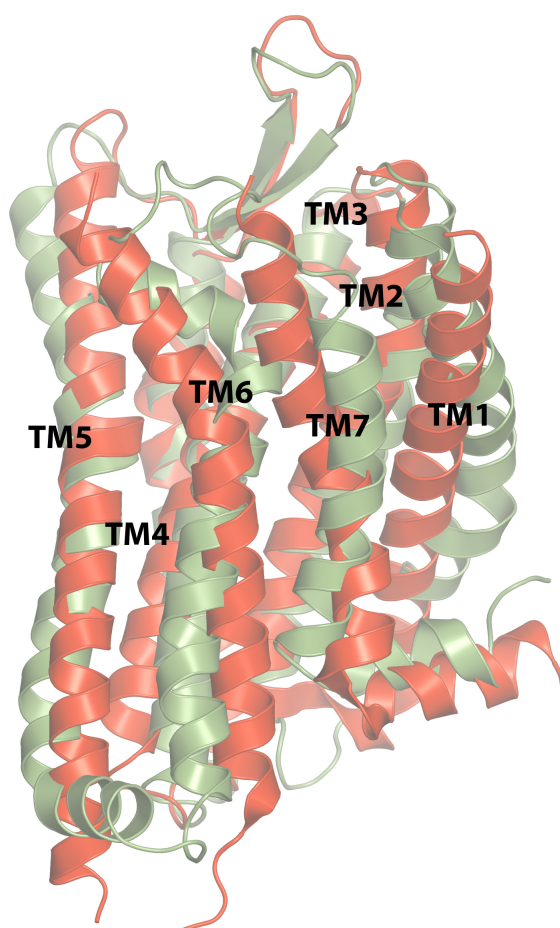


Figure 4.18. Overlaid and aligned conformations for crystal structure (red) and representative structure of the most sampled conformation during the simulation (green), RMSD = 4.447 Å.

Figure 4.18 shows the overlaid conformation of highest sampled conformation for KOR-RB64 system and the conformation of the KOR-JDTic crystal structure. Compared to the crystal structure, significant variations were seen in KOR-RB64-rep-1 conformations. The inward movement of TM6 at His^{6.52} (a turn above Pro^{6.50}) driven by interactions with Asp3.32 is seen to induce a sharp kink the helix, while both the top and the bottom of the helix move outwards. The extracellular helix of TM7 unravels and the intracellular part of the TM7 moves inwards. Outward movements were also seen in TM1 and TM2.

A complete protein trajectory study was undertaken (including both backbone and side chains) for further analysis of conformational sampling of the simulation. Following parameters associated with ‘active-like’ state of the receptor were analyzed:

a) Movements in P-I-F motif

As discussed previously characteristic conformational changes are observed at the P-I-F motif in agonist bound GPCRs. Pro^{5.50} moves inwards, while the Phe^{6.44} side chain rotates towards TM5, and the Ile^{3.40} side chain shifts to the position previously held by Phe^{6.44}. As a result phenyl ring of the Phe^{6.44} moves towards Pro^{5.50}. This movement was analyzed by studying the evolution of distances between the center of mass of Phe^{6.44} phenyl ring and the Pro^{5.50} backbone nitrogen. (Figure 4.19) The distance between the two is ~ 8-10 Å in starting conformations, and remains fairly constant through the simulation, especially in the most sampled conformation population. Figure 4.20 shows the conformation state of the P-I-F motif in the representative of the most

sampled conformation. No ‘active-like’ movements were observed for Pro^{5.50} (brown sticks), Ile^{3.40} (green sticks) or Phe^{6.44}.

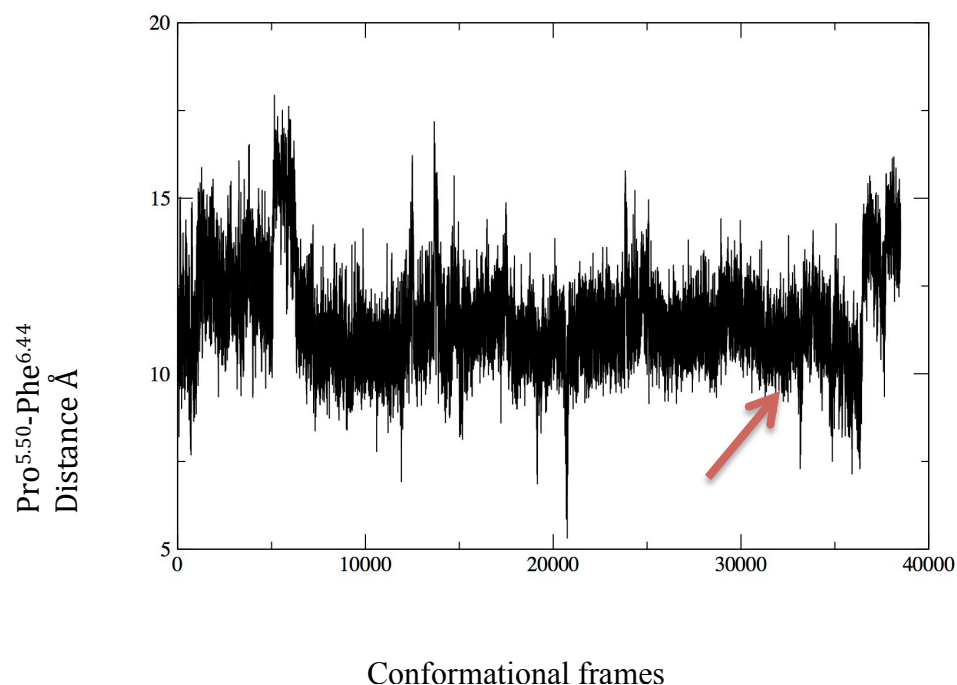


Figure 4.19. Evolution of distance between center of mass of phenyl ring of Phe^{6.44} and nitrogen atom of Pro^{5.50}. Each frame = 2 ps, red arrow indicates the ‘switch time’ (58 ns).

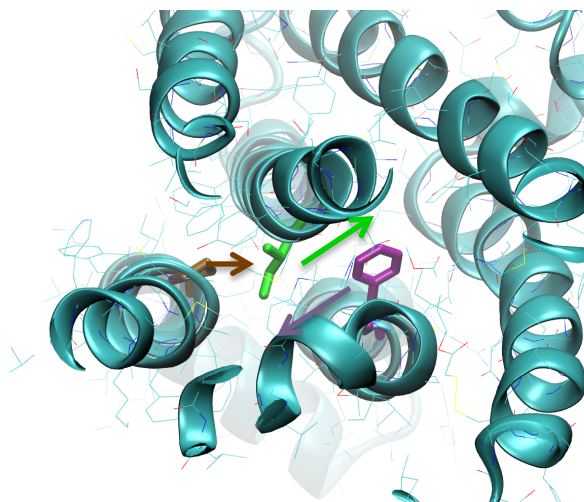


Figure 4.20. Conformational state of P-I-F motif in the highest sampled population in the simulation. Phe^{6.44} (magenta), Pro^{5.50} (brown), Ile^{3.40} (green). Arrows indicate expected active-state like movements in respectively colored residues.

b) Hydrogen bond network between Tyr^{5.58} and Tyr^{7.53}

Another characteristic active state GPCR movement is inward movement of the cytoplasmic end of TM7 towards the position vacated by outward movement of TM6. This inward movement of TM7 brings Tyr^{7.53} close Tyr^{5.58}, and the resulting hydrogen bond network through waters stabilizes the active state of the receptor. The evolution of distances between the hydroxyl oxygen of the tyrosines is shown in Figure 4.21. The distance between Tyr^{5.58} and Tyr^{7.53} increased during the simulation, instead of the expected decrease.

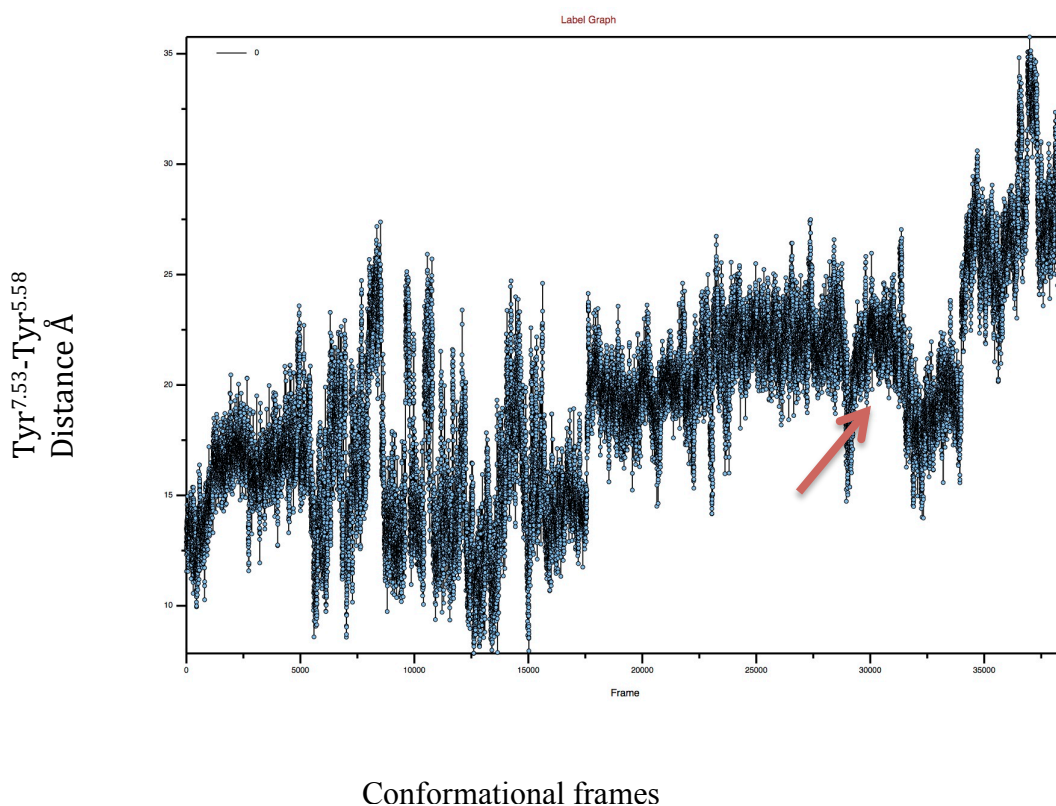


Figure 4.21. Evolution of distance between hydroxyl oxygen atoms of Tyr^{5.58} and Tyr^{7.53}. Each frame = 2 ps, red arrow indicates the 'switch time' (58 ns).

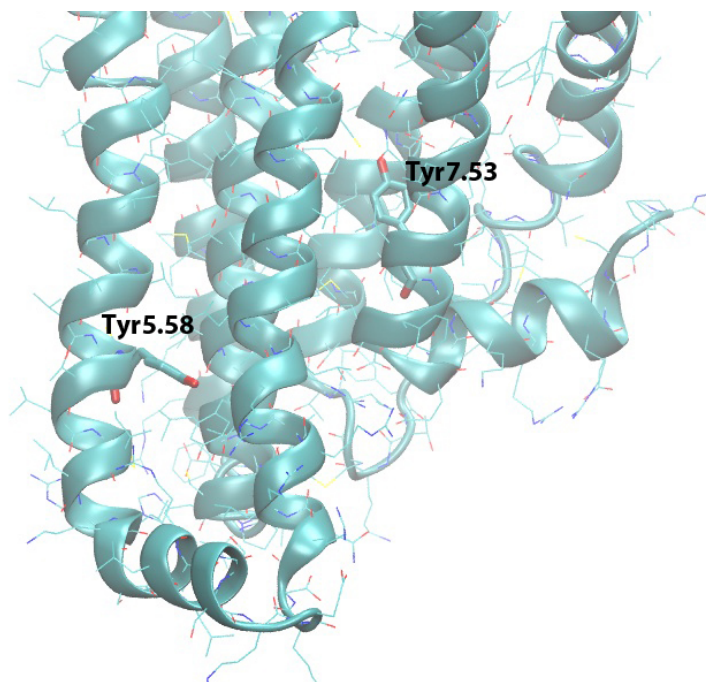


Figure 4.22. Conformational state of Tyr^{7.53} and Tyr^{5.58} in the most highly sampled population in the simulation.

c) Movement of cytoplasmic domain of TM6

Agonist-bound crystal structures show varying degrees of outward movements in TM6. It is more pronounced in the presence of the G protein or a G protein mimic; however, limited outward movement of the cytoplasmic domain of TM6 has been a constant feature in all agonist-bound receptor crystal structures. Figure 4.23 depicts the evolution of distance between center of mass of the protein and center of mass of the cytoplasmic domain of TM6. An outward movement of ~ 2 Å is observed during the simulation.

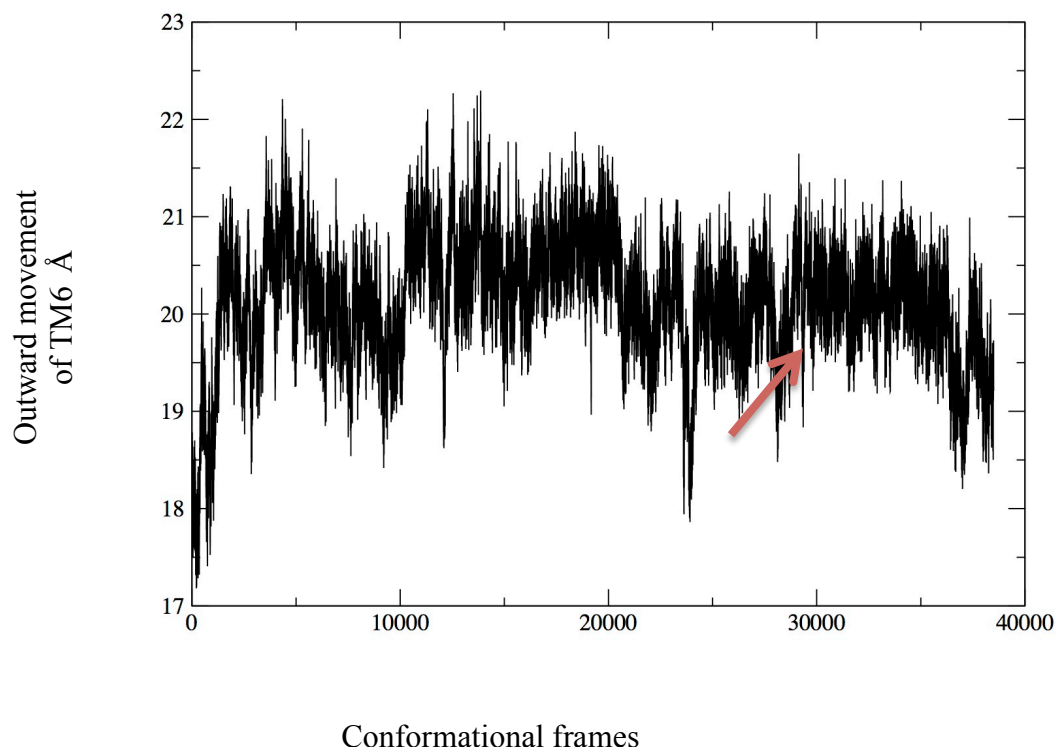


Figure 4.23. Evolution of distance between center of mass of the receptor and center of mass of cytoplasmic domain of TM6. Each frame = 2 ps, red arrow indicates the ‘switch time’ (58 ns).

Effectively, the major conformation observed, although different from the antagonist bound crystal structure conformation, showed little evidence for the ‘active-like’ state. The most prominent change observed in the receptor conformation was development of a sharp kink in TM6 at the His^{6.52} residue. (Figure 4.24) This is possibly due to a salt bridge interaction between carboxylate of the highly conserved Asp^{3.32} residue and the δ N of the His^{6.52}.

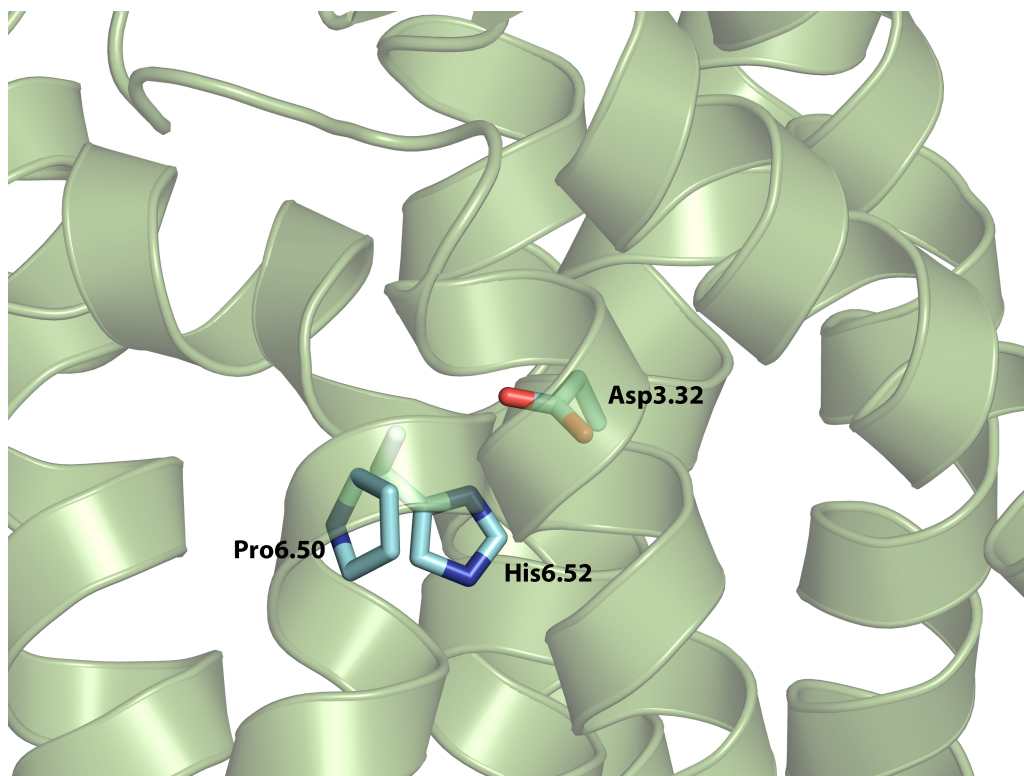


Figure 4.24. Sharp kink in TM6 at His^{6.52}, a half turn above Pro^{5.50} in KOR.

4.3.2.c Analysis of apoprotein KOR lipid embedded complex simulations

Analysis of the apo-KOR-allosteric sodium complex simulation demonstrates a constrained conformation sampling compared to the conformations observed without allosteric sodium in Apo-KOR. However, conformations with similar projections were sampled most often in both cases. A plausible cause could be the loss of sodium from its allosteric site outside the interhelical region, early in the simulation. The sampled conformations showed a sharp TM6 kink similar to those seen in RB-64 model.

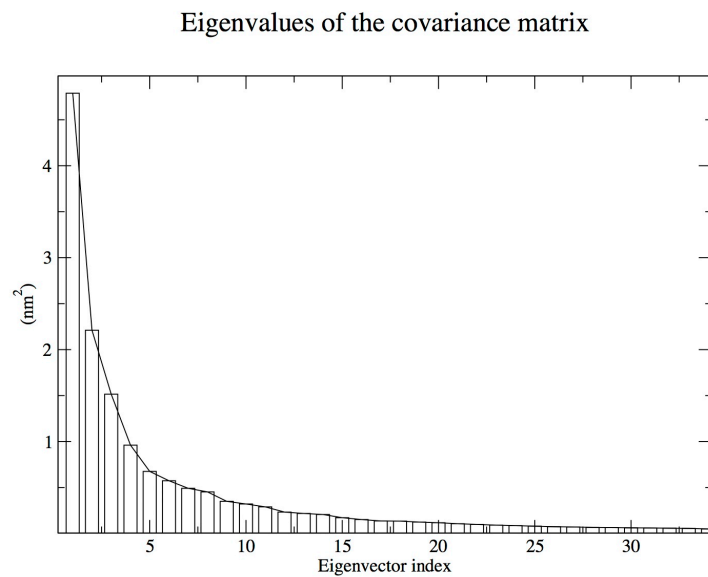


Figure 4.25. Eigenvalues (Y axis) associated with principal components (X axis) for Apo-KOR system.

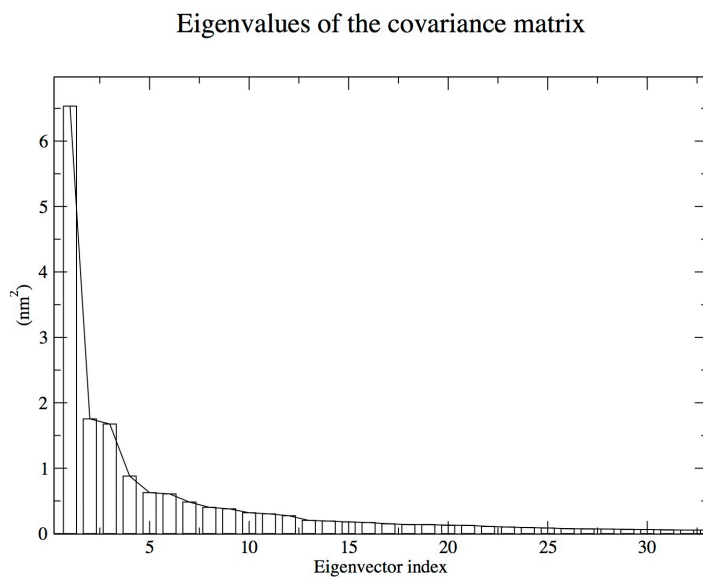


Figure 4.26. Eigenvalues (Y axis) associated with principal components (X axis) for Apo-KOR-allosteric sodium system.

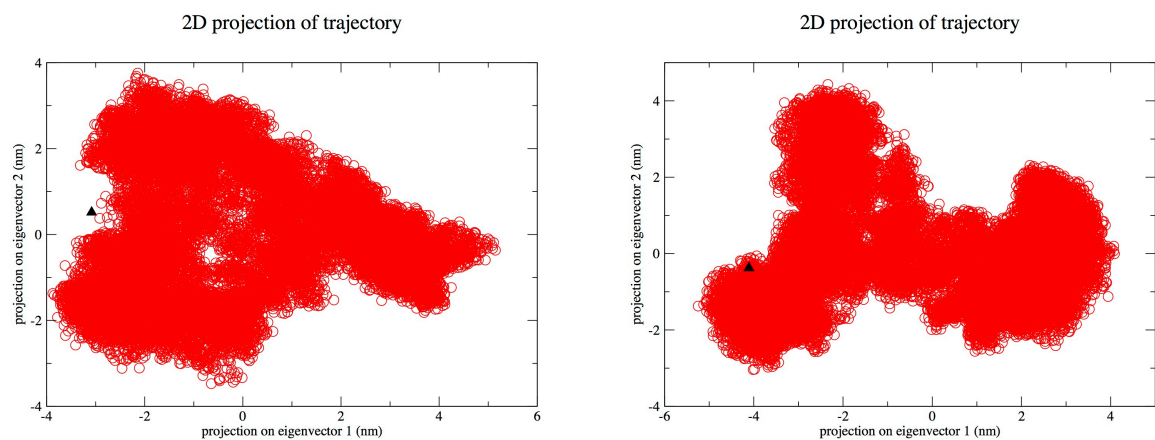


Figure 4.27. Projection of the receptor conformational space onto the two most significant principal components. A. apo-KOR system B. apo-KOR-allosteric sodium system.

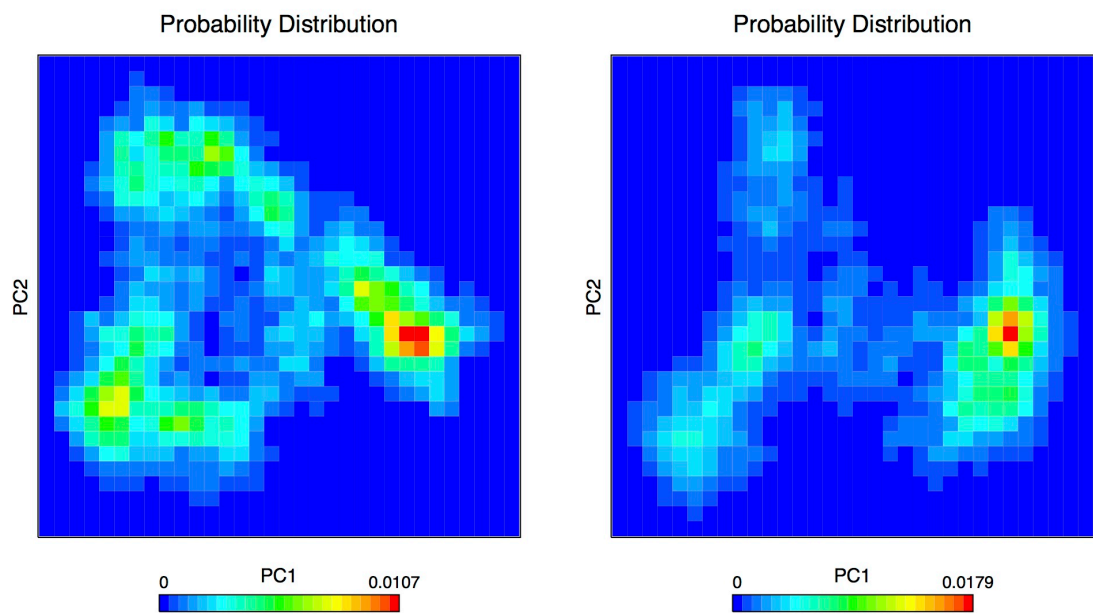


Figure 4.28. Sampling probabilities of the projections. A. apo-KOR system B. apo-KOR-allosteric sodium system.

4.4 Discussion

Advancement in crystallographic techniques in the past decade has resulted in structure elucidation of many GPCRs and the number of these structures is expected to grow. However, each of these structures represents only one plausible conformation of the receptor under the given experimental conditions, not least of which is the co-crystallized ligand. In fact, deviations observed in receptor conformations while they are co-crystallized with ligands of different functionality (agonism/antagonism/inverse agonism) are being employed to develop models for receptor activation and functional selectivity.

This report describes an attempt to model the agonist bound KOR protein conformation by utilizing the enhanced sampling capabilities of accelerated molecular dynamics. Four different lipid embedded-water enveloped systems were built – KOR-agonist, KOR-antagonist, apoprotein-KOR and apoprotein-KOR-allosteric sodium, and accelerated MD simulations were carried out for > 60 ns after equilibrating via conventional molecular dynamics. All four systems remained stable during the simulation and conformational sampling revealed major clusters of similar conformations for each simulation. In the KOR–JDTic system (antagonist), the major conformation was close to the crystallographic conformation observed for the protein in JDTic co-crystallized KOR, indicating a fair reproducibility of experimental observations in the simulation. For the KOR-RB-64 system (agonist), two major clusters of receptor conformation populations were observed. Of these clusters, the minor population conformation was closer to the conformations observed in antagonist-bound KOR, while the major population showed divergence from the crystal structure conformations. However, analysis of the trajectory revealed the absence of ‘signature’ active state conformational changes and the observed major

conformational change was apparently effected by hydrogen bond interactions between His^{6.52} and Asp^{3.32}.

The strong interactions between His^{6.52} and Asp^{3.32} resulted in a sharp kink in TM6 and the unraveling of the extracellular domain of TM7 due to the strain in ECL3. Interestingly, B factors for ECL3 are high for all three opioid receptor crystal structures and the ECL3 loop remained unresolved in the KOR–JDTic crystal structure. His^{6.52} previously has been implicated in opioid receptor agonist activation; mutagenesis studies have observed increased intrinsic activity as well as conferring agonist-like actions to antagonists.⁴⁶ Similar TM6 kinks were also observed in apoprotein KOR simulations, these could reflect conformations responsible for basal activity of the receptor.

Regardless, the observed TM6 kink could be an artifact of the simulation parameters. The protonated imidazole form of histidine was used in the simulation, a choice that was based on several test simulations that demonstrated the ability of protonated histidine to maintain the surrounding water network as observed in the KOR crystal structure. However, this also ‘loaded’ the charged His^{6.52} with an additional hydrogen bond donor, which found a ready acceptor in Asp^{3.32}. An elementary remedy would be parameterizing non-protonated form of the histidine for the simulation or to increase the simulation time period. Furthermore, the ionization state of the solvent accessible histidine is likely to be in equilibrium, which may not be adequately represented by either extreme.

The work detailed here presents an initial effort of building agonist phase models of the kappa opioid receptor. Although the classical ‘active’ state conformation of the KOR receptor was not achieved, the study does provides a good template for future studies. Notably, seemingly

adequate conformational sampling was achieved within ~80 ns of accelerated molecular dynamic simulation. Hence, optimization of the energy boosts for the accelerated simulation was realized while maintaining the overall robustness of the system. The future studies require detailed analysis of changes in the charged state of ionizable residues due to the structural changes in the protein, particularly of the residues close to the ligand and to the allosteric sodium site. Following successful building and validation of agonist–KOR complex models, correlational conformation analysis of the residues can bring new insights into mechanism of GPCR activation and functional selectivity of the ligands. Similar approaches can also be utilized to study other opioid receptors as well as other GPCRs.

Reference:

- (1) Irannejad, R.; Tomshine, J. C.; Tomshine, J. R.; Chevalier, M.; Mahoney, J. P.; Steyaert, J.; Rasmussen, S. G. F.; Sunahara, R. K.; El-Samad, H.; Huang, B.; von Zastrow, M. Conformational Biosensors Reveal GPCR Signalling from Endosomes. *Nature* **2013**, *495*, 534–538.
- (2) Sheikh, S. P.; Zvyaga, T. A.; Lichtarge, O.; Sakmar, T. P.; Bourne, H. R. Rhodopsin activation blocked by metal-ion-binding-site linked transmembrane helices C and F. *Nature* **1996**, *383*, 347-350.
- (3) Sheikh, S. P.; Vilardarga, J.-P.; Baranski, T. J.; Lichtarge, O.; Iiri, T.; Meng, E. C.; Nissenson, R. A.; Bourne, H. R. Similar Structures and Shared Switch Mechanisms of the Beta 2-Adrenoceptor and the Parathyroid Hormone Receptor. Zn(II) BRIDGES BETWEEN HELICES III AND VI BLOCK ACTIVATION. *J. Biol. Chem.* **1999**, *274*, 17033–17041.
- (4) Palczewski, K. Crystal Structure of Rhodopsin: A G Protein-Coupled Receptor. *Science* **2000**, *289*, 739–745.
- (5) Deupi, X. Relevance of Rhodopsin Studies for GPCR Activation. *Biochim. Biophys. Acta* **2013**, *1837*, 674–682.
- (6) Nakamichi, H.; Okada, T. Crystallographic Analysis of Primary Visual Photochemistry. *Angew. Chem. Int. Ed. Engl.* **2006**, *45*, 4270–4273.
- (7) Nakamichi, H.; Okada, T. Local Peptide Movement in the Photoreaction Intermediate of Rhodopsin. *Proc. Natl. Acad. Sci. U. S. A.* **2006**, *103*, 12729–12734.
- (8) Choe, H. W.; Kim, Y. J.; Park, J. H.; Morizumi, T.; Pai, E. F.; Krauss, N.; Hofmann, K. P.; Scheerer, P.; Ernst, O. P. Crystal Structure of Metarhodopsin II. *Nature* **2011**, *471*, 651–655.
- (9) Scheerer, P.; Park, J. H.; Hildebrand, P. W.; Kim, Y. J.; Krauss, N.; Choe, H. W.; Hofmann, K. P.; Ernst, O. P. Crystal Structure of Opsin in Its G-Protein-Interacting Conformation. *Nature* **2008**, *455*, 497–502.
- (10) Standfuss, J.; Edwards, P. C.; D'Antona, A.; Fransen, M.; Xie, G.; Oprian, D. D.; Schertler, G. F. X. The Structural Basis of Agonist-Induced Activation in Constitutively Active Rhodopsin. *Nature* **2011**, *471*, 656–660.
- (11) Rosenbaum, D. M.; Cherezov, V.; Hanson, M. A.; Rasmussen, S. G. F.; Thian, F. S.; Kobilka, T. S.; Choi, H. J.; Yao, X. J.; Weis, W. I.; Stevens, R. C.; Kobilka, B. K. GPCR

- Engineering Yields High-Resolution Structural Insights into beta2-Adrenergic Receptor Function. *Science* **2007**, *318*, 1266–1273.
- (12) Rasmussen, S. G. F.; Choi, H. J.; Fung, J. J.; Pardon, E.; Casarosa, P.; Chae, P. S.; Devree, B. T.; Rosenbaum, D. M.; Thian, F. S.; Kobilka, T. S.; Schnapp, A.; Konetzki, I.; Sunahara, R. K.; Gellman, S. H.; Pautsch, A.; Steyaert, J.; Weis, W. I.; Kobilka, B. K. Structure of a Nanobody-Stabilized Active State of the $\beta(2)$ Adrenoceptor. *Nature* **2011**, *469*, 175–180.
- (13) Rasmussen, S. G. F.; DeVree, B. T.; Zou, Y.; Kruse, A. C.; Chung, K. Y.; Kobilka, T. S.; Thian, F. S.; Chae, P. S.; Pardon, E.; Calinski, D.; Mathiesen, J. M.; Shah, S. T. a; Lyons, J. a; Caffrey, M.; Gellman, S. H.; Steyaert, J.; Skiniotis, G.; Weis, W. I.; Sunahara, R. K.; Kobilka, B. K. Crystal Structure of the β_2 Adrenergic Receptor-Gs Protein Complex. *Nature* **2011**, *477*, 549–555.
- (14) Lebon, G.; Warne, T.; Edwards, P. C.; Bennett, K.; Langmead, C. J.; Leslie, A. G. W.; Tate, C. G. Agonist-Bound Adenosine A2A Receptor Structures Reveal Common Features of GPCR Activation. *Nature* **2011**, *474*, 521–525.
- (15) Xu, F.; Wu, H.; Katritch, V.; Han, G. W.; Jacobson, K. a; Gao, Z. G.; Cherezov, V.; Stevens, R. C. Structure of an Agonist-Bound Human A2A Adenosine Receptor. *Science* **2011**, *332*, 322–327.
- (16) Kruse, A. C.; Ring, A. M.; Manglik, A.; Hu, J.; Hu, K.; Eitel, K.; Hübner, H.; Pardon, E.; Valant, C.; Sexton, P. M.; Christopoulos, A.; Felder, C. C.; Gmeiner, P.; Steyaert, J.; Weis, W. I.; Garcia, K. C.; Wess, J.; Kobilka, B. K. Activation and Allosteric Modulation of a Muscarinic Acetylcholine Receptor. *Nature* **2013**, *504*, 101–106.
- (17) Wacker, D.; Wang, C.; Katritch, V.; Han, G. W.; Huang, X. P.; Vardy, E.; McCorvy, J. D.; Jiang, Y.; Chu, M.; Siu, F. Y.; Liu, W.; Xu, H. E.; Cherezov, V.; Roth, B. L.; Stevens, R. C. Structural Features for Functional Selectivity at Serotonin Receptors. *Science* **2013**, *340*, 615–619.
- (18) Schwartz, T. W.; Frimurer, T. M.; Holst, B.; Rosenkilde, M. M.; Elling, C. E. Molecular Mechanism of 7TM Receptor Activation-a Global Toggle Switch Model. *Annu. Rev. Pharmacol. Toxicol.* **2006**, *46*, 481–519.
- (19) Pellissier, L. P.; Sallander, J.; Campillo, M.; Gaven, F.; Queffeuilou, E.; Pillot, M.; Dumuis, A.; Claeysen, S.; Pardo, L. Conformational Toggle Switches Implicated in Basal Constitutive and Agonist-Induced Activated States of 5-Hydroxytryptamine-4 Receptors. *Mol. Pharmacol.* **2009**, *75*, 982–990.

- (20) Jensen, A. S. M.; Sparre-Ulrich, A. H.; Davis-Poynter, N.; Rosenkilde, M. M. Structural Diversity in Conserved Regions Like the DRY-Motif among Viral 7TM Receptors-A Consequence of Evolutionary Pressure? *Adv. Virol.* **2012**, *2012*, 231813.
- (21) Manglik, A.; Kobilka, B. The Role of Protein Dynamics in GPCR Function: Insights from the β 2AR and Rhodopsin. *Curr. Opin. Cell Biol.* **2014**, *27*, 136–143.
- (22) Cooper, A. Energy uptake in the first step of visual excitation. *Nature* **1979**, *282*, 531-533.
- (23) Tehan, B. G.; Bortolato, A.; Blaney, F. E.; Weir, M. P.; Mason, J. S. Unifying Family A GPCR Theories of Activation. *Pharmacol. Ther.* **2014**, *143*, 51–60.
- (24) Roth, B. L.; Baner, K.; Westkaemper, R.; Siebert, D.; Rice, K. C.; Steinberg, S.; Ernsberger, P.; Rothman, R. B. Salvinorin A: A Potent Naturally Occurring Nonnitrogenous Kappa Opioid Selective Agonist. *Proc. Natl. Acad. Sci. U. S. A.* **2002**, *99*, 11934–11939.
- (25) Ansonoff, M. A.; Zhang, J.; Czyzyk, T.; Rothman, R. B.; Stewart, J.; Xu, H.; Zjawiony, J.; Siebert, D. J.; Yang, F.; Roth, B. L.; Pintar, J. E. Antinociceptive and Hypothermic Effects of Salvinorin A Are Abolished in a Novel Strain of κ -Opioid Receptor-1 Knockout Mice. **2006**, *318*, 641–648.
- (26) Yan, F.; Mosier, P. D.; Westkaemper, R. B.; Roth, B. L. $G\alpha$ -Subunits Differentially Alter the Conformation and Agonist Affinity of κ -opioid receptor. *Biochemistry* **2008**, *47*, 1567–1578.
- (27) Vortherms, T. A.; Mosier, P. D.; Westkaemper, R. B.; Roth, B. L. Differential Helical Orientations among Related G Protein-Coupled Receptors Provide a Novel Mechanism for Selectivity: STUDIES WITH SALVINORIN A AND THE κ -OPIOID RECEPTOR. *J. Biol. Chem.* **2006**, *282*, 3146–3156.
- (28) Yan, F.; Mosier, P. D.; Westkaemper, R. B.; Stewart, J.; Zjawiony, J. K.; Vortherms, T. A.; Sheffler, D. J.; Roth, B. L. Identification of the Molecular Mechanisms by Which the Diterpenoid Salvinorin A Binds to Kappa-Opioid Receptors. *Biochemistry* **2005**, *44*, 8643–8651.
- (29) Yan, F.; Bikbulatov, R. V.; Mocanu, V.; Dicheva, N.; Parker, C. E.; Wetsel, W. C.; Mosier, P. D.; Westkaemper, R. B.; Allen, J. a; Zjawiony, J. K.; Roth, B. L. Structure-Based Design, Synthesis, and Biochemical and Pharmacological Characterization of Novel Salvinorin A Analogues as Active State Probes of the Kappa-Opioid Receptor. *Biochemistry* **2009**, *48*, 6898–6908.
- (30) Wu, H.; Wacker, D.; Mileni, M.; Katritch, V.; Han, G. W.; Vardy, E.; Liu, W.; Thompson, A. a; Huang, X. P.; Carroll, F. I.; Mascarella, S. W.; Westkaemper, R. B.; Mosier, P. D.;

- Roth, B. L.; Cherezov, V.; Stevens, R. C. Structure of the Human K-Opioid Receptor in Complex with JDTic. *Nature* **2012**, *485*, 327–332.
- (31) Costa, T.; Lang, J.; Gless, C.; Herz, A. Spontaneous Association between Opioid Receptors and GTP-Binding Regulatory Proteins in Native Membranes: Specific Regulation by Antagonists and Sodium Ions. *Mol. Pharmacol.* **1990**, *37*, 383–394.
- (32) Hamelberg, D.; Mongan, J.; McCammon, J. A. Accelerated Molecular Dynamics: A Promising and Efficient Simulation Method for Biomolecules. *J. Chem. Phys.* **2004**, *120*, 11919–11929.
- (33) Pierce, L. C. T.; Salomon-Ferrer, R.; Augusto F de Oliveira, C.; McCammon, J. A.; Walker, R. C. Routine Access to Millisecond Time Scale Events with Accelerated Molecular Dynamics. *J. Chem. Theory Comput.* **2012**, *8*, 2997–3002.
- (34) Fenalti, G.; Giguere, P. M.; Katritch, V.; Huang, X. P.; Thompson, A. A.; Cherezov, V.; Roth, B. L.; Stevens, R. C. Molecular Control of Δ -Opioid Receptor Signalling. *Nature* **2014**, *506*, 191–196.
- (35) Fiser, A.; Do, R. K.; Sali, A. Modeling of Loops in Protein Structures. *Protein Sci.* **2000**, *9*, 1753–1773.
- (36) Valiev, M.; Bylaska, E. J.; Govind, N.; Kowalski, K.; Straatsma, T. P.; Van Dam, H. J. J.; Wang, D.; Nieplocha, J.; Apra, E.; Windus, T. L.; de Jong, W. A. NWChem: A Comprehensive and Scalable Open-Source Solution for Large Scale Molecular Simulations. *Comput. Phys. Commun.* **2010**, *181*, 1477–1489.
- (37) Grosdidier, L.; Michielin, O.; Zoete, V.; Cuendet, M. A. SwissParam : A Fast Force Field Generation Tool for Small Organic Molecules. *J. Comput. Chem.* **2011**, *32*, 2359-2368.
- (38) Mackerell, A. D.; Feig, M.; Brooks, C. L. Extending the Treatment of Backbone Energetics in Protein Force Fields: Limitations of Gas-Phase Quantum Mechanics in Reproducing Protein Conformational Distributions in Molecular Dynamics Simulations. *J. Comput. Chem.* **2004**, *25*, 1400–1415.
- (39) Feller, S. E.; Gawrisch, K.; MacKerell, A. D. Polyunsaturated Fatty Acids in Lipid Bilayers: Intrinsic and Environmental Contributions to Their Unique Physical Properties. *J. Am. Chem. Soc.* **2002**, *124*, 318–326.
- (40) Buck, M.; Bouguet-Bonnet, S.; Pastor, R. W.; MacKerell, A. D. Importance of the CMAP Correction to the CHARMM22 Protein Force Field: Dynamics of Hen Lysozyme. *Biophys. J.* **2006**, *90*, L36–8.

- (41) Humphrey, W.; Dalke, a; Schulten, K. VMD: Visual Molecular Dynamics. *J. Mol. Graph.* **1996**, *14*, 33–38, 27–28.
- (42) Lomize, M. A.; Lomize, A. L.; Pogozheva, I. D.; Mosberg, H. I. OPM: Orientations of Proteins in Membranes Database. *Bioinformatics* **2006**, *22*, 623–625.
- (43) Phillips, J. C.; Braun, R.; Wang, W.; Gumbart, J.; Tajkhorshid, E.; Villa, E.; Chipot, C.; Skeel, R. D.; Kalé, L.; Schulten, K. Scalable Molecular Dynamics with NAMD. *J. Comput. Chem.* **2005**, *26*, 1781–1802.
- (44) Wang, Y.; Harrison, C. B.; Schulten, K.; McCammon, J. A. Implementation of accelerated molecular dynamics in NAMD. *Comput. Sci. Discov.* **2012**, *4*, 1–14.
- (45) Frishman, D.; Argos, P. Knowledge-based protein secondary structure assignment. *Proteins* **1995**, *23*, 566-579.
- (46) Spivak, C. E.; Beglan, C. L.; Seidleck, B. K.; Hirshbein, L. D.; Blaschak, C. J.; Uhl, G. R.; Surratt, C. K. Naloxone Activation of Mu-Opioid Receptors Mutated at a Histidine Residue Lining the Opioid Binding Cavity. *Mol. Pharmacol.* **1997**, *52*, 983–992.

CHAPTER 5

CONCLUSIONS

This report describes various strategies for protein structure-based drug design. In chapter 2, due to the unavailability of the target protein (CCR5) structure, a homology modeling approach was employed. The homology model of CCR5 was built based on the closely related CXCR4 template, following a rigorous sequence alignment including that of the secondary structural features such as the disulfide bonds. The ligand binding site of the homology model and the ligand docking scoring function were validated by examining the top scored docking solutions with respect to the available site-directed mutagenesis data for binding affinities of known CCR5 antagonists. The docking modes of the lead compound (anibamine) were then proposed for the validated binding pocket of the homology model. The exploration of anibamine docking modes inside the receptor revealed weak interactions due to the high conformational flexibility of the ligand inside the primarily hydrophobic and aromatic ligand binding pocket. In consideration of the model, second generation anibamine compounds were designed with amine-linked aromatic substitutions. Furthermore, water sites were generated inside the ligand binding pocket of the CCR5 homology model. The superimposition of the generated water map on the docking modes

of the previously docked ligands suggests entropy-driven binding of CCR5 antagonists due to displacement of the conserved and highly ordered water molecules close to the crucial acidic Glu283 residue. Some plausible hydrogen bonding interactions through the water bridges were also observed. The results suggest the importance of including water molecules in receptor-ligand interaction studies.

In chapter 3, the selectivity profile of the naltrexone derived compounds was explored with respect to the opioid receptors. The lead compounds, NAP and NAQ, were originally designed on the basis of the identification of ‘address’ sites on the rhodopsin template homology model of the opioid receptors. The results shown here validated the address sites of original homology-based model and also proposed new address sites. The results indicate that the naltrexone derivatives can interact with multiple address sites, depending on the position of the substitutions attached, as well as the conformation a ligand may prefer inside the binding pocket.

In the MOR, two primary address sites were identified on the receptor for the 6-substituted naltrexamine derivatives based on the docking experiments and sequence alignment studies. The first site had aromatic as well as hydrogen bond donor moieties (Trp318 and Lys303), which is a validation of the original homology based model. An alternate address site was also identified, present close to the top of TM5 and ECL2. The second generation analogs of NAP and NAQ were designed on the basis of the address sites identified here. However, loss in relative selectivity of some of the second generation analogs was observed. Long term molecular dynamic (MD) simulation experiments were performed with a representative of the second generation analogs (NNQ) in complex with opioid receptors in a ‘plasma membrane-like’ environment. The results suggest that the ligand recognizes the address sites identified earlier in

MOR; however, the functionalized moiety of the ligand interacts with the alternate regions in KOR and DOR, which may compensate for lack of MOR ‘address’ site recognition. The non-bonded interaction energies calculated between the ligand and the opioid receptor validated the compensation hypothesis.

The docking studies of 14-substituted ester-linked naltrexone derivatives on the opioid receptor revealed another ‘address’ region in the MOR. This ‘address’ region was postulated due to the variations in the conformation assumed by the conserved glutamate residue in the ligand binding pocket following short term MD simulation experiments. In the MOR, the conserved glutamate residue provided a hydrogen bond donor group to the 14-substituted naltrexone derivatives because of its interactions with a non-conserved asparagine residue, present one turn above. However, the conserved glutamate in KOR and DOR was ill directed for hydrogen bonding, thus explaining the selectivity of the 14-substituted ester-linked naltrexone derivatives towards MOR. However, this selectivity was lost for amine-linked derivatives, possibly because of stronger conserved interactions between the amide linker and the conserved aspartate of TM3 in all three opioid receptors. Overall results suggest the presence of a good operational model for understanding opioid selectivity for both 6- and 14-position substituted naltrexone derivatives.

Finally in chapter 4, structural insights from the recently crystallized ‘active-like’ GPCRs were employed to identify ‘signature’ conformational changes that induce receptor activation. Long-term accelerated MD simulation experiments were performed on the KOR-RB-64 (agonist) complex in a lipid bilayer inside a water box. Distinct and highly populated receptor conformations were achieved in the KOR-agonist simulation experiments that were significantly different from the KOR-antagonist crystal structure conformation. However, these structures

lacked the ‘signature’ conformational changes associated with receptor activation. The protonation state of the crucial histidine in TM6 was identified as a plausible cause of ‘artifactual’ conformation. The study provides a template for future such experiments, particularly the optimization of the energy acceleration such that significant conformational sampling is achieved without damaging stability and integrity of the system. These studies are promising for understanding receptor activation mechanism, the role of receptor residues and motifs in ligand functions, functional selectivity of the ligand etc.

Overall, the studies reported here represent the evolution of molecular modeling techniques with the advent of the GPCR crystal structures. For the majority of the past decade, the receptor structure based computational studies were generally limited to homology modeling approaches. However, with the advancement of crystallization techniques and the surge in the number of available crystal structures, more comprehensive and extensive ligand-receptor interaction and selectivity studies have come to fruition. Furthermore, the availability of active-like structures of GPCRs has opened a new paradigm of modeling ligand functions on the receptor.